OPTICAL ABSORPTION STUDIES OF Mn^{2+} IN CRYSTALS

A THESIS

submitted to the

INDIAN INSTITUTE OF TECHNOLOGY, KANPUR

in partial fulfilment of the requirements

for the degree of

DOCTOR OF PHILOSOPHY

I. I. T. KANPUR
CENTRAL LIBRARY
Acc. No: 75382

Thesis
532.6
M474o

by

ANJANI K. MEHRA

TH
PHY/1967/D
M474o

DEPARTMENT OF PHYSICS

INDIAN INSTITUTE OF TECHNOLOGY, KANPUR, INDIA

JANUARY, 1967

PHY- 1967-D-MEH-OPT

Certified that the work presented in this thesis has been done by Mr. Anjani Kumar Mehra under my supervision.

Putcha Venkateswarlu

Putcha Venkateswarlu
Professor of Physics

Feb. 3, 1967

Department of Physics
Indian Institute of Technology
Kanpur, India.

ACKNOWLEDGEMENTS

This research has been carried out under the kind supervision of Professor Putcha Venkateswarlu, whose continuing encouragement and many valuable suggestions are gratefully acknowledged.

I am grateful to Dr. P.K. Kelkar, Director, Indian Institute of Technology, Kanpur, for his interest in the progress of this work.

Thanks are due to friends and colleagues, Dr. K.N. Shrivastava and M/s. V.N. Sarin, S.S. Dua, S. Mohanty, M.D. Sastry, B.V.R. Chowdary, J.P. Shrivastava and A.K. Bhargava for their encouragement and friendly cooperation. Thanks are also due to Mr. Surendra Kapoor and Mr. Ravi Kumar of computer center I.I.T. Kanpur for their valuable help in computations.

The work of machine shop under the supervision of Mr. J.S. Sharma, the glass blowing of Mr. R.A. Thakur and the typing of Mr. R. Singh are much appreciated.

Financial assistance from the Council of Scientific and Industrial Research, India in the form of a Junior Research Fellowship is gratefully acknowledged.

PREFACE

Optical absorption studies of Mn^{2+} in some crystals are described in this thesis. The crystals that have been studied are: $RbMnF_3$, $Mn(CH_3COO)_2 \cdot 4H_2O$ and Mn^{2+}-doped alkali halides. The spectra have been studied at room- and liquid nitrogen temperatures. The observed spectra are analyzed in the framework of crystal (or ligand) field theory. The band positions are fitted with four parameters, Racah's parameters B and C, cubic field parameter Dq and Trees correction parameter α. The fit obtained with the observed energies is fairly satisfactory. The parameters for room- and liquid nitrogen temperature spectra are evaluated separately. The increase in Dq value found in all the crystals on cooling is associated with the contraction in lattice size. Fine structure of the bands is analyzed by considering the spin-orbit interaction, the coupling of vibrations with the electronic states, and the lower symmetry crystalline fields. The spin-orbit splitting is calculated by diagonalizing the complete energy matrices involving the five parameters B, C, Dq, α and ξ (the spin-orbit coupling parameter) in the strong field scheme. The dimensions of the matrices are: Γ_6, 20 x 20; Γ_7, 22 x 22 and Γ_8, 42 x 42. In these calculations the matrix elements of Trees correction factor α in the strong field scheme are required and these have been calculated in the present work.

The thesis has six chapters and five appendices. Chapter I is a brief description of transition metal complexes and crystal field theory. The basic features of the theory of optical spectrum of Mn^{2+} used in the present work are developed in Chapter II.

Chapter III deals with the absorption spectrum of $RbMnF_3$. Intensities of the two sharp bands assigned to ($^4A_{1g}(G)$, $^4E_g(G)$) and $^4E_g(D)$ levels are found to be higher than those of the broad bands. This enhancement of the intensities of the sharp bands is compared with the similar observations of earlier workers. Measurements performed in the ultraviolet region reveal the presence of an abnormally intense broad band with f-value 6.6×10^{-6}. This band is assigned to $^4T_{2g}(F)$ level. Fine structure observed in $^4T_{2g}(D)$ band is attributed to the spin-orbit splitting and the analysis yields a value of $320cm^{-1}$ for the spin-orbit coupling parameter ζ. Vibrational structure of the bands is analyzed by finding the vibrational modes of perovskite structured $RbMnF_3$.

The absorption spectrum of $Mn(CH_3COO)_2 \cdot 4H_2O$ is discussed in Chapter IV. As the structure of this crystal is not known, tetragonal and rhombic perturbations are invoked for explaining the observed structure of the bands and it is concluded that the site symmetry of Mn^{2+} in the crystal should be very low, may be rhombic. It is found that in spite of site symmetry being much lower than cubic, the cubic field calculations give a

fairly good fit to the observed band positions.

In Chapter V, the absorption spectra of Mn^{2+}-doped alkali halides are described over a wide range of dopant concentration (0.1 to 10 mole per cent). The different types of Mn^{2+} centers in alkali halides at different concentrations are discussed in the light of observed spectra.

A comparative study of Mn^{2+} spectra in different ligand coordinations is presented in Chapter VI. Well defined spectrochemical and nephelauxetic series of ligands are found to exist for Mn^{2+}. A comparative study of the spectra of hydrated salts supports the view point that the oxygen of the acetic groups occupy the two opposite vertices of octahedron of ligands around Mn^{2+} in $Mn(CH_3COO)_2 \cdot 4H_2O$.

The group theoretical preliminaries are given in Appendix I. The cubic field energy matrices for the quartet levels of Mn^{2+} are in Appendix II. Matrix elements of Trees correction factor α in the strong field are tabulated in Appendix III along with the procedure for determining them. Appendix IV is a reproduction of paper entitled : Absorption Spectrum of Mn^{2+} in KCl: published by author and Venkateswarlu in the Journal of Chemical Physics 45, 3381 (1966) and supplements the study of Mn^{2+}-doped alkali halides given in Chapter V. Experimental details and computations are described in Appendix V.

References are numbered consequetively and placed at the end of the thesis. Figures and tables are given at their appropriate places.

Anjani Kumar Mehra

December, 1966

Physics Department
Indian Institute of Technology,
Kanpur.

CONTENTS

CHAPTER I

INTRODUCTION

CHAPTER I

INTRODUCTION

The elements in the third column of periodic table from titanium to zinc, constitute the first group of transition metals. The atomic 3d orbitals get successively filled with electrons as one passes along this group of elements. Two extreme classes of transition-metal compounds are conveniently distinguished-the metallic and nonmetallic. The former class includes the alloys, borides, carbides and the metals themselves. Typical members of the later class are inorganic complexes such as nickel sulphate and ferric chloride. From a theoretical standpoint the essential distinction between the two classes is that in the later the d-electrons may be assigned individually to particular metal atoms. Each metal atom (or ion) in a non-metallic compound has its own set of d-electrons localized near it, having little interaction with the sets belonging to neighbouring metal atoms. In a metallic compound the d-electrons are owned collectively by all the metal atoms and they can not be separated into nearly non-interacting sets.

The peculiar interest of the transition metals is generally agreed to be connected with their ability to form the non-metallic compounds in which the 3d electron configuration of the metal ion is only partially filled. It is the presence of incomplete d-electron shells which

is responsible in one way or another for the varied colours and also for the paramagnetism which many transition metal compounds (or complexes) display and with which we shall be concerned in the present work.

Divalent and trivalent transition metal ions have the electronic structure $1s^2\ 2s^2\ 2p^6\ 3s^2\ 3p^6\ 3d^n$. First 18 electrons form a closed argon shell while the outer n electrons fill the 3d orbit partially. The absorption spectra of complexes of these ions in infrared and visible regions generally consist of a number of weak bands which are recognized with the parity forbidden intersystem transitions within the d^n configurations of the metal ion[1]. In order to explain these spectra and also the other properties of transition metal complexes it is necessary to find out how the electronic energy levels of the central metal ion are affected by the presence of surrounding groups called ligands placed around the ion in some definite pattern. In an isolated ion all the five d orbitals have same energy but when it is perturbed due to the surrounding ligands, the degeneracy may get partially or completely removed. If the perturbation can be represented by an electrostatic field we can speak of this as electrostatic splitting. Such situations arise particularly in ionic crystals or complexes. It was in connection with this that Bethe[2] first studied the splitting of energy levels of ions in crystals of different symmetries. For this reason it is frequently referred to as crystal field splitting and the underlying theory, which has been very successful in explaining the properties of transition

metal complexes, as crystal field theory.

The theory concerns itself with the behaviour of rare-earth and transition metal ions in crystal, their salts, solutions and complexes. The original theory as given by Bethe[2] treats the metal ions as if they were subjected to electrostatic fields of force arising from the ions or groups by which they are surrounded. Thus the anions, the water of crystallization or of solvation and the other ligands with which they are most intimately associated are originally assigned to some extent rather passive roles. These may be polarized by the presence of the cation they stabilize, but the motions of their electrons are assumed to remain unaffected by such factors as the optical excitation of the cation. The ligands are supposed to provide a potential field for the central ion which is the same for its ground state as for its lower excited states. In other words, the theory completely neglects the covalent bonding. Later developments of the subject showed a need for more active participation of ligands in the bonding. Quite apart from the more indirect evidences such as the impossibility of fitting certain magnetic experimental data[3] and absorption band intensities[4] without the use of molecular orbital scheme, a very direct proof for the presence of covalency in certain complexes and ionic crystals has come up with the observation of super-hyperfine structure by a number of workers in electron paramagnetic resonance, for instance, the super-hyperfine structure (the extra hyperfine structure)

of Mn^{2+}, Fe^{2+} and Co^{2+} in the fluoride crystals[5] and, more recently, of Cu^{2+} in NH_4Br observed[6] in our laboratory. These experiments give a clear proof that the metal electrons move in a molecular orbital extending over the entire complex or the neighboring ions. The Bethe's crystal field theory with the necessary extension to incorporate the effects of the finite extension of ligand orbitals and the overlap of the metal ion and ligand orbitals has been termed as ligand field theory.[1] Nearly all the results of Bethe's simple crystal field theory are valid in the ligand field theory as the later theory is more general in its approach. However, as the things stand now in such a developed subject, this simple difference of nomenclature should not put any restrictions on the ideas to be presented and in the spirit of this, we shall use both the names, crystal field theory and ligand field theory, to mean the theory that arises out of the hybridization of original crystal field theory of Bethe and molecular orbital theory of Mulliken.

Nearly 30 years have passed since Van Vleck[7,8] demonstrated the effectiveness of crystal field approach in the discussion of optical and magnetic properties of transition metal complexes. In the past decade the theory has seen a rapid development and a large amount of experimental data on these complexes has been successfully analyzed.[1] It has been also successful in explaining the spectra of transition metal ion and rare-earth ion

doped crystals[9] of different symmetries. The possible application of the crystals doped with transition metals and rare earths as solid state laser devices[10] has added much interest to these studies in the recent years. The famous ruby laser, Cr^{3+} doped Al_2O_3, is one such example.

The absorption spectrum of Mn^{2+} in certain crystal systems has been investigated in the present work. The d^5 configuration of Mn^{2+} is unique among the d^n configurations in the sense that all the transitions in its absorption spectrum are spin forbidden, besides being parity forbidden which is common to all transition metal spectra. This fact is reflected in the low extinction coefficients observed for the Mn^{2+} spectra.[11-13] Because of the weak intensities of the observed spectra, pure manganous compounds[14,15] have been mostly studied in the previous years and very little amount of work has been done on Mn^{2+} -doped crystals as very high concentrations of the dopant are required for observing the absorption spectrum.[16] In the present work the alkali halide crystals were grown from melt with sufficient quantity of Mn^{2+} as added impurity and the absorption spectra of these crystals have been studied. Mn^{2+}-doped alkali halides are long known to have fluoroscent properties[17] and it is hoped that the present study might help in understanding the nature of these fluoroscent centers.

Some of the bands in the Mn^{2+} spectrum show well

developed fine structure at low temperature. It is felt that a study of such structure might throw some light on the spin-orbit interaction in Mn^{2+} in crystals. The study of $RbMnF_3$ whose cubic structure makes such an analysis simpler, was undertaken with this purpose in mind. The results obtained are discussed in Chapter III.

In addition to these, the absorption spectrum of a pure crystal of $Mn(CH_3COO)_2.4H_2O$ has also been investigated. It is relatively a new compound whose properties have been of interest in the recent years.[18] Its crystal structure is not known in detail as yet and information about the coordination of Mn^{2+} in the crystal has been obtained from the observed spectrum.

Finally, a comparative study of Mn^{2+} in crystals having different ligands e.g. F^-, H_2O, Cl^- and Br^- has been made and well defined spectrochemical and nephelauxetic series[1] of ligands are found to exist.

....

This Chapter is based on the following books and review articles:

a. C.J. Ballhausen: "Introduction to Ligand Field Theory", McGraw-Hill Book Company, Inc.,N.Y.,1962.

b. D.S. McClure: Solid State Physics, Vol.9, Academic Press, Inc., New York, 1959.

c. J.S. Griffith, The Theory of Transition Metal Atoms, Cambridge University Press, 1960.

d. Leslie E. Orgel: An Introduction to Transition Metal Chemistry, John Wiley and Sons, Inc., New York, 1960.

e. W. Moffit and C.J. Ballhausen: Ann. Rev. Phys. Chem. 7, 107 (1956).

f. C.K. Jorgensen: Absorption Spectra and Chemical Bonding in Complexes, Pergamon Press, Inc., New York, 1962.

g. H. Bethe: Ann. Physik,[5], 3, 133 (1929).

...

CHAPTER II

THEORY OF THE OPTICAL SPECTRUM OF Mn^{2+} ION

CHAPTER II

THEORY OF THE OPTICAL SPECTRUM OF Mn^{2+} ION

The basic features of crystal field theory, as applied to Mn^{2+} in particular, will be briefly discussed in this Chapter. The topics that will be discussed are the calculation of energy levels in free ion and in cubic crystalline field, spin-orbit interaction, intensities and widths of the absorption bands and the effect of temperature on them, spectrochemical and nephelauxetic series of ligands and the lower symmetry crystalline fields. The general features of the observed Mn^{2+} spectra and the assignments of the bands to the cubic field levels will also be presented.

The manganese ion Mn^{2+} has the electronic structure $1s^2\ 2s^2\ 2p^6\ 3s^2\ 3p^6\ 3d^5$. The first 18 electrons form a closed argon shell. The last five electrons fill the d-orbitals partially and transitions may be possible among the different states arising from d^5 configuration. The present work deals with the optical spectra arising from such transitions. In the case of absorption spectrum the transitions take place from the ground state to the excited levels of d^5 configuration.

Free Mn^{2+} Ion:

The d^5 configuration of free Mn^{2+} ion gives rise to one sextet, four quartets and eleven doublets. In

confirmity with the Hunds rule, its ground state is ^6S. Since there are no other sextet levels present in the d^5 configuration, all the transitions in the observed absorption spectrum of Mn^{2+} violate the selection rule $\triangle S = 0$. Transitions from ground state to excited quartet levels have been observed and their experimental energies[19] are given in Table 2.1. Transitions to the doublet levels have not been observed because of their very low intensities ($\triangle S = 2$).

The quantitative calculations of energy levels of free transition metal ions have been thoroughly reviewed by Slater.[20] The prominent interactions in the free ion are the electrostatic repulsion between the electrons and the spin-orbit coupling. The electrostatic interaction term gives rise to difference in energies of different multiplet terms whereas the spin-orbit coupling which is found to be much smaller than the electrostatic interaction, splits each of these multiplet levels into the levels characterized by total J value. The spin-orbit splittings are particularly small in Mn^{2+} because of its being a half filled shell and therefore, can be neglected in comparison to the electrostatic energies of the levels (first order spin-orbit interaction will be zero in Mn^{2+}). The electrostatic energies of the levels can be expressed in terms of interelectronic repulsion integrals designated F^2 and F^4. More frequently F_2 and F_4 orB and C are used and these are given by the

Table 2.1

The observed and calculated energies of the quartet levels in free Mn^{2+} ion. The calculated energies before and after the inclusion of α are in columns 4 and 5 respectively.

Term	Theoretical energy	Observed energy(cm^{-1})	Calculated energy (cm^{-1}) B=950 C=3275 α=0	B=915 C=3235 α=76
^4G	10B+5C+20α	26,850	25,875	26,845
^4P	7B+7C+2α	29,200	29,575	29,202
^4D	17B+5C+6α	32,340	32,550	32,186
^4F	22B+7C+12α	43,620	43,860	43,687
^2I	11B+8C+42α	---	36,650	39,137

following relations:

$F_2=F^2/49$, $F_4=F^4/441$, $B=F_2-5F_4$ and $C=35F_4$.

We shall use the parameters B and C. The electrostatic energies of all the levels have been found by Racah[21] in terms of B and C.

The ratio F^4/F^2 has got some theoretical significance and has been discussed by Slater[20] and Watson[22]. This ratio, based on Watson's calculation on transition metal ions, has a value slightly below 0.649 (hydrogenic wave function ratio). It serves as a measure of the departure of true d-electron wave functions from a hydrogenic function. The analogous hydrogenic wave function ratio for C/B is nearly 3.96.

Trees[23] has shown that the agreement of the calculated values with the observed energies in iron group spectra can be very much improved if a term equal to $\alpha L(L+1)$ is added to the theoretical electrostatic energies. The significance of this correction term has been discussed by Racah.[24] This type of the refinement of the theory is called the polarisation effect. We shall show that the inclusion of this correction term causes a marked improvement in the agreement for Mn^{2+} also.

The theoretical energies in terms of B,C and α are given in Table 2.1 for all the quartet levels and also for the lowest doublet level ^2I.

Griffith[25] has discussed the fitting of the free ion energy levels by means of empirical parameters. The selection of suitable values of parameters is made on the basis of the fit obtained with the observed energy levels. An arbitrary basis of best fit such as least-squares analysis has been criticized in the recent years and it has been suggested that a more critical procedure which takes into account the possible departures from the theory should be adopted.[26] However, as our aim is just to show the fruitfulness of including the α correction, we shall find the suitable values of parameters from least-squares fitting.

The fits obtained with and without including the α term are given in Table 2.1. Values of parameters determined in the two cases respectively are:

B=915, C=3235 and α=76cm^{-1}; B=950 and C=3275cm^{-1}. The mean deviations with and without α term are 540 and 84cm^{-1} respectively. The marked improvement in the agreement with the observed energies on including α shows the importance of α term in Mn^{2+}.

The splittings due to spin-orbit interaction are of second order in half filled shells like Mn^{2+}. However, a greater significance to spin-orbit interaction in Mn^{2+} is imparted by the spin forbidden nature of the transitions. The spin forbidden transitions can only be observed if there is a mixing of levels having different multiplicities. The spin-orbit interaction between the

levels is the cause of such a mixing.

It is not possible to obtain significant experimental value of spin-orbit coupling parameter ξ by a least-squares fit to the Mn^{2+} spectrum, because the small second order spin-orbit splitting coming from d^5 wave functions only is no larger than the first order spin-orbit contributions coming from non-half-filled configurations mixed into the d^5 states by the electrostatic electron-electron interaction. Shadmi[27] has shown however, using a least squares fit over the spectra of the doubly ionized iron series elements, that the interpolated ξ value for Mn^{2+} is $\sim 300cm^{-1}$. The theoretical calculations using Watson's wave functions for the free ion ground state of Mn^{2+} give a slightly higher ξ value of $376cm^{-1}$.[28] It is not possible to decide between the two values at present.

Mn^{2+} in Cubic Symmetry:

In crystal field theory the central metal ion in a complex is supposed to be subjected to an electric field originating from the surrounding ligands. Such a crystalline field reduces the spherical symmetry of the free ion and a splitting of the energy levels of the ion takes place. A quantitative treatment for such a model can be easily formulated. The Hamiltonian for the electrons of the metal ion consists of two terms:

$$H = H_F + V$$

H_F is the Hamiltonian for the free ion which has been discussed in the last section and V is the potential provided by the ligands. However, when we are going to perturb the eigenvalues of H_F for the free ion with V, it is very important to know that how V compares with electrostatic and spin-orbit interactions constituting H_F. It is found in transition metals that V and electrostatic interaction are of the same order of magnitude and spin-orbit interaction is much smaller than them. Consequently, one can first consider the electrostatic and crystal field interactions, and can later perturb them by spin-orbit interaction. The splitting of each multiplet levels of the ion in the crystalline field is first determined and the spin orbit interaction is added, if required, for understanding the fine structure of these Stark levels. The general theory has been discussed in quite a length in several text books[1,9,25] and in the following sections we shall discuss only the basic features.

The qualitative splittings of the atomic levels can be easily found out by the methods of group theory. Appendix I gives the representations of the O_h group. The reductions of atomic states into the irreducible representations of the O_h group are also given there.

The form of octahedral potential V can be determined from the requirement that it must remain invariant under all the operations of the O_h group. The form of V for

d electrons in an O_h symmetry is:[9]

$$V = D(x^4 + y^4 + z^4 - \frac{3}{5} r^4)$$

in which $D = 35e_i/4R^5$, e_i is the charge on each ligand and R is the metal-ligand distance. The form of the basis functions to be used in finding the matrix elements can also be determined from the symmetry requirements. For a single d-electron the orbitals have symmetry t_{2g} and e_g.

While finding the matrix elements of V one comes across integrals involving radial functions which are not known a priori, and these integrals are replaced by empirical parameters. The separation between t_{2g} and e_g is 10Dq (Fig. 2.1), q is found to be $2e\langle r^4\rangle/105$ so that in this simple model $Dq=ee_i\langle r^4\rangle/6R^5$, where e is the electron charge.

Fig. 2.1

Splitting of the d-orbitals in an octahedral field

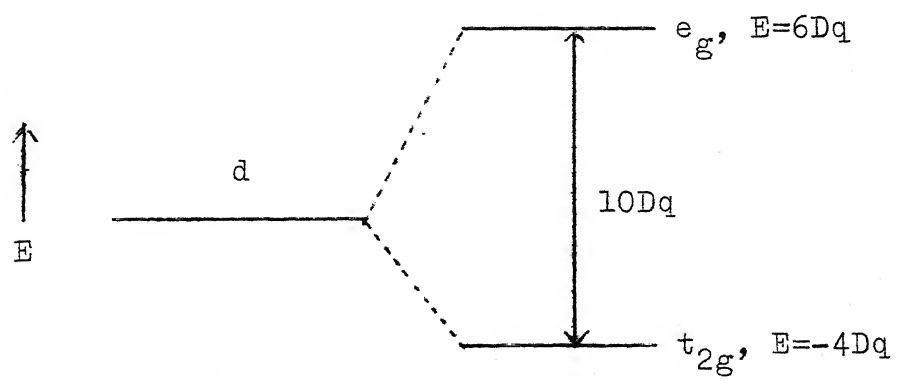

In the case of Mn^{2+} one has to consider the total Hamiltonian and the wave functions arising out of all the five d-electrons. For calculating the matrix elements of the Hamiltonian two extreme representations, according to the choice of basic orbitals, are in practice. One is called weak field scheme and the another as strong field scheme. Basic orbitals used in the weak field scheme are the five d-orbitals characterized by their m_l values. The electrostatic term is diagonal in this scheme and V is non-diagonal. Weak field matrices for Mn^{2+} in cubic symmetry have been calculated by Orgel.[29]

The basic orbitals used in the strong field scheme are t_{2g} and e_g. The advantage of this scheme of calculation is that the chosen orbitals transform according to the O_h group. V is therefore diagonal in this scheme but the electrostatic term is non-diagonal. Tanabe and Sugano[30] have calculated the strong field matrices for all the d^n configurations in cubic field.

These two representations are connected by unitary transformation and the results of calculations in both of them should be same if one diagonalizes the energy matrices.[31] However, if one uses the perturbation approach, which is, of course, not valid in our case, one has to be cautious in choosing the suitable scheme. In our calculations we have always diagonalized the matrices and it makes little difference whether one uses the weak field or strong field scheme.

These matrices involve three parameters B,C (coming from electrostatic term) and Dq (coming from crystal potential). Because of the deformation of the free ion orbitals, the free ion values of B and C are not expected to hold in the crystals. These two and also Dq are treated as adjustable parameters in the theory. What one usually does is that one varies the three until a reasonably good fit with the experimental energies is obtained. The calculations of this type for Mn^{2+} have been done by Heidt, Koster and Johnson.[13]

It has been observed[13,14] that a unique set of B, C and Dq does not give very good agreement with all the observed transition energies of Mn^{2+}. We observed that, similar to the case of free ion, the inclusion of Trees correction term α causes a marked improvement in this agreement and hence the parameter α has also been included in the calculation. To reduce the number of adjustable parameters the value of α has always been fixed at the free ion value of $76cm^{-1}$. In fact, its value may be slightly different in different cases but since the correction term introduced by it is relatively small, a change in the value of α causes only a very little change on the values of other parameters and energies and therefore it may be conveniently fixed at some value , most suitable being the free ion one. The inclusion of this correction term causes an addition of $\alpha L (L+1)$ term to the diagonal

elements in the weak field matrices. The correction term is non-diagonal in strong field scheme.

Only the transitions from the ground state to higher quartet levels are expected to have appreciable intensities and therefore the observed bands are assigned to the quartet levels. The energy matrices of all the quartet levels are given in Appendix II. These contain four parameters B, C, Dq and α. The matrices are given in the strong field scheme since the use of such a scheme is found to be more convenient for reasons discussed in the next section. The eigenvalues of these matrices obtained on varying only Dq give the energy level diagram for d^5 configuration for chosen values of fixed parameters B,C and α. A typical energy level diagram of Mn^{2+} is shown in Fig. 2.2 which has been plotted for free ion values of B,C and α.

Spin-Orbit Coupling:

The need for including the spin-orbit interaction for Mn^{2+} in crystals arises due to the following reasons: firstly, for explaining the mechanism of transitions all of which are spin forbidden, secondly, for understanding the fine structure of the bands observed in low temperature spectra, and lastly, for explaining the splitting of spherically symmetric ground state by crystalline fields observed in paramagnetic resonance experiments.[28] One of the prominent reasons suggested for the anomalous splitting of an S state by crystalline fields is the

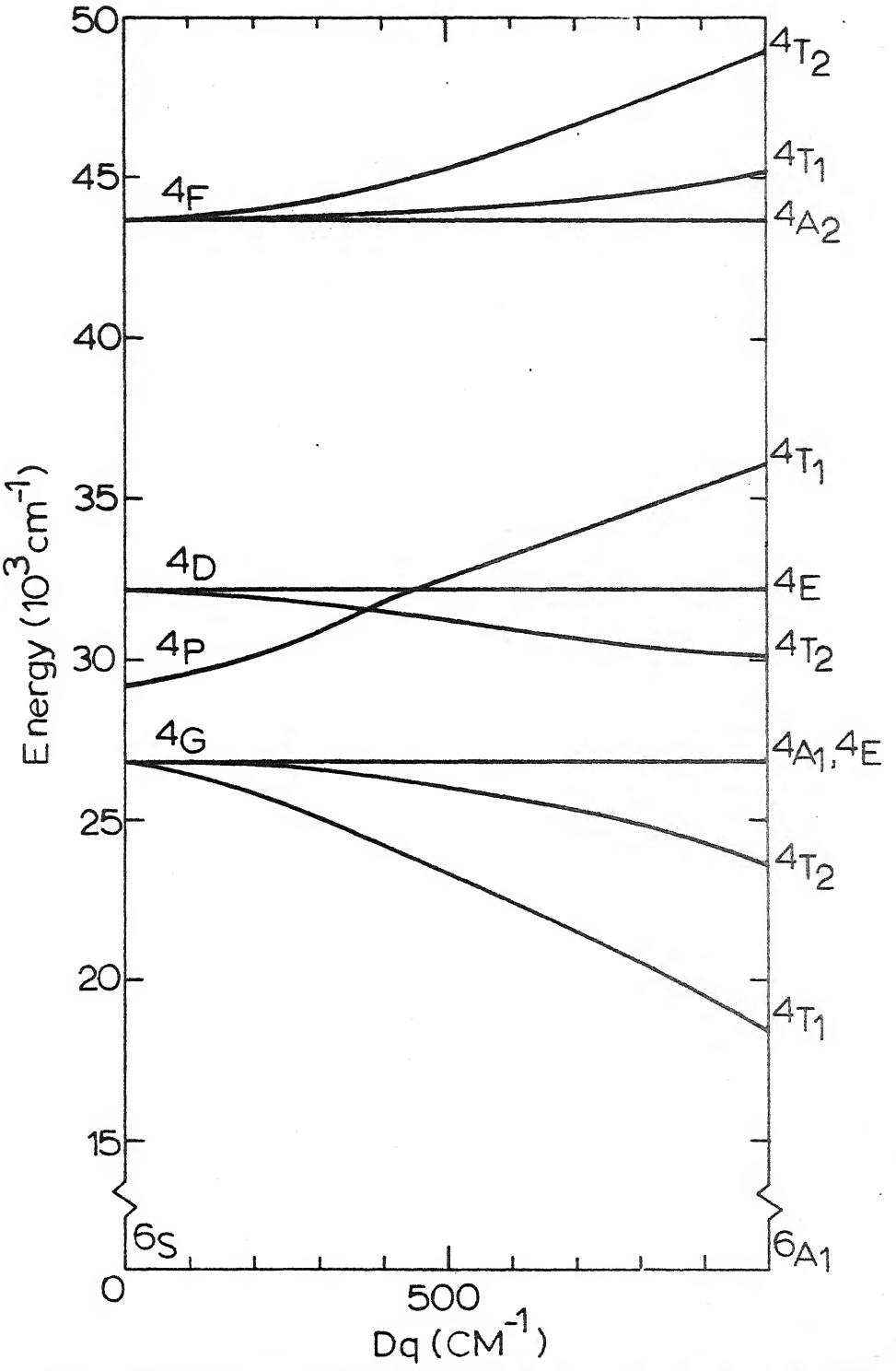

Fig. 2.2 Energy level diagram for Mn^{2+} in octahedral symmetry for free ion values of the parameters B, C α which are 915, 3270 and 76 cm^{-1} respectively.

mixing of non-spherically symmetric excited states in the ground state via the spin-orbit interaction.

The d^5 configuration has ~~got~~ an odd number of electrons so that all the levels in a crystalline field should be atleast doubly degenerate according to Kramers theorem. One uses in this case octahedral double group representations (Appendix I). Bethe's notation is used here for the states obtained after including the spin-orbit interaction while Mulliken's notation is used for the states existing before including spin-orbit interaction. Thus we shall use Bethe's notation for double group representations and Mulliken's notation for normal O_h group representations. The correlation between the two notations is given in Appendix I.

The spin-orbit states arising out of any level can be easily determined by reducing the direct product of the spin and orbital parts of the level into the irreducible representations of the double group. The spin part for quartet levels has Γ_8 symmetry. The reductions of the direct product of Γ_8 and orbital parts of quartet levels are given in Appendix I. The total number of states coming out of the complete d^5 configuration are: 20 of Γ_6, 22 of Γ_7 and 42 of Γ_8 symmetry. The dimensions of energy matrices obtained on including the spin-orbit interaction are also same. The matrix elements of spin-orbit interaction in the strong field scheme have been published by Schroeder.[32]

The first order splitting of the levels may be conveniently obtained from Landé's formula using a fictitious L value.[9] For example a $^4T_2$ state ($L' = 1$, $S = 3/2$) splits into three levels having energies:

$E=3a$(six fold $\Gamma_7+\Gamma_8'$), $-2a$(four fold Γ_8) and $-5a$(two fold Γ_6)

where a is a proportionality constant which depends on the constitution of the level.

From the exact spin-orbit calculations Goode[33] has found that though the order of levels is preserved, the exact splittings differ from the first order ones. Therefore, the diagonalization of the matrices, rather than the perturbation approach, becomes necessary if one wants to correlate the observed splittings with the calculated ones. Goode[33] has done the spin-orbit calculations in the strong field scheme considering four parameters B, C, Dq and ζ. Our calculations differ from those of Goode in the sense that we include the additional factor α in our calculations.

Recently, Low and Rosengarten[34] have also performed the spin-orbit calculations for Mn^{2+} but in the weak field scheme. They however, have not published the spin-orbit and crystal field matrices used by them in the weak field scheme. Although α can be more easily incorporated into the weak field scheme by adding a term $\alpha L(L+1)$ to the diagonal elements, the unavailability of spin-orbit and complete crystal field matrices which include doublet levels, makes the use of weak field

scheme less attractive. The calculation of spin-orbit and crystal field matrices is quite involved and therefore, it was found convenient to find the matrix elements of α in the strong field scheme where both spin orbit[32] and crystal field matrices[30] are available. The strong field matrices of α term and the method by which these have been found are given in Appendix III.

The complete energy matrices of the d^5 configuration in terms of the five parameters B,C,Dq, α and ξ can be obtained by adding these α matrices to the known spin-orbit and crystal field matrices. When this is done, three large matrices, F_6 of dimension 20 x 20, F_7 of dimension 22 x 22, and F_8 of dimension 42 x 42 are obtained. The eigenvalues of these matrices were obtained by diagonalizing them on an IBM 7044 computer. As usual an iterative method was employed in finding the eigenvalues and it was observed that the method gives eigenvalues correct upto 6th place.

Since the matrices are quite large, these were thoroughly checked by several means. Firstly, the separate diagonalizations of B,C,Dq, α and ξ parts of these matrices were carried out to check the numerical coefficients in the matrices. The relative signs of different terms were then checked by taking several combinations of the parameters. Finally, a comparison with calculated energies of Goode[33] was made by using his values of the parameters. The calculated energies

were found to be in agreement with those of Goode[33].

The detailed results of these spin-orbit calculations will be given in the later chapters along with the observed fine structure of the bands.

Transitions to the Doublet Levels:

The problem of transitions to doublet levels has been discussed in detail by Goode[33] and our results do not appreciably differ from his. In short, we found that by considering only the spin orbit mixing of the different multiplicity terms, the intensities of transitions to most of the doublet levels should be more than thousand times smaller than the intensities of transitions to quartet levels. In the case of the doublet levels which lie quite close to the quartet levels these calculations become quite uncertain but nevertheless even in these cases the intensities are expected to be 100 times smaller.

Band Widths:

It was first pointed out by Orgel[35] that the band widths in the Mn^{2+} spectrum are proportional to $dE/d(Dq)$ where E is the energy of the transition. The basic reason for such a behaviour has been successfully explained with the help of Franck-Condon principle. It is now clear that the transitions to levels having large slope in the energy level diagram give rise to broad bands while the transitions to levels having lesser slope give rise to sharp bands. In general, the transitions to

levels having same configuration as the ground state are expected to be sharper.

Intensities of Transitions:

Electric dipole transitions in Mn^{2+} are spin and parity forbidden. The relaxing of spin selection rule is explained with the help of the spin-orbit interaction. The parity forbidden nature of the electric dipole transitions is common to all the transition metal ions and explains the low intensities of the observed spectra of these ions. This prohibition is removed by mixing the orbitals having odd parity with even parity d-orbitals. Such mixing may be induced by (a) absence of a center of symmetry of the crystal field (hemihedral field) (b) destruction of center of symmetry by vibrations in the case of crystal field having center of symmetry (holohedral field).[36]

For Mn^{2+} in cubic symmetry, it is necessary to consider vibrational-electronic and spin orbit interactions simultaneously, to account for the violation of both the selection rules. This explains the very low intensities of the Mn^{2+} spectra. Koide and Pryce[37], and Englman[38] have made detailed calculations of these induced intensities for Mn^{2+} in cubic fields.

Other type of transitions which can occur are of magnetic dipole and electric quadrupole type. The former type of transitions have been observed[39] in the case of some of the transition metal ions but not the

later type. The nature of transitions can be determined by using polarized light.[9] The intensities of the above two types of transitions are expected to be smaller than those of the electric dipole transitions.

Effect of Temperature:

Because of the freezing of the lattice vibrations the widths and intensities of the observed bands decrease on going to low temperatures. It is therefore natural to relate the temperature dependence of these with the vibrational frequencies of the crystal and obtain some information about the vibrational modes of the crystal.

Homes and McClure[12] fit the temperature dependence of the oscillator strength (f) of a particular band using the formula

$$f = f_0(1+\exp(-\omega/kT))$$

where f_0 is a constant equal to the f-value at $T=0^\circ K$ and ω is the energy of an antisymmetric vibration. The present studies have been made at room temperature ($\sim 300^\circ K$) and also at liquid nitrogen temperature ($\sim 80^\circ K$). From above expression the ratio of f-values at these two temperatures can be written as

$$\frac{f_{80^\circ}}{f_{300^\circ}} = \frac{1+e^{-\omega/201}}{1+e^{-\omega/53.6}}$$

where ω is to be expressed now in cm^{-1}.

No satisfactory theory for the temperature dependence of the band widths has been given as yet. Finlayson et.al.[16] fit the temperature dependence of the widths of the absorption bands of MnF_2 using the following expression found by Klick and Schulman[40] from their studies on the widths of fluorescence emission bands of Mn^{2+}:

$$\mu \text{ (band width)} \alpha \ (h\omega_g/2k) \coth(h\omega_g/2kT)$$

where ω_g is the ground state vibrational frequency in sec^{-1}. Its applicability to the absorption bands may be questioned, but in the absence of any other satisfactory formulation we shall also use the above expression. Extending the expression to a general vibrational frequency in cm^{-1}, the ratio of band widths at 80^oK and 300^oK comes out as

$$\mu_{80^oK}/\ \mu_{300^oK} = \coth(\omega/402)/\coth(\omega/107.2)$$

Lower Symmetry Fields:

A crystalline field of symmetry lower than cubic can be thought of as a sum of cubic field and a lower symmetry field. Accordingly, one may first approximate the problem to the cubic case to simplify the analysis, and then add the lower symmetry field as a perturbation over the cubic field. It is encouraging to find that this scheme works in most of the cases and even in those cases where the actual site symmetry of the metal ion is known to be much lower than cubic. The band positions

in the observed spectra are very well explained by the cubic approximation and it is only for explaining the finer details that one has to bring in the lower symmetry fields.

The qualitative splittings of the cubic field levels by the lower symmetry perturbations can be determined from the group theory. The number of levels in which a cubic field level splits depends on the point group of the lower symmetry under consideration. The quantitative splittings can be determined by adding the appropriate lower symmetry crystal field potential to the Hamiltonian. Goode[33] has recently done extensive calculations on Mn^{2+} in tetragonal field .

Spectrochemical Series:

It has been found empirically that many of the more frequent ligands can be arranged in a series such that Dq increases as we pass along this series. The precise values of Dq depend, of course, on the choice of central metal atom, but the spectrochemical series, as it is called,[41] is almost independent of this choice. The series in the order of increasing Dq is

I^-, Br^-, Cl^-, F^-, C_2H_5OH, H_2O, NH_3, CN^-.

For the same metal ion the Dq value increases if one replaces the ligand by the one which is higher in this series. The crystal field in cynide of Mn^{2+} is so high that the complex is of low spin t_2^5 configuration.

This series has been found to be valid for several transition metal ions and its validity for Mn^{2+} is confirmed in the present work.

Other features regarding Dq that are observed are:

1. Dq is virtually independent of the ligands (or ions) which are not directly attached to the metal ion.
2. Dq depends largely on the nearest neighbours.

Nephelauxetic Series:

It is nearly always found that in order to fit the absorption bands of the complex ions to theoretical level schemes, one needs to deminish the parameters B and C from the values obtained from the spectra of free ions. This corresponds to a reduction of the term separations that are obtained by extrapolating the crystal field strength to zero. The question that arises is whether it is possible to arrange the ligands in a series which is based upon their power of deminishing the term separations of the metal ion? Investigations show that such a series can indeed be constructed and one gets the following series[42] of the ligands in the order of increasing power of deminishing the term separations in the metal ion.

$$F^-,\ H_2O,\ NH_3,\ Cl^-,\ Br^-.$$

The applicability of this series to Mn^{2+} is explored in the present work.

The interest in this series arises due to its closeness to the one which a chemist working with complexity constants would device in order to illustrate the increasing power of ligands for complexing.

Observed Mn^{2+} Spectra and Fitting of Parameters:

A typical Mn^{2+} spectrum in the visible region looks like Figures 3.2, 4.1 and 5.3 given in the later chapters. Leaving aside the shifts along the energy scale and the relative intensities of the bands, the overall features of the spectra in different crystals are found to be very much similar. The two sharp peaks around 4100A° and 3400A° regions observed in all the cases are characteristic of Mn^{2+}.

Assignments of the observed bands to the cubic field levels are now well established. These are discussed here and will not be treated in detail in later chapters. The fine structure of the cubic field levels will be taken up in the later chapters.

The bands are assigned to transitions from the ground state $^6A_{1g}(S)$ to excited quartet levels (p.17). The first two levels on the lower energy side of the energy level diagram have a large slope and correspondingly the first two bands in the spectra are found to be quite broad. In accordance with the energy level diagram, the lower energy band is assigned to $^4T_{1g}(G)$ level and the higher energy band to $^4T_{2g}(G)$ level. These bands

are respectively named as A and B in the present work. The next two levels $^4A_{1g}(G)$ and $^4E_g(G)$ are degenerate in a cubic field and have zero slope. The accidental degeneracy of these levels can be removed by considering additional factors like covalency effects and lower symmetry fields but the levels are still expected to lie quite close to one another. The next absorption band named C consists of a sharp peak accompanied by a shoulder. It has been suggested that these two could be due to the transitions to the two closely spaced levels. The sharpness of the band is in confirmity with the vanishing slope of the levels. However, in spite of the extensive studies[14,43,44] on this sharp band, a unique order of the two levels has not yet been established and it is not possible to assign the peak and shoulder individually to the two levels. Koide and Pryce[37] considered the differential deformation of t_{2g} and e_g orbitals due to the covalency of the crystal as responsible for the removal of the degeneracy. This simple model suggested that $^4A_{1g}(G)$ could be $\sim 100 cm^{-1}$ below $^4E_g(G)$.

There should be one more sharp band corresponding to $^4E_g(D)$ level which again has a vanishing slope and accordingly other sharp band, named E, is assigned to this level. There is a band, denoted by D, in between the two sharp bands and according to the energy level

diagram this is assigned to $^4T_{2g}(D)$ level which always lies in between the two sharp levels. The broad band found on the higher energy side is assigned to $^4T_{1g}(P)$ level. This band is named F in the present work.

The next group of three levels arising from the ^4F level of the free ion lies in the ultraviolet region. Because of the high background absorption of the crystals in the ultraviolet region the bands corresponding to these three levels are not observed with that clarity as the visible region bands and the exact nature of these bands is not very clear. What one expects according to the energy level diagram is a sharp band corresponding to $^4A_{2g}(F)$ level followed by two broad bands on higher energy side corresponding to $^4T_{1g}(F)$ and $^4T_{2g}(F)$ levels. These bands are termed as G, H and I respectively.

A very clear cut example of the reduction of free ion term separations in crystals is provided by the two sharp bands C and E. The lower energy sharp band C arising from ($^4A_{1g}(G)$, $^4E_g(G)$) levels should have an energy equal to that of the ^4G level of the free ion ($26850cm^{-1}$). However, it is found that the band lies at energies lower than this, for example, in fluorides[14] it lies around $25000cm^{-1}$ which means that the equivalent $^6S - {}^4G$ separation in the fluorides is reduced to about $25000cm^{-1}$. Same applies to $^4E_g(D)$ band which should have an energy equal to that of the ^4D level of the free ion

but is found to have lower energies. In terms of parameters this means a reduction in parameters B and C from the free ion values. The positions of these bands vary from crystal to crystal and same set of parameters B and C can not hold in all the crystals. Since we intend to do a comparative study of different crystal systems it is necessary that a systematic procedure is followed in finding the values of the parameters. The procedure adopted in the present work is as follows. The parameter α is always fixed at the free ion value of $76cm^{-1}$. The energies of $^4A_{1g}(G)$ and $^4E_g(D)$ levels are independent of Dq and as α has already been fixed they are functions of only parameters B and C. The values of parameters B and C which give a close fit to the observed energies of these two levels are first calculated. Since the positions of the two sharp bands can be found out quite accurately this ensures a reasonably accurate value for B and C, atleast for a comparative study. After this, a preliminary Dq value is obtained by fitting the observed energy of $^4T_{1g}(G)$ level which has the largest slope in the energy level diagram and for which a change in Dq value affects the calculated energy most. The energies of all the levels are then calculated using this initial set of parameters and compared with the observed energies. It has been found that this initial set of parameters gives a reasonably good agreement to most of the levels. However, if necessary, these

initial values could be slightly varied so as to give a good fit to all the possible levels. It is interesting to find that there are in all nine observed energies to be fitted with only three parameters but the agreement between the calculated and observed energies is found to be fairly satisfactory.

CHAPTER III

ABSORPTION SPECTRUM OF $RbMnF_3$

CHAPTER III

ABSORPTION SPECTRUM OF $RbMnF_3$

INTRODUCTION

Perovskite fluorides of the form ABF_3 in which B is a divalent transition metal ion, have been of considerable interest in the recent years. These crystals generally display antiferromagnetism below the Neel temperature and evidences of magnetic exchange interactions have been found in their optical spectra.[45] Theoretical studies[46] of these crystals have yielded valuable informations about the role of covalency in the so called ionic crystals.

Among the perovskite fluorides of Mn, $RbMnF_3$ has received particular attention as its cubic structure which does not distort below the Neel temperature,[47] provides unusual opportunities for experimental and theoretical investigations. Its absorption spectrum is reported in the present work. Recently, Ferguson, Guggenheim and Tanabe[48] studied the fine structure of the two sharp bands C and E of Mn^{2+} in fluoride crystals including $RbMnF_3$, for the purpose of finding the effects of magnetic exchange interaction in them. Stevenson[49] has also measured the spectra of several manganese fluorides. Our studies on $RbMnF_3$ are more extensive and attempts have been made for analyzing most of the

interesting features observed in the absorption spectrum. In addition to fitting the observed band energies to theoretical cubic field levels, fine structure of the bands has been examined in the light of spin-orbit and vibrational-electronic interactions.

The Neel temperature T_N of $RbMnF_3$ was originally estimated[47] as 54.5°K but recently Moruzzi and Teaney[50] have found from specific heat measurements that T_N should be 82±1°K. The higher T_N value is in line with the observation of anisotropy in susceptibility at 66°K and neutron diffraction peaks at 77°K.[50]

CRYSTAL STRUCTURE

Perovskite structure of $RbMnF_3$ is shown in Fig. 3.1. Mn^{2+} is located at the body centered position of the cubic cell while six F^- ions located at the face centered positions form a regular octahedron around Mn^{2+}. Rubidium ions are found at the corners. The edge of the cell[51] is 4.2396±.0002A° and this determines all the distances in the crystal. Same structure is retained below the Neel temperature.

EXPERIMENTAL

$RbMnF_3$ crystal was obtained from the Semi-elements, Inc., Saxonberg, Pennsylvania, U.S.A. The original piece was irregular in shape and a fairly uniform crystal was cleeved out of this for the present work. It was found by taking an X-ray Laue pattern

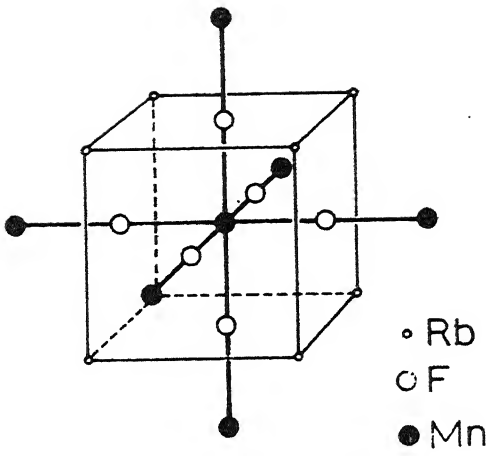

Fig. 3.1 Crystal structure of cubic perovskite $RbMnF_3$.

that the cleavage plane of the crystal is a {100} plane. The thickness of this specimen was found to be 0.121cm. Absorption spectrum was measured with a Cary 14 spectrophotometer at room temperature and also at liquid nitrogen temperature.

The recorded absorbances were converted to molar extinction coefficients ε using the relation $\varepsilon = (M/1000D\,t) \times$ Absorbance. M is the molecular weight of the crystal (197.5) and t is the thickness of the specimen used. Density D of $RbMnF_3$ could not be obtained from the literature and was determined from the size of the cubic cell and the molecular weight. The calculated density is 4.32gm/cc. The reported ε of the peaks have been corrected for the background absorption. The oscillator strengths of the bands were found by measuring the area under the absorption curves.

RESULTS

A. Visible Region Spectrum

Fig. 3.2 shows the absorption spectrum in the visible region at room temperature. The results of measurements are given in Table 3.1 along with the assignments of the bands.

On cooling the crystal, fine structure of the bands becomes clear and a variety of other changes occur. Results of measurements at liquid nitrogen temperature

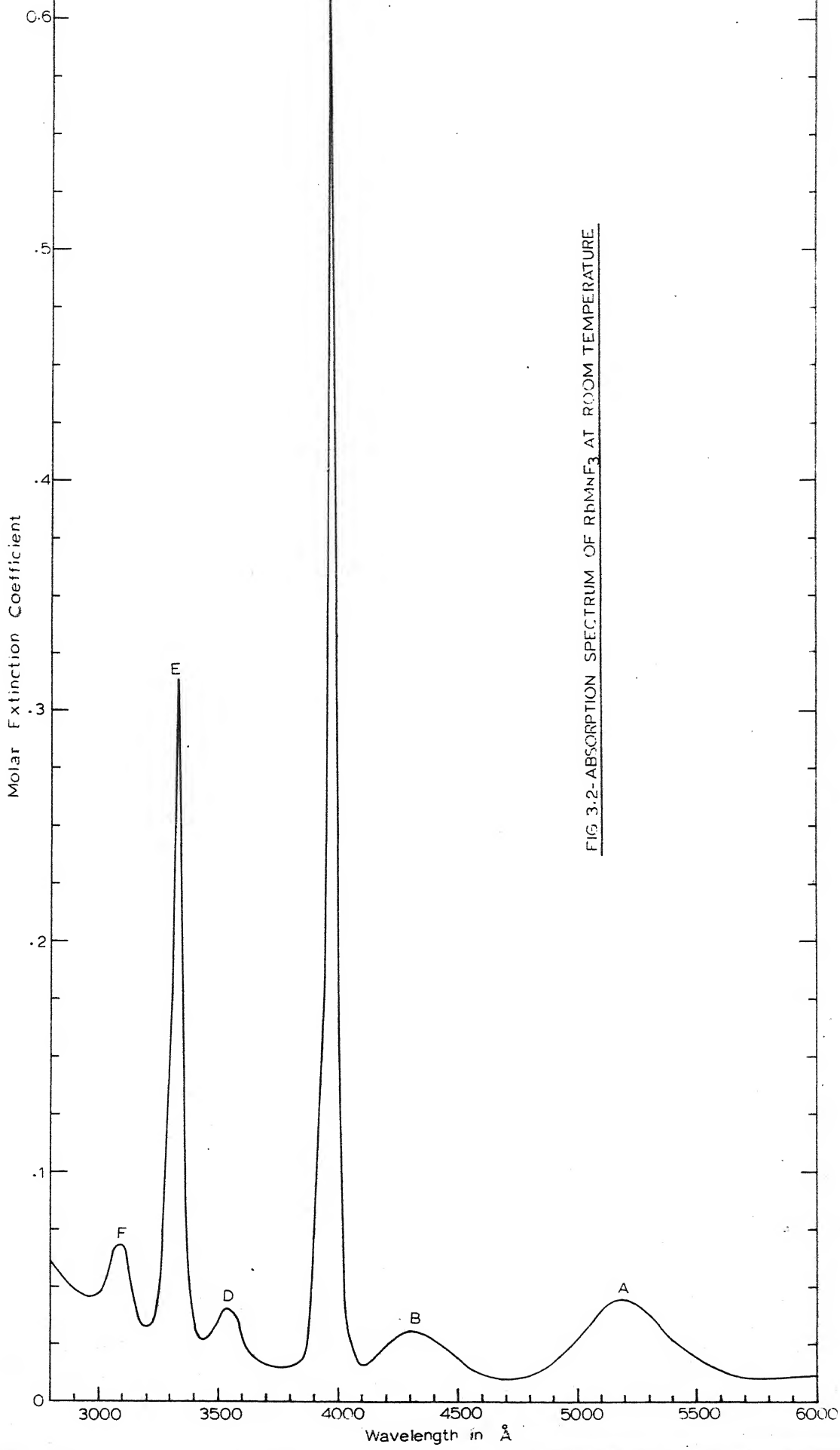

FIG 3.2-ABSORPTION SPECTRUM OF $RbMnF_3$ AT ROOM TEMPERATURE

Table 3.1

Experimental data and analysis of the absorption spectrum of $RbMnF_3$ at room temperature.

Absorption peaks	Wave length A^o	Wave number cm^{-1}	Width[a] cm^{-1}	ε (peak)	f-value x 10^7	Transition $^6A_{1g}(S) \rightarrow$	Calculated[b] energy cm^{-1}
A	5185	19,286	1500	0.035	2.4	$^4T_{1g}(G)$	19,204
B	4295	23,282	1800	0.021	2.0	$^4T_{2g}(G)$	23,311
C_1	3976	25,151					
C	3956	25,278[c]	140	0.602	9.2	$^4E_g(G)$ $^4A_{1g}(G)$	25,270
C_2	3924	25,484					
C_3	3891	25,700					
D	3526	28,362	900	0.022	1.4	$^4T_{2g}(D)$	28,423
E	3326	30,067	360	0.284	7.1	$^4E_g(D)$	30,051
E_1	3290	30,395					
F	3085	32,414	1100	0.031	1.8	$^4T_{1g}(P)$	32,747
X	~2565	39,000					
G	2430	41,152				$^4A_{2g}(F)$	40,842
I	2265	44,249	1700	0.457	45.0	$^4T_{2g}(F)$	44,429

a. Width at half intensity.

b. B = 835, C = 3080, Dq = 760 and $\alpha = 76 cm^{-1}$.

c. Ferguson et.al.[48a] report 25280 cm^{-1} for this peak.

are given in Table 3.2 while the bands themselves are shown in Figs. 3.3, 3.4, 3.5 and 3.6.

An interesting feature of the observed spectrum is the abnormally high intensities of the two sharp bands. A comparison of the observed spectrum with that of MnF_2[14] shows that while the intensities of the broad bands are of the same order, the intensities of the sharp bands are much higher in the present case. The molar extinction coefficient of the peak of C band in MnF_2 is only 0.16 as compared to the 0.602 of the present case. Similar high intensities for the sharp bands have been observed by Ferguson et.al.[48] in $KMnF_3$ also. They have proposed that the magnetic interactions between manganese ions in the crystals are responsible for these abnormal intensities.

Transition to the pair of closely spaced $^4A_{1g}(G)$ and $^4E_g(G)$ levels gives rise to the first sharp band seen around 4000A^o. At room temperature, it consists of a sharp peak C accompanied by a shoulder C_1 on higher wavelength side and two, C_2 and C_3, on lower wavelength side (Fig. 3.4a). On going to liquid nitrogen temperature, the peak C shows a blue shift of 58cm^{-1} and similar shifts are observed in the shoulders so that the relative separations are nearly preserved. The higher wavelength shoulder C_1 developes into a separate sharp peak and the two lower wavelength shoulders also become more apparent (Fig. 3.4b). The

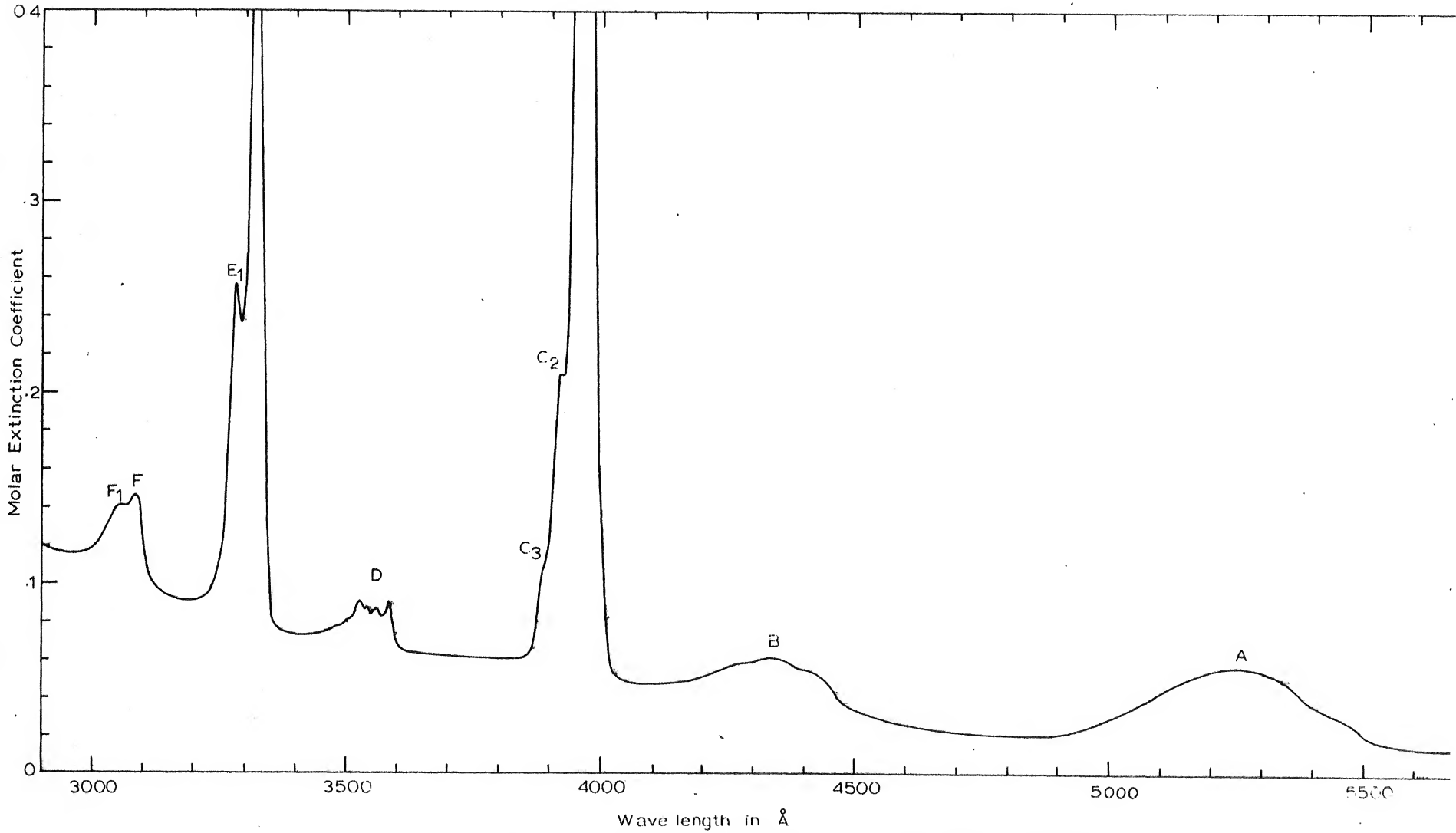

FIG 3.3 - ABSORPTION SPECTRUM OF $RbMnF_3$ AT LIQUID NITROGEN TEMPERATURE

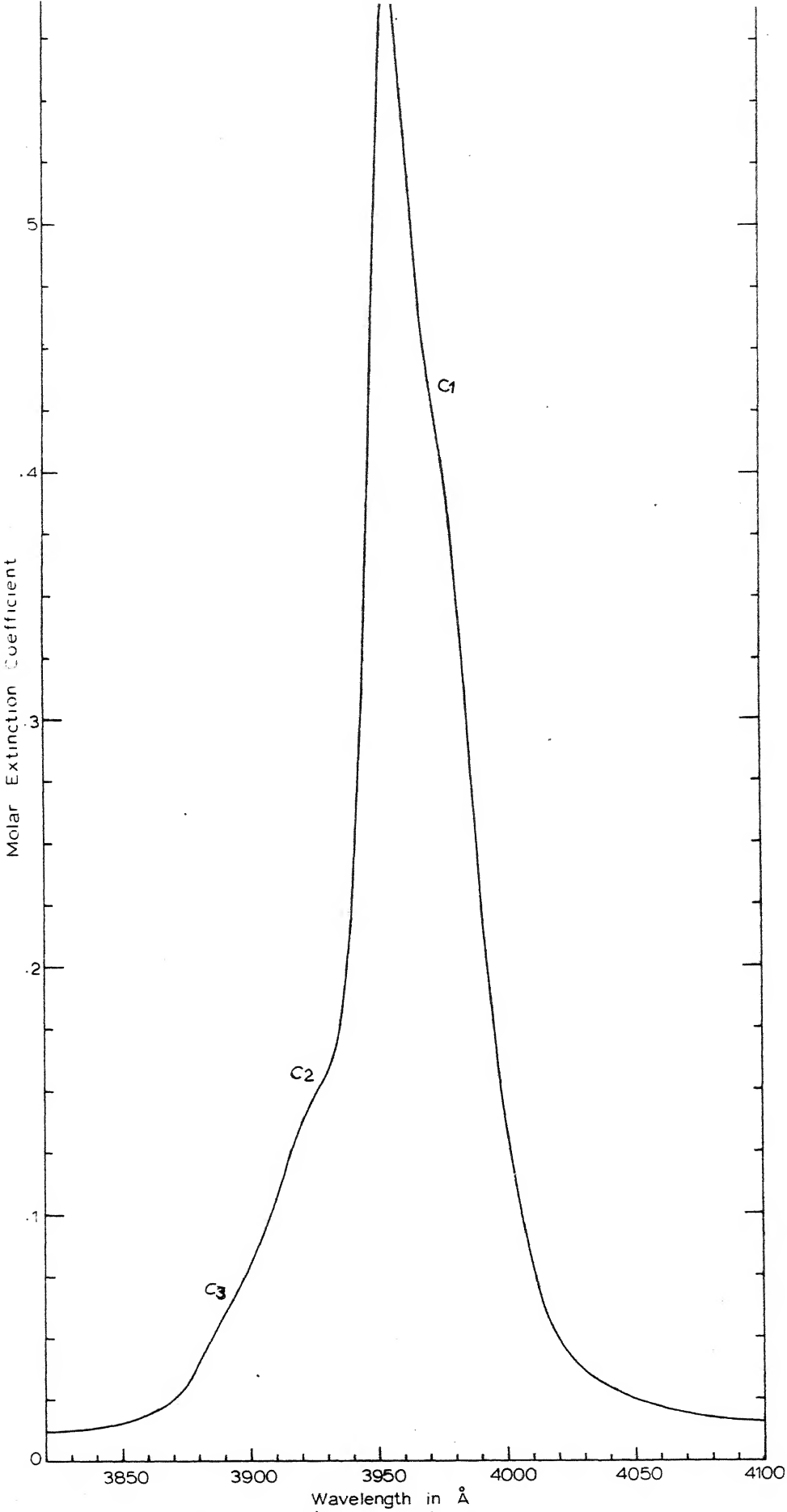

Fig. 3.4: $^6A_{1g}(S) \rightarrow {}^4A_{1g}(G)$, $^4E_g(G)$ band in $RbMnF_3$ at room temperature.

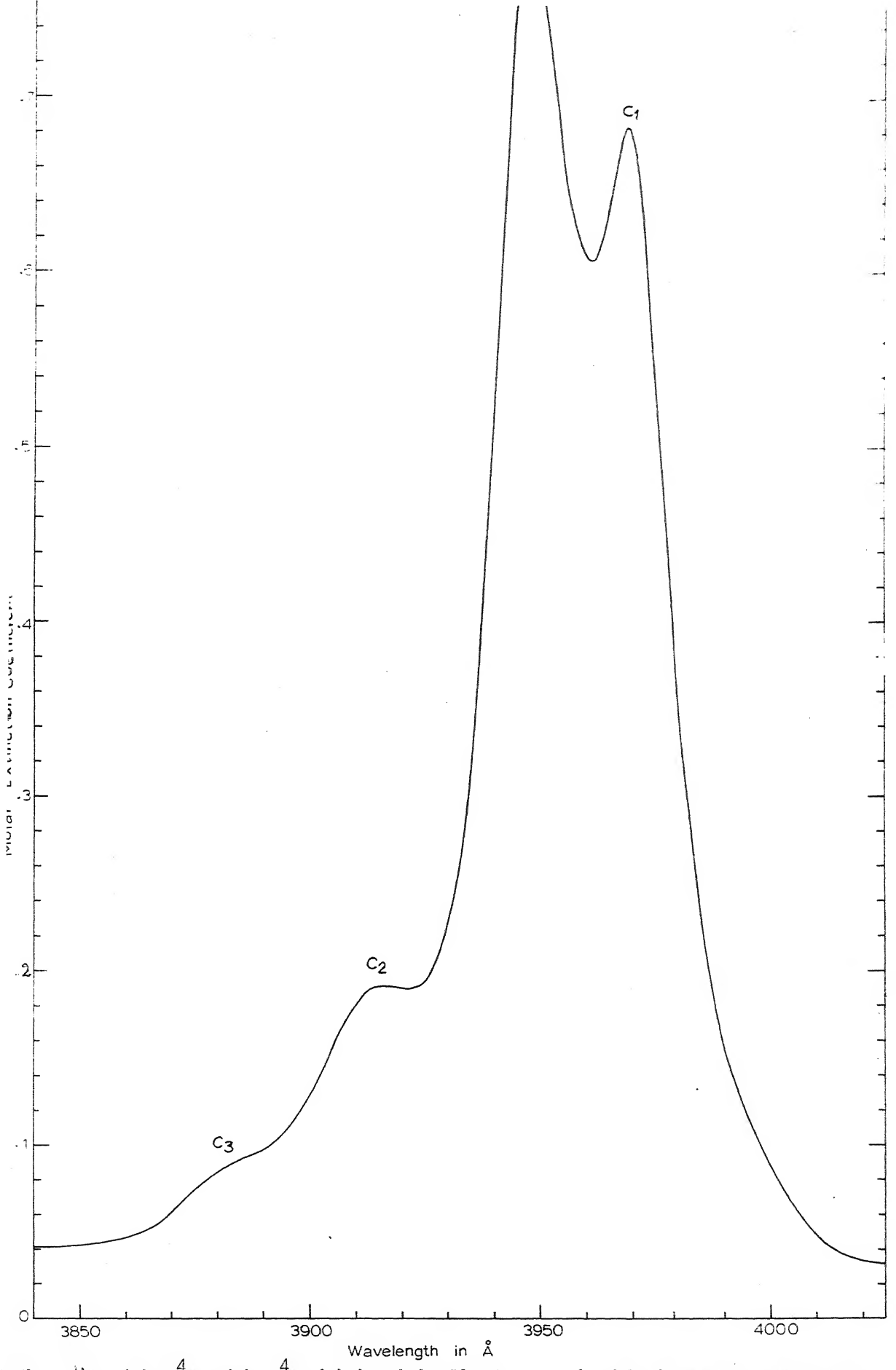

5.4b $^4A_{1g}(S) \rightarrow {}^4A_{1g}(G)$, $^4E_g(G)$ band in $RbMnF_3$ at liquid nitrogen temperature.

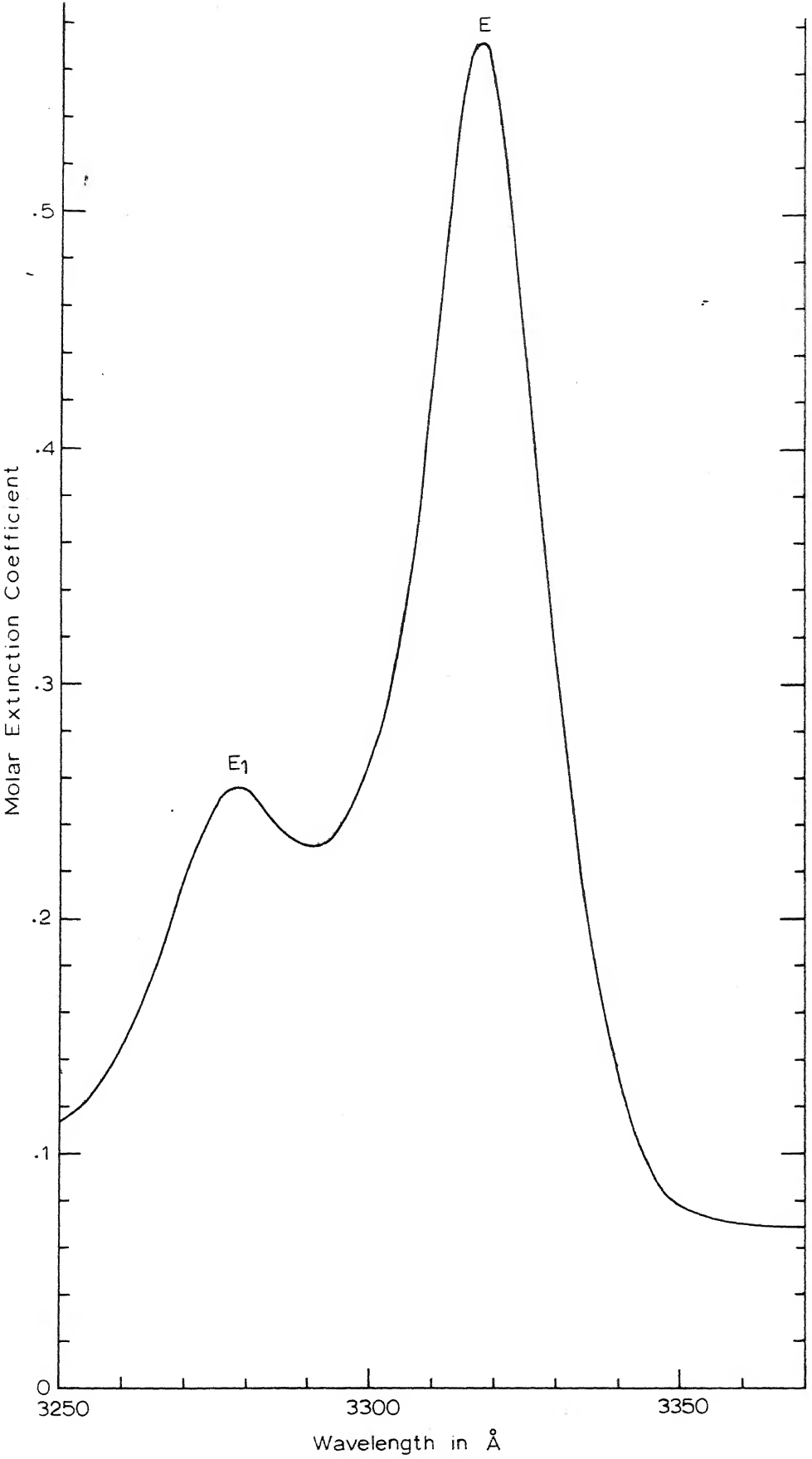

Fig. 3.5 $^6A_{1g}(S) \rightarrow {}^4E_g(D)$ band in $RbMnF_3$ at liquid nitrogen temperature.

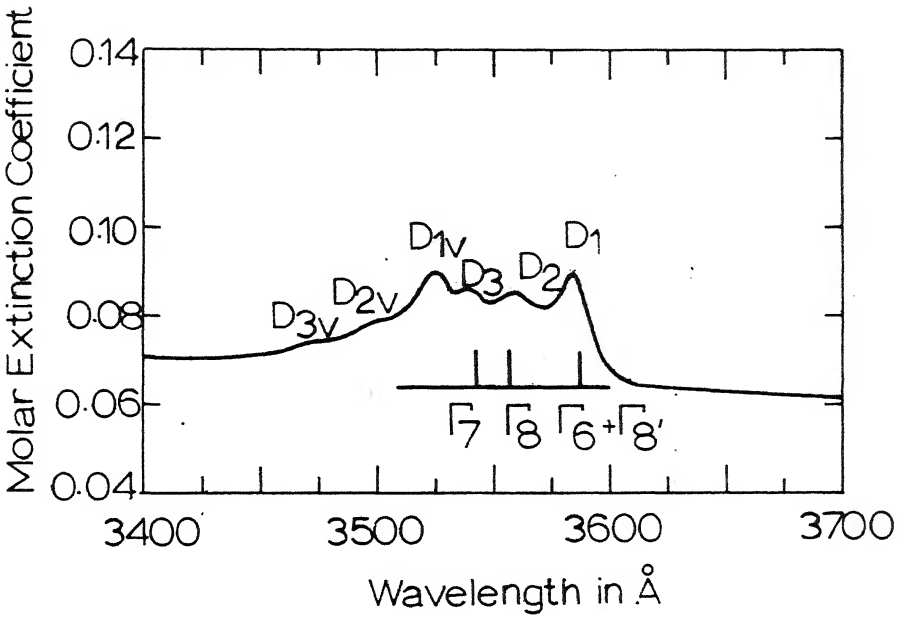

Fig. 3.6 $^6A_{1g}(S) \rightarrow {}^4T_{2g}(D)$ band in $RbMnF_3$ at liquid nitrogen temperature. The calculated spin-orbit components of $^4T_{2g}(D)$ level for $\xi=320cm^{-1}$ are marked for comparison.

Table 3.2

Experimental data and analysis of the absorption spectrum of $RbMnF_3$ at liquid nitrogen temperature.

Absorption peaks	Wave length A^o	Wave number cm^{-1}	Width cm^{-1}	f-value x 10^7	Transition $^6A_{1g}(S) \rightarrow$	Calculated[a] energy cm^{-1}
A	5222	19,150	1100	2.0	$^4T_{1g}(G)$	19,060
B	4328	23,106	1300	1.6	$^4T_{2g}(G)$	23,257
C_1	3969	25,195				
C	3947	25,336	130	9.2	$^4E_g(G)$ $^4A_{1g}(G)$	25,320
C_2	3915	25,543				
C_3	3882	25,759				
D_1	3582	27,917				
D_2	3555	28,129		1.1	$^4T_{2g}(D)$	28,463
D_3	3539	28,258				
D_{1v}	3523	28,385				
E	3318	30,140	220	7.0	$^4E_g(D)$	30,136
E_1	3281	30,478				
F	3082	32,446		1.5	$^4T_{1g}(P)$	32,927
F_1	3049	32,798				
	~2630	38,000				
	~2520	39,700				
G	2428	41,158			$^4A_{2g}(F)$	40,952
H	2385	41,926			$^4T_{1g}(F)$	41,877
I	2277	43,914			$^4T_{2g}(F)$	44,687

a. B = 840, C = 3080, Dq = 780 and α = 76 cm^{-1}.

integrated band intensity does not show any change within experimental error, on cooling. This makes one think that inspite of its abnormally high intensity, the underlying transitions do not involve vibrations to any large extent. Ferguson et.al.[48] have measured this band and also the corresponding band of $KMnF_3$ upto $4.2^{\circ}K$ and have also reached similar conclusions.

The second abnormally intense band seen around $3300A^{\circ}$ in Fig. 3.2 is assigned to $^4E_g(D)$ level. The weak shoulder E_1 seen on the lower wavelength side of its peak E becomes quite clear at liquid nitrogen temperature (Fig. 3.5). The peak E shows a blue shift on cooling like the other sharp peak C, but the shift is slightly larger in this case, the shift being $76cm^{-1}$. Similar blue shift is observed in the shoulder, marked as E_1 in Fig. 3.5. Although the halfwidth of the peak E shows appreciable decrease on cooling, the small decrease in its f-value which is within the possible experimental error, is not very striking. From the temperature independence of intensity it seems that this transition is also not much dependent on the vibrational perturbations.

The first two bands A and B on higher wavelength side in Fig. 3.2 are quite broad and arise respectively from transitions to $^4T_{1g}(G)$ and $^4T_{2g}(G)$ levels. On going to liquid nitrogen temperature, peaks of A and B bands shift towards lower energies. The

half widths and oscillator strengths of the bands decrease appreciably showing thereby that the underlying transitions are largely assisted by vibrations.

The weak band D seen around 3500A° in Fig. 3.2 is assigned to $^4T_{2g}(D)$ level. This level does not have a very large slope in the energy level diagram and therefore the low temperature spectrum is expected to reveal fine structure of the level. This is found to be so in the present case and also in other cases discussed in the later chapters. The spectrum at liquid nitrogen temperature shows the presence of four prominent peaks marked as D_1, D_2, D_3 and D_{1v} in Fig. 3.6. The total intensity of this band decreases on cooling.

The last band F seen around 3000A° in Fig. 3.2 arises from the transition to $^4T_{1g}(P)$ level. Its low temperature record given in Fig. 3.3 shows a shoulder F_1 on the lower wavelength side of the peak. The decrease in its f-value on cooling shows its dependence on vibrational perturbations.

75382

B. Spectrum in the Ultraviolet Region

Transitions to the three highest levels $^4A_{2g}(F)$, $^4T_{1g}(F)$, and $^4T_{2g}(F)$ arising from ^4F level of the free ion are expected to lie in the ultraviolet region. From the slopes of these levels one expects a sharp $^4A_{2g}(F)$ band followed by two broad bands on higher energy side arising from $^4T_{1g}(F)$ and $^4T_{2g}(F)$ levels. Reliable

experimental results available on the observed Mn^{2+} bands in this region i.e. below 3000A°, are very few as the high background absorptions which set up in this region obscure the true nature of these bands. Finlayson et.al.[16] observed three weak bands in the case of MnF_2 but their assignments of the bands are doubtful.

Fig. 3.7 shows the ultraviolet spectrum observed in the present case at room temperature. Three bands are seen in it. High background absorption conceals the true nature of the first band marked X on higher wavelength side which is seen to be quite broad. The second band marked G is observed with more clarity because of its sharpness. A prominent feature of the observed spectrum is the anomalously high intensity of the last band marked I which surpasses even the sharp bands C and E of the visible region in intensity. Such an intense band does not seem to be previously reported in the manganese fluorides. The band observed in MnF_2[16] at the similar position is very weak. It may be mentioned that although the enhancement of the intensities has been observed for the sharp bands, C and E in some cases[48], for a broad band it is reported here for the first time.

At liquid nitrogen temperature the broad band X around 39000cm^{-1} shows very complex structure which could not be measured with certainty. Broadly speaking,

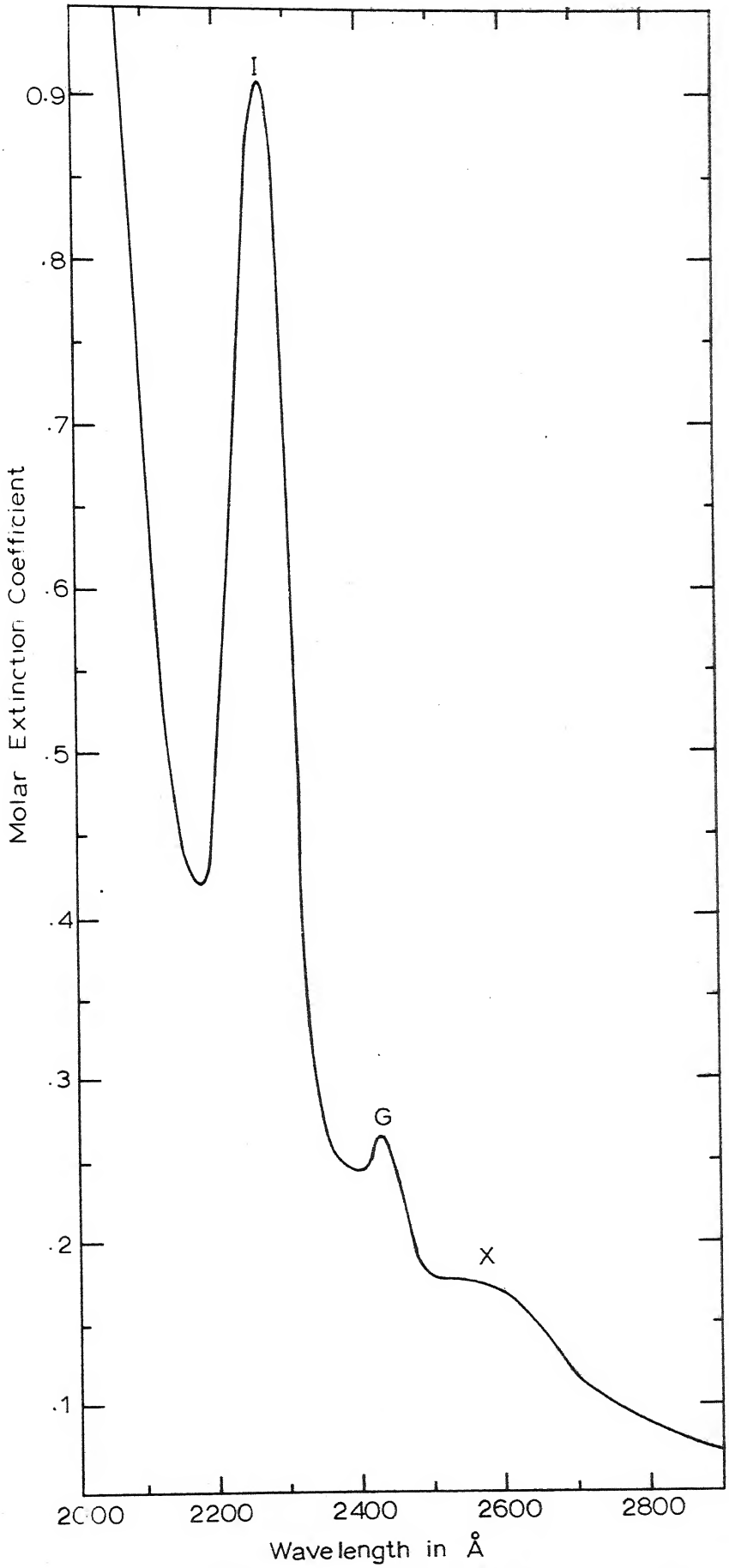

Fig. 3.7 Absorption spectrum of $RbMnF_3$ in the ultraviolet region at room temperature.

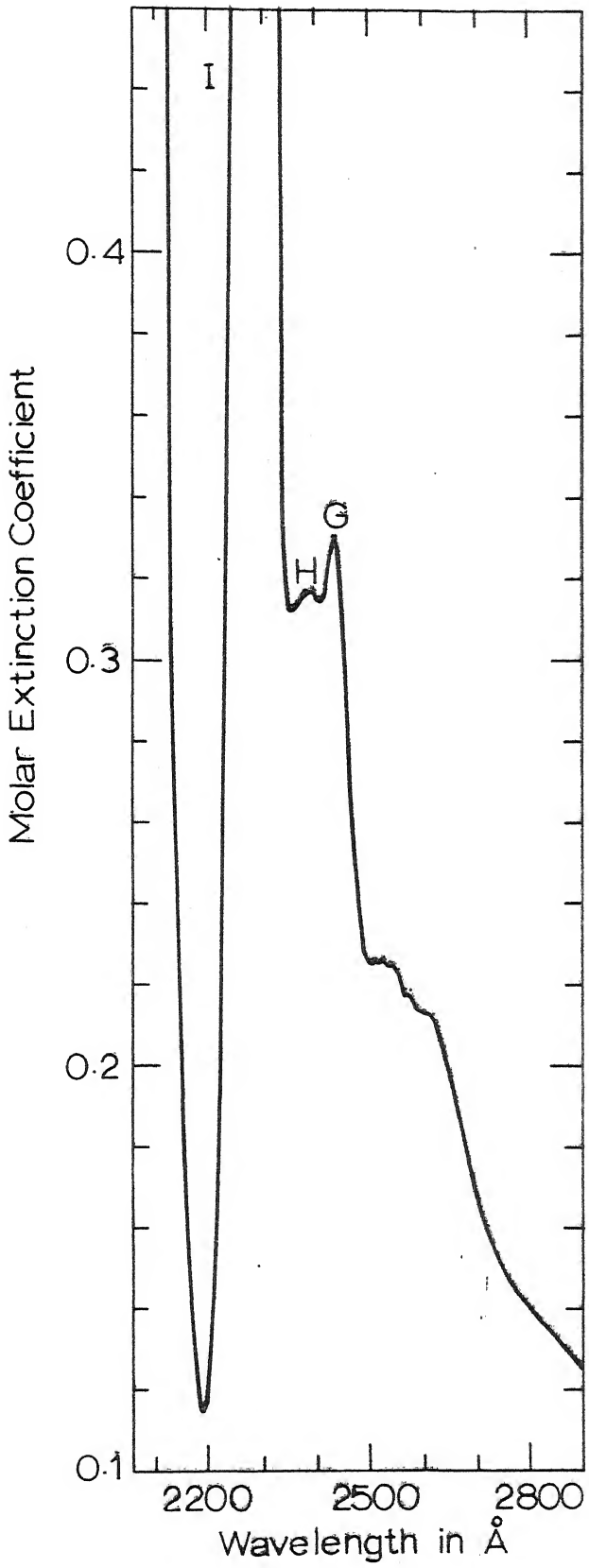

Fig. 3.8 Absorption spectrum of $RbMnF_3$ in the ultraviolet region at liquid nitrogen temperature. The peak of I band which lies outside the figure is not shown.

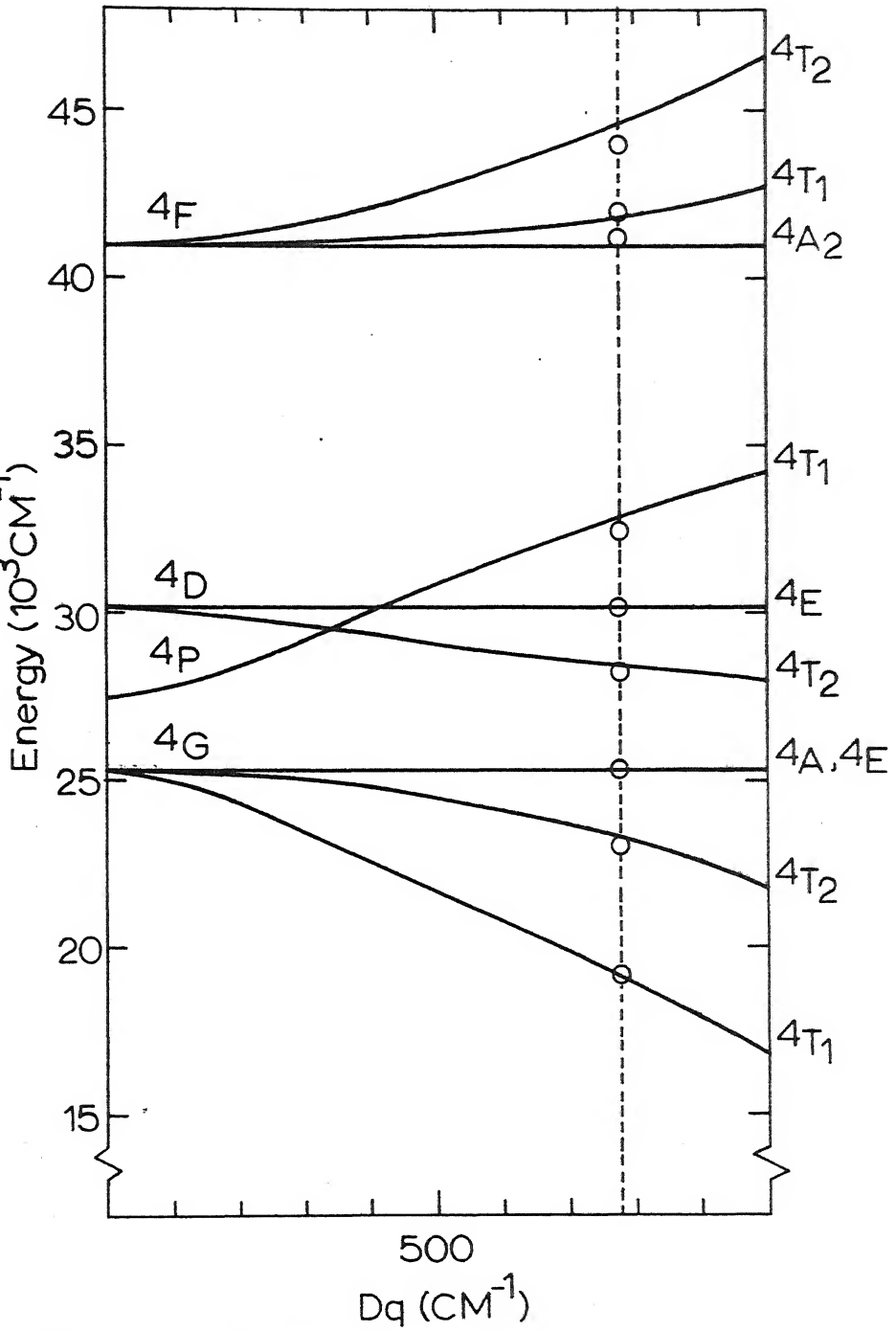

Energy level

Fig. 3.9 diagram of Mn^{2+} in octahedral symmetry for B= 840, C= 3080, and α = 76 cm^{-1}. The observed band energies in the spectrum of $RbMnF_3$ at liquid nitrgen temperature are marked o at Dq= 780 cm^{-1}.

it splits into two bands centered around 38000 and 39700cm^{-1} (Fig. 3.8). The sharp band G shows a small red shift in contrast to the blue shifts of the sharp bands of visible region. No structure is seen in this sharp band. An additional weak band marked H is seen to have come up on lower wavelength side of the sharp band G (Fig. 3.8). The corresponding peak in the room temperature spectrum is not clear. The intense band I becomes a little sharper and the peak height increases on cooling. Reliable measurements could not be made on this band at liquid nitrogen temperature because of the increased peak absorption which goes outside the reliable measurement limits of the spectrophotometer. However, a red shift of about 300cm^{-1} is noticed in this band.

If one assigns the three bands observed at room temperature to the three levels arising from ^4F of the free ion in their respective order of energies i.e. broad band X to $^4A_{2g}(F)$, sharp band G to $^4T_{1g}(F)$ and intense band I to $^4T_{2g}(F)$, one finds that the observed widths of the bands are not in agreement with the theoretically expected widths. Any other alternative assignments of the bands will not fit in the theoretical level scheme(Fig. 3.9).

This anomaly however, is resolved by the coming up of additional band H between the sharp and intense bands at low temperature. Assignments of sharp band G

to $^4A_{2g}(F)$, this new band H to $^4T_{1g}(F)$ and intense band I to $^4T_{2g}(F)$ levels very well fit in the theory. The probable upper state $^4T_{1g}(F)$ of the weak band H lies quite close to $^4A_{2g}(F)$ state and it is possible that at room temperature the weak band H is merged in the neighboring intense bands. Because of the sharpening of the bands it comes up at liquid nitrogen temperature.

The origin of the first broad band X is not very clear. It may arise from a transition to some doublet level but its observed intensity is a little large for such a transition.

CUBIC FIELD CALCULATIONS

The Mn^{2+} ion sees a cubic crystalline field at room temperature as well as at liquid nitrogen temperature. We shall first calculate the cubic field energy levels to fit the peak positions of the observed bands. Fine structure of the bands will be then analyzed by finding the effects of spin orbit and vibrational interactions on these cubic field levels.

The procedure of fitting the observed energies has been described earlier in chapter II. One uses the matrices given in Appendix II which involve four parameters B, C, Dq, and α. The parameter α is fixed at $76cm^{-1}$ so that there are only B, C and Dq to be adjusted.

The parameters can have slightly different

values at different temperatures because of the changes produced in the properties of crystal on changing the temperature. The observed shifts of the bands along the energy scale on cooling the crystal support this viewpoint. We shall evaluate the parameters for the spectra at room and liquid nitrogen temperatures separately.

Values of parameters calculated for the room temperature spectrum are B=835, C=3080, and Dq=760cm^{-1}. The calculated energies given in Table 3.1 are seen to be in very good agreement with the observed energies. The deviations for the five lower energy levels are less than 100cm^{-1}. Larger deviations for higher lying states are probably because of the more vulnerability of these states to configurational interactions. Still, the reasonably good agreement obtained in the case of the ultraviolet bands confirms our assignments based on the observed widths of the bands.

To account for the small blue shifts of the two sharp peaks C and E of the visible region, the parameter B for liquid nitrogen temperature spectrum is arbitrarily increased by 5cm^{-1} over its room temperature value of 830cm^{-1}. This accounts for the observed blue shift of 58cm^{-1} (= 10δB) of the first sharp band C.

Because of the contraction of the lattice size, the parameter Dq is expected to increase on cooling. Red shifts of $^4T_{1g}(G)$ and $^4T_{2g}(G)$ levels which have

negative slopes and blue shift of $^4T_{1g}(P)$ level which has positive slope confirm an increase in Dq. Slightly increased Dq value of 780cm^{-1} will explain the observed red shifts of the bands involving $^4T_{1g}(G)$ and $^4T_{2g}(G)$ levels. The calculated energies for low temperature spectrum using B=~~855~~ 840, C=3080, and Dq=780cm^{-1} are given in Table 3.2. The calculated energy of $^4T_{1g}(F)$ level, which could not be compared with the observed energy in room temperature spectrum, is 41877cm^{-1} and the close agreement with the observed energy, 41926cm^{-1}, of the weak band H which comes up at liquid nitrogen temperature supports our assignments of ultraviolet bands.

ANALYSIS OF THE FINE STRUCTURE: THEORETICAL FORMULATION

Calculated cubic field levels account very well for the overall band positions. We shall now consider the effects of spin orbit and vibrational interactions on these levels for explaining the observed fine structure of the bands. A theoretical estimation of the possible splittings produced by these is first made and the observed structures are then correlated with the expected ones.

A. Spin-Orbit Interaction

Qualitative splittings of the cubic field levels under the spin-orbit interaction have been discussed along with the general theory of Mn^{2+} in

Chapter II. Quantitative splittings of the levels can be found by diagonalising the energy matrices obtained on adding the matrices of α term to the spin orbit and crystal field matrices. Dimensions of the matrices are Γ_6: 20 x 20, Γ_7: 22 x 22 and Γ_8: 42 x 42. The calculations involve five parameters B, C, Dq, α and ξ. It is found that the spin orbit splittings are sensitive functions of only ξ and so the other parameters can be conveniently fixed at the values which fit the band positions without spin orbit coupling. Values of parameters obtained from liquid nitrogen temperature spectrum in which the fine structures are easily measurable, are used in the calculation. These values are B = 840, C = 3080, Dq = 780 and $\alpha = 76 cm^{-1}$.

Reliable value of spin orbit coupling parameter for Mn^{2+} is neither known in free ion nor in any crystal. For free Mn^{2+} ion Shadmi's[27] extrapolated value is $\sim 300 cm^{-1}$ while the calculated value[28] using Watson's ground state wavefunction is $376 cm^{-1}$. No reliable ξ value for Mn^{2+} has been reported in crystals. Such being the case, we calculated the splittings for various values of ξ between 0 and $400 cm^{-1}$ and selected the ξ value which gave a good fit to the observed splittings. It has been found that a ξ value of $320 cm^{-1}$ is quite probable. As it is unnecessary to give the calculated splittings for all the ξ values, these are given in Table 3.3 for the estimated value of $320 cm^{-1}$.

Table 3.3

Energies of the quartet terms and their splitting when spin orbit interaction is introduced. B=840, C=3080, Dq=780, α=76 and ξ =320 cm^{-1}.

Term	Energy without s.o. int. cm^{-1}	s.o. level[a] t	s.o. splitting cm^{-1}
$^6A_{1g}(S)$	0	7	-19.971
		8	-19.969
$^4T_{1g}(G)$	19,060	7	-98
		8′	-65
		8	-03
		6	+43
$^4T_{2g}(G)$	23,257	7	-120
		8	-76
		6	+27
		8′	+33
$^4A_{1g}(G)$	25,320	8	-34
$^4E_g(G)$	25,320	7	-36
		6	-17
		8	-15
$^4T_{2g}(D)$	28,463	8′	-173
		6	-158
		8	+74
		7	+176
$^4E_g(D)$	30,136	7	-54
		8	-34
		6	-16
$^4T_{1g}(P)$	32,927	8′	-101
		7	-23
		8	+33
		6	+78
$^4A_{2g}(F)$	40,952	8	+189
$^4T_{1g}(F)$	41,877	6	-239
		8	-90
		8′	+69
		7	+73
$^4T_{2g}(F)$	44,687	6	-250
		8′	-235
		7	-135
		8	+67

a. $\Gamma_6, \Gamma_7, \Gamma_8$ and $\Gamma_{8'}$ have been abbreviated here to 6,7,8 and 8′ for convenience.

Calculated splittings for all the quartet levels are given in this Table.

B. Vibrational Modes of $RbMnF_3$

Electric dipole moment has the symmetry T_{1u} in O_h group. The selection rule says that for electric dipole transition to occur, the product of the initial and final state representations must contain T_{1u} representation. This would be possible if a vibrational state having an appropriate representation is coupled to the initial or the final electronic states. Because of such coupling of vibrations with the electronic states, vibrational structures are expected in the present case. For an analysis of the observed structures a knowledge of vibrational modes of $RbMnF_3$ is necessary and accordingly we shall proceed to find them.

In perovskite structure $RbMnF_3$ there are five atoms per unit cell. Group theoretical analysis of the fifteen degrees of freedom, based on the symmetry operations of the space group O_h^1, shows that the fifteen dimensional mechanical representation T_m breaks into following irreducible representations (Appendix I):

$$T_m = 4T_{1u} + T_{2u}$$

Out of these five three fold degenerate modes, one T_{1u} representation is pure translation.[52] From Table 3.4

Table 3.4

Reductions of the products $T_{exc} \otimes T_{vib}$ for $RbInF_3$ in O_h symmetry.

T_{exc}	$T_{exc} \times T_{vib}$	
	$T_{vib} = T_{1u}$	$T_{vib} = T_{2u}$
A_{1g}	T_{1u}	T_{2u}
A_{2g}	T_{2u}	T_{1u}
E_g	$T_{1u}+T_{2u}$	$T_{1u}+T_{2u}$
T_{1g}	$A_{2u}+E_u+T_{1u}+T_{2u}$	$A_{1u}+E_u+T_{1u}+T_{2u}$
T_{2g}	$A_{1u}+E_u+T_{1u}+T_{2u}$	$A_{2u}+E_u+T_{1u}+T_{2u}$

Foot Note: Explanation of notation:
T_{exc} is the irreducible representation of the electronic state and T_{vib} is that of the vibrational mode.

one finds that for excited states of symmetry E_g, T_{1g} and T_{2g} both the vibrational modes have appropriate symmetry to make the electric dipole transition possible whereas for A_{1g} only T_{1u} modes and for A_{2g} state only T_{2u} mode can be effective.

The experimental frequencies of vibrational modes of $RbMnF_3$ are not available with which we may correlate our observed spectral structures. However, infrared measurements have recently been reported for $KNiF_3$ and $KMgF_3$ both of which have the same perovskite structure as that of $RbMnF_3$. Reported frequencies of the three T_{1u} modes in $KNiF_3$ at 90°K are $\nu_1 = 144$, $\nu_2 = 248$ and $\nu_4 = 452$ cm^{-1}, while the T_{2u} mode is inactive in the infrared.[52] Corresponding frequencies[53] in $KMgF_3$ are 140, 295 and 450 cm^{-1} respectively. The vibrational structure observed by Ferguson and Guggenheim[45] in the optical spectrum of $KNiF_3$ has been found to be in good agreement with the frequencies determined from infrared measurements. From the measurements of Ferguson and Guggenheim[45], the probable frequency ν_3 of the infrared inactive mode T_{2u} in $KNiF_3$ seems to be around 330cm^{-1}. Closeness between the vibrational frequencies of $KMgF_3$ and $KNiF_3$, in spite of Mg being much different from Ni, suggests that the vibrational frequencies of $RbMnF_3$ may also be of similar order.

C. Jahn-Teller Effect

As some of the excited states of Mn^{2+} are degenerate

there is a possibility that a dynamic Jahn-Teller effect might operate in these states to remove the degeneracies. However, the dynamical Jahn-Teller effect can only occur for excited states of symmetry E_g, T_{1g} and T_{2g} if there are fundamental vibrational modes of symmetry T_{2g} or E_g.[1] As the analysis of the vibrational modes of the crystal has shown that there are no fundamental modes belonging to these symmetry representations, only dynamical instabilities which are second order in nuclear displacements are possible (Renner effect). These are expected to be very small and can be excluded from the analysis of the observed fine structure.

ANALYSIS OF THE FINE STRUCTURE: INTERPRETATION

A. $^6A_{1g}(S) \rightarrow {}^4T_{1g}(G)$ and $^4T_{2g}(G)$ Transitions

The $^4T_{1g}$ and $^4T_{2g}$ types of levels undergo first order spin-orbit splitting. No spin orbit splitting however, is observed in $^4T_{1g}(G)$ and $^4T_{2g}(G)$ bands since any such splitting, which is expected to be less than $200cm^{-1}$, is perhaps masked by the large widths of the bands. However, some weak structures extending throughout the widths of the bands ($\sim 1000cm^{-1}$) are observed but no reliable measurements are possible. These could be vibrational in origin and from their large extension one concludes that several vibrational levels are involved. No regularity could be established in these structures to allow any reliable estimate of vibrational frequencies.

B. $^6A_{1g}(S) \rightarrow {}^4T_{2g}(D)$ Transition

The band D involving $^4T_{2g}(D)$ level shows four prominent peaks marked D_1, D_2, D_3 and D_{1v} (Fig. 3.6 and Table 3.2). The splitting produced by spin orbit coupling is expected to be large in this level (Table 3.3). Since the slope of the level is small it is possible that this splitting may be resolved in low temperature spectra and therefore, we shall analyse the observed structure from the point of view of spin orbit splitting.

The level splits under spin orbit coupling as:

$$\Gamma_8 \times T_{2g} = \Gamma_6 + \Gamma_7 + 2\Gamma_8$$

First order splittings calculated from Landes formula using fictitious $L' = 1$ are:

$E = 5a$ (two fold Γ_7), $2a$ (Γ_8), and $-3a$ ($\Gamma_6 + \Gamma_{8'}$).

The calculated splittings obtained by diagonalizing the matrices are drawn in Fig. 3.10 for ξ values ranging from 0 to 400cm^{-1}. The degeneracy of Γ_6 and Γ_8 levels is removed in exact calculations but the levels still lie quite close to one another. Therefore, only three out of the four observed lines should be spin orbit in origin. The lines D_1, D_2 and D_3 fit the expected splitting pattern well. The separations D_3-D_2 and D_2-D_1 are in the ratio 129:212 = 3:5, which agrees with the first order splitting ratio. From the magnitude of the observed splittings the ξ value is estimated to be 320 ± 10cm^{-1} (See Figs. 3.6 and 3.10 for

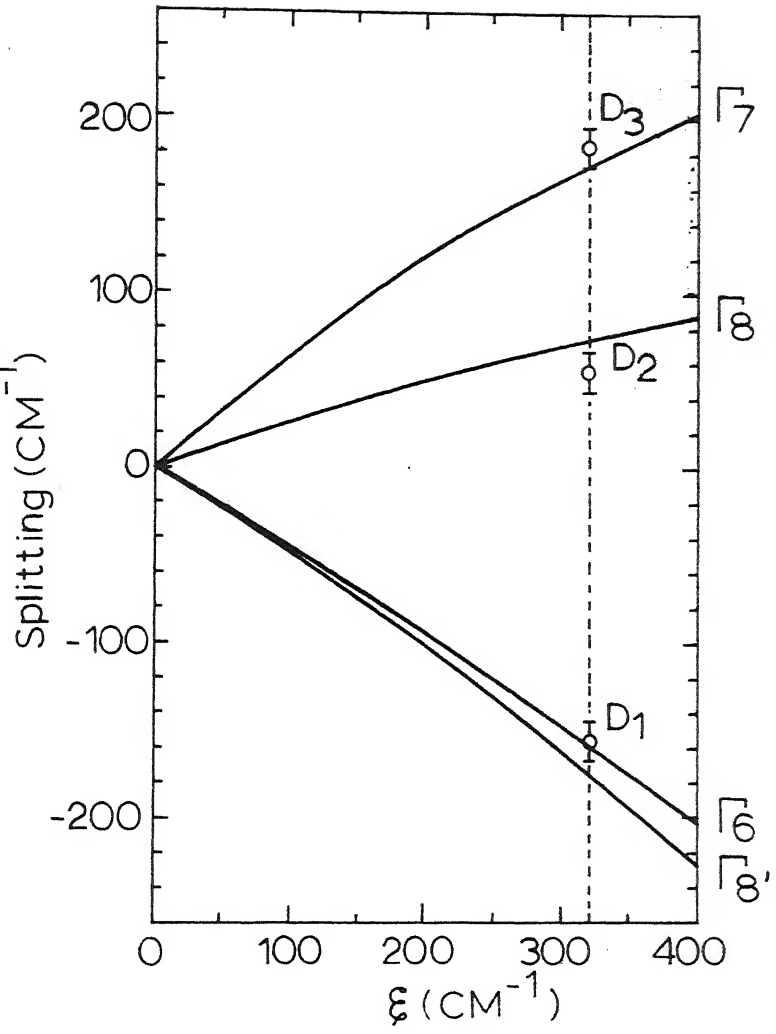

Fig. 3.10 Spin-orbit splitting diagram of $^4T_{2g}(D)$ level in Mn^{2+} for ξ between 0 to 400 cm^{-1}, B = 840, C = 3080, Dq = 780 and α = 76 cm^{-1}. The observed fine structure components of the level are marked $\overset{\circ}{\underset{\mid}{\mid}}$ at ξ = 320 cm^{-1}.

comparison between the observed and calculated values).

The line D_{1v} probably belongs to another vibrational level of $^4T_{2g}(D)$. From the similarity in the shapes of D_1 and D_{1v} lines it looks as if D_{1v} is the first spin orbit component in that vibrational state. In that case there should be two more lines on the higher energy side of D_{1v}. Indications of the presence of such two lines can be seen in Fig. 3.6 where they are marked as D_{2v} and D_{3v}.

C. $^6A_{1g}(S) \rightarrow {}^4T_{1g}(P)$ Transition

The band F having $^4T_{1g}(P)$ as the upper state shows a prominent shoulder separated by $352 \pm 20 cm^{-1}$ from the peak on the higher energy side. The estimated spin orbit splitting of this level is $179 cm^{-1}$ which is much less than this separation and therefore the shoulder is probably vibrational in origin. The separation $352 cm^{-1}$ perhaps represents the frequency ν_3 of the T_{2u} vibrational mode of the upper electronic state.

D. $^6A_{1g}(S) \rightarrow {}^4E_g(D)$ Transition

This transition shows two lines E and E_1 separated by $338 \pm 10 cm^{-1}$. This can not be the spin orbit splitting of $^4E_g(D)$ level, since the estimated spin orbit components are spread over less than $40 cm^{-1}$ (Table 3.3). This structure is perhaps the vibrational

structure of the level. The separation between E and E_1 is of the expected order of ν_3 frequency in the upper electronic state.

E. $^6A_{1g}(S) - {}^4A_{1g}(G)$, $^4E_g(G)$ Transition

The band involving these levels has two prominent peaks C_1 and C and two weak shoulders C_2 and C_3. The two intense peaks C and C_1 probably arise due to the transitions to the two closely spaced electronic states but it is difficult

to assign them individually to the two states. The spin orbit splitting of the $^4E_g(G)$ level is expected to be less than $20cm^{-1}$ while $^4A_{1g}(G)$ does not split (Table 3.3). The shoulders C_2 and C_3 therefore should be vibrational in nature and could be associated with anyone of the two peaks C and C_1. The frequency differences involved are of the order of magnitude expected for vibrational frequencies of the upper states.

EFFECT OF TEMPERATURE ON BAND WIDTHS AND INTENSITIES

The widths and f-values of broad bands A,B,and F appreciably decrease on reducing the temperature which may be associated with the freezing of lattice vibrations. The observed ratios f_{80^oK}/f_{300^oK} for A and F bands are ~ 0.83 and for B band ~ 0.80. Using the formulation discussed in Chapter II, the involved vibrational

frequency ω_0 for A and F bands comes $\sim 320 cm^{-1}$ and for B band comes $\sim 270 cm^{-1}$. Thus the magnitude of ω_0 comes out to be of the magnitude expected for vibrational frequencies.

The widths of A and B bands decrease by factors of 0.73 and 0.72 respectively on cooling to liquid nitrogen temperature. The formation given previously (Chapter II) yields $\omega_0 \sim 370 cm^{-1}$ which is again of the right order of magnitude for a vibrational frequency.

The above analysis has been done just to show the correctness of explaining the decrease in widths and intensities of the bands from the point of view of freezing of lattice vibrations and it can be seen that though the vibrational frequencies determined from the temperature dependence of these may not be exactly equal to any actual vibrational frequency of the crystal, the magnitudes of the vibrational frequencies are of the right order.

CHAPTER IV

ABSORPTION SPECTRUM OF $Mn(CH_3COO)_2 \cdot 4H_2O$

CHAPTER IV

ABSORPTION SPECTRUM OF $Mn(CH_3COO)_2 \cdot 4H_2O$

INTRODUCTION

Hydrated manganous crystals have long been employed for the study of Mn^{2+} spectrum as these can be easily grown from the aqueous solutions. Gielessen's[57] study of hydrated crystals is perhaps the first detailed investigation on Mn^{2+} spectrum in crystals. Pappalardo[54] has measured the low temperature spectra of several hydrated crystals. Tsujikawa[44] has studied the absorption spectrum of $MnSiF_6 \cdot 6H_2O$ between 20^oK and 1.2^oK in various external magnetic fields. Koide and Pryce[37] and Englman[38] have done theoretical calculations on the intensities of absorption bands in hydrated salts.

The absorption spectrum of manganese acetate tetrahydrate has been studied in the present work. This is a comparitively new system whose properties have been of interest in the recent years. Flippen and Friedberg[18] studied the magnetization of this crystal below 20^oK and found a transition temperature at 3.18^oK. The possible ordered states discussed by them are ferrimagnetic and parasitic ferromagnetic states. Tsujikawa[55] measured the absorption spectrum in the region of sharp ($^4A_1(G)$, $^4E(G)$) band of Mn^{2+} and found five sharp lines. From the magnetic field dependence of the intensities of these five sharp lines below the

transition temperature, he has concluded that the ordered state is ferrimagnetic.

CRYSTAL STRUCTURE

The space group of the crystal belongs to the monoclinic system. The detailed crystal structure is not known. The crystallographic data given by Groth[56] shows that a:b:c = 0.5265:1:1.112 and $\beta = 94^{\circ}58'$. The a and b axes are in the plane of broad face. Preliminary results of X-ray analysis of Iwasaki and of Baughman have been quoted by Tsujikawa.[55] According to Iwasaki's results a = 9.13 ± .04A, b = 17.62 ± .03A, c = 19.76±.08A, and $\beta = 94.5^{\circ}$ while according to Baughman's results they are: a = 9.17 ± .02A, b = 17.61 ± .02A, c = 19.60 ± .10A and $\beta = 95^{\circ}$. In the Iwasaki's analysis a unit cell contains twelve Mn^{2+} ions out of which eight Mn^{2+} occupy eight equivalent sites and the other four occupy the remaining four equivalent sites. From the consideration of overall symmetry it has been concluded that the eight equivalent Mn^{2+} in a unit cell see a crystal field without center of symmetry while the four equivalent Mn^{2+} see a crystal field with center of symmetry. It has been conjectured that the two acetic groups occupy the two opposite vertices and four water molecules occupy the other four coplanar vertices of octahedron of ligands around eight equivalent Mn^{2+} while in the case of the four equivalent Mn^{2+} all the six vertices may be occupied by water molecules. In the case of

nickelous and cobaltous acetate tetrahydrates the oxygen of acetic groups occupy the opposite vertices of octahedron. These salts however, are not isomorphic to manganese acetate tetrahydrate. From the above discussion it becomes clear that the actual crystalline field may have a rhombic symmetry but an approximation to tetragonal field will not be very unreasonable.

We shall first correlate the band positions with the cubic field levels and shall then apply the lower symmetry perturbations for analysing the fine structure.

EXPERIMENTAL

The crystals were grown from saturated water solution at room temperature. The crystals grow in the form of thin six sided plates and out of these a uniform crystal of thickness 3.4 mm was chosen for the present study. The absorption spectra were recorded on a Cary-14 spectrophotometer at room and liquid nitrogen temperatures. Broad face of the crystal was perpendicular to the path of light beam in the spectrophotometer.

Molecular weight of the crystal is 245.08 and the density is 1.589. For 3.4 mm thick sample, the recorded optical densities were converted to molar extinction coefficients by multiplying by a factor of 0.454. Oscillator strengths were determined by measuring the area under the absorption curves. Although some bands show fine structure at low temperature, the total f-values

nickelous and cobaltous acetate tetrahydrates the oxygen of acetic groups occupy the opposite vertices of octahedron. These salts however, are not isomorphic to manganese acetate tetrahydrate. From the above discussion it becomes clear that the actual crystalline field may have a rhombic symmetry but an approximation to tetragonal field will not be very unreasonable.

We shall first correlate the band positions with the cubic field levels and shall then apply the lower symmetry perturbations for analysing the fine structure.

EXPERIMENTAL

The crystals were grown from saturated water solution at room temperature. The crystals grow in the form of thin six sided plates and out of these a uniform crystal of thickness 3.4 mm was chosen for the present study. The absorption spectra were recorded on a Cary-14 spectrophotometer at room and liquid nitrogen temperatures. Broad face of the crystal was perpendicular to the path of light beam in the spectrophotometer.

Molecular weight of the crystal is 245.08 and the density is 1.589. For 3.4 mm thick sample, the recorded optical densities were converted to molar extinction coefficients by multiplying by a factor of 0.454. Oscillator strengths were determined by measuring the area under the absorption curves. Although some bands show fine structure at low temperature, the total f-values

are computed in these cases as the measurements of the f-values of individual components would have been very uncertain.

RESULTS

The observed spectra at room and liquid nitrogen temperatures are shown in Figs. 4.1 and 4.2 and the corresponding measurements are given in Tables 4.1 and 4.2.

The widths and the intensities of the two bands marked A and B decrease on cooling the crystal but no structure is resolved. These two bands have $^4T_1(G)$ and $^4T_2(G)$ respectively for their upper states.

The sharp band C is shown in Fig. 4.3 as observed at liquid nitrogen temperature. The band maximum consists of two strong lines C and C_1. A weak sharp line C_o is also seen in Fig. 4.3. The shoulder around 4015A° does not show any marked sharpening or structure on cooling though there are indications of its splitting into two weak components C_2 and C_3. An overall blue shift is found in this band on cooling. Tsujikawa[55] has studied the fine structure of this sharp band. Since he used a high resolution instrument and carried out his experiments at very low temperature, the lines C and C_1 were observed by him as doublets. A comparison of his five lines with our lines is given in Table 4.3.

The band D, assigned to $^4T_2(D)$ state, shows

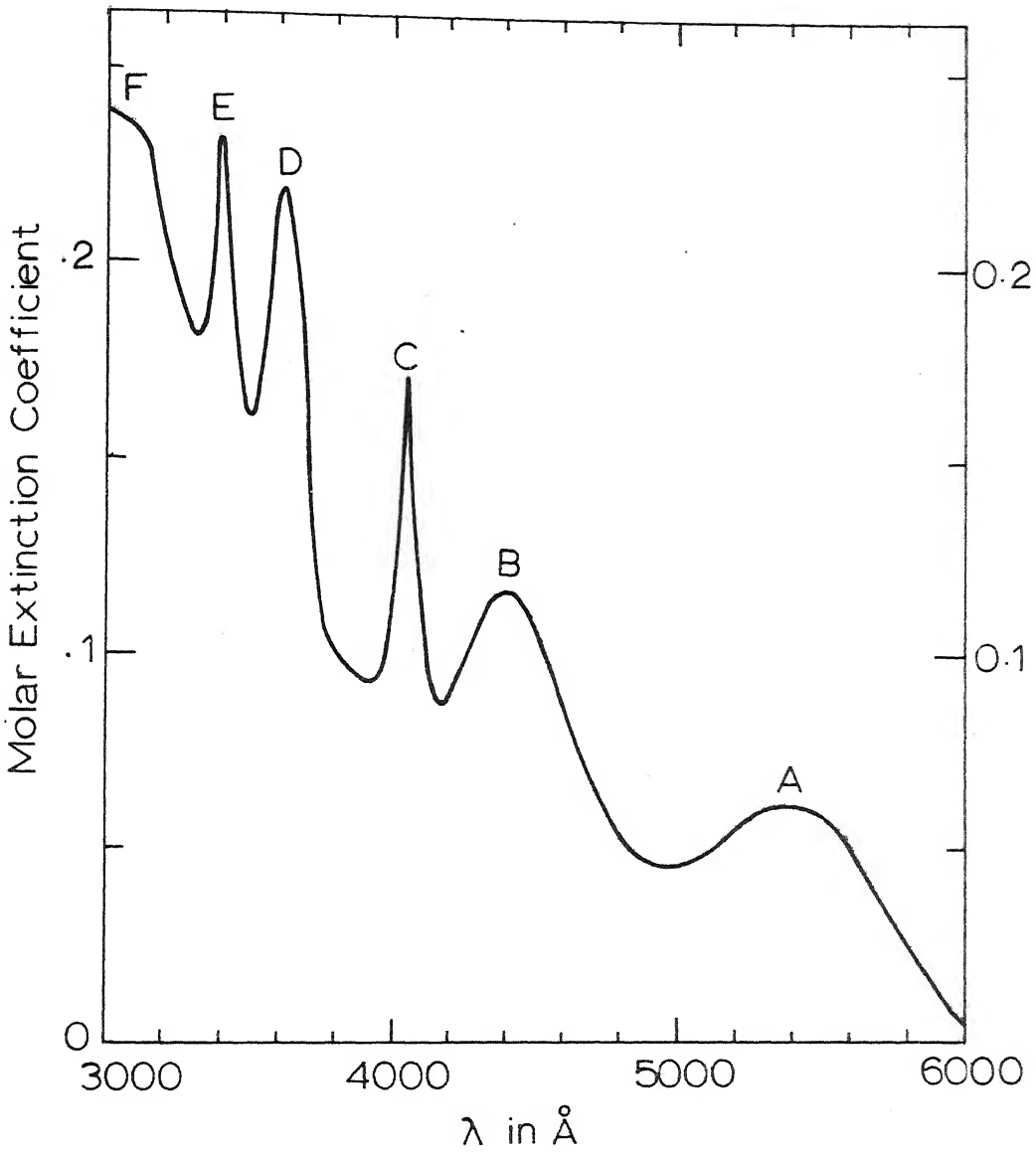

Fig. 4.1 Absorption spectrum of $Mn(CH_3COO)_2 \cdot 4H_2O$ at room temperature.

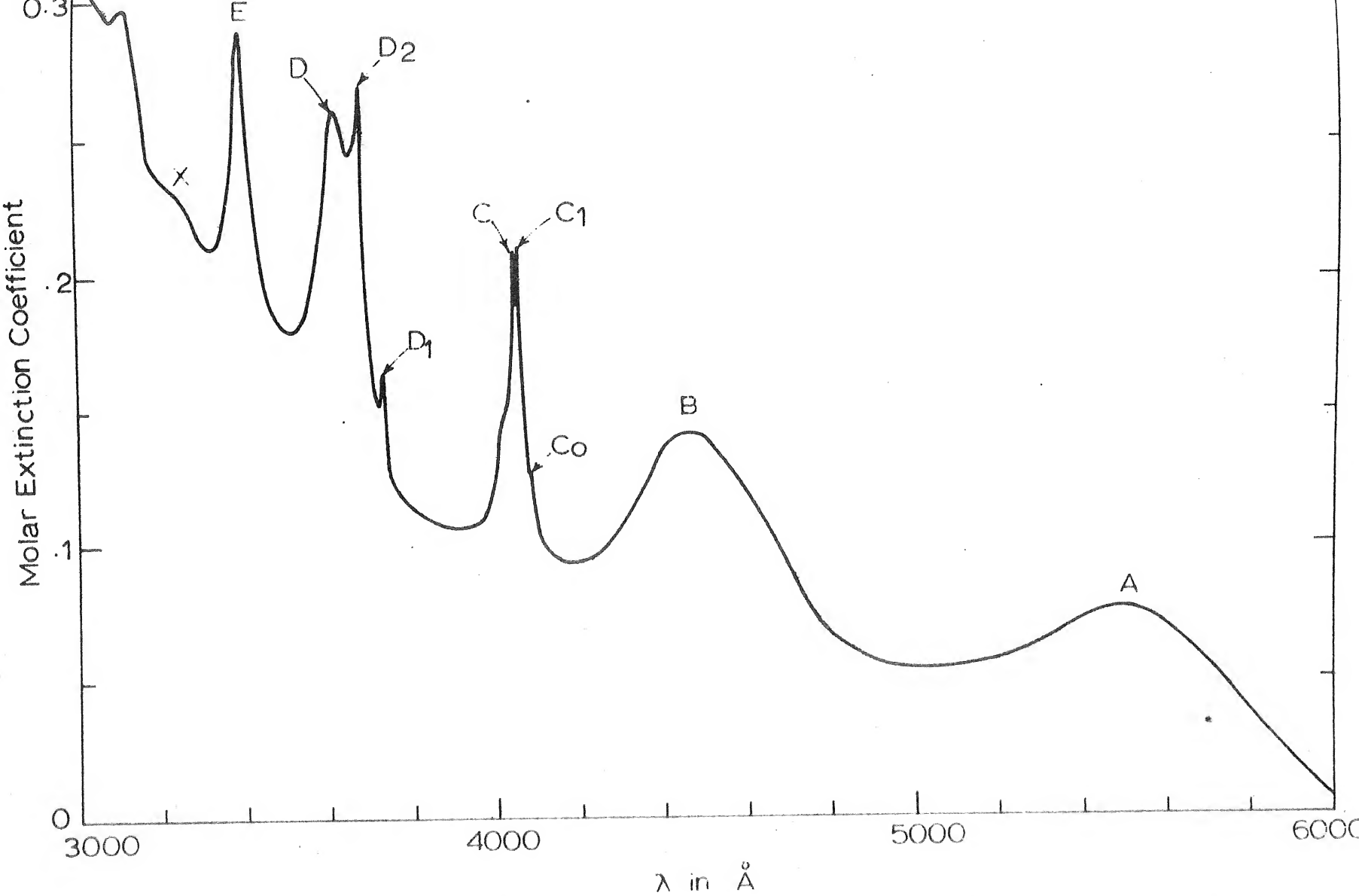

Fig. 4.2 Absorption spectrum of $Mn(CH_3COO)_2 \cdot 4H_2O$ at liquid nitrogen temperature.

Table 4.1

Experimental data and analysis of the absorption spectrum of $Mn(CH_3COO)_2 \cdot 4H_2O$ at room temperature.

Absorption peaks	Wave length A^o	Wave number cm^{-1}	Width[a] cm^{-1}	Transition $^6A_1(S) \rightarrow$	Calculated[b] energy cm^{-1}
A	5405	18,502	2000	$^4T_1(G)$	18,604
B	4400	22,727	1750	$^4T_2(G)$	22,709
C_o	4080	24,510			
C_1	4051	24,685	460	$^4A_1(G)$, $^4E(G)$	24,720
C	4042	24,740			
	4015	24,907			
D	3628	27,564	900	$^4T_2(D)$	27,770
E	3395	29,454	520	$^4E(D)$	29,396
F	3130	31,949		$^4T_1(P)$	32,108

a. Width at half intensity.

b. Calculated with B = 820, C = 3000, Dq = 760 and $\alpha = 76\ cm^{-1}$.

Table 4.2

Experimental data and analysis of the absorption spectrum of $Mn(CH_3COO)_2 \cdot 4H_2O$ at liquid nitrogen temperature.

Absorption peaks	Wave length A^o	Wave number cm^{-1}	Width[a] cm^{-1}	Transition $^6A_1(S) \rightarrow$	f-value[c] x 10^7	Calculated[b] energy cm^{-1}
A	5470	18,282	1800	$^4T_1(G)$	2.6	18,271
B	4450	22,472	1600	$^4T_2(G)$	3.7	22,502
C_o	4079	24,515		$^4A_1(G)$		
C_1	4049	24,697			1.3	24,720
C	4039	24,759		$^4E(G)$		
D	3622	27,609		$^4T_2(D)$	4.8	27,703
E_1	3490	29,336		$^4E(D)$	1.8	29,396
E	3392	29,481				
X	3225	31,008				
F	3125	32,000		$^4T_1(P)$		32,307

a. Width at half intensity.

b. Calculated with B = 820, C = 3000, Dq = 795 and $\alpha = 76\ cm^{-1}$.

c. Integrated band intensities are given.

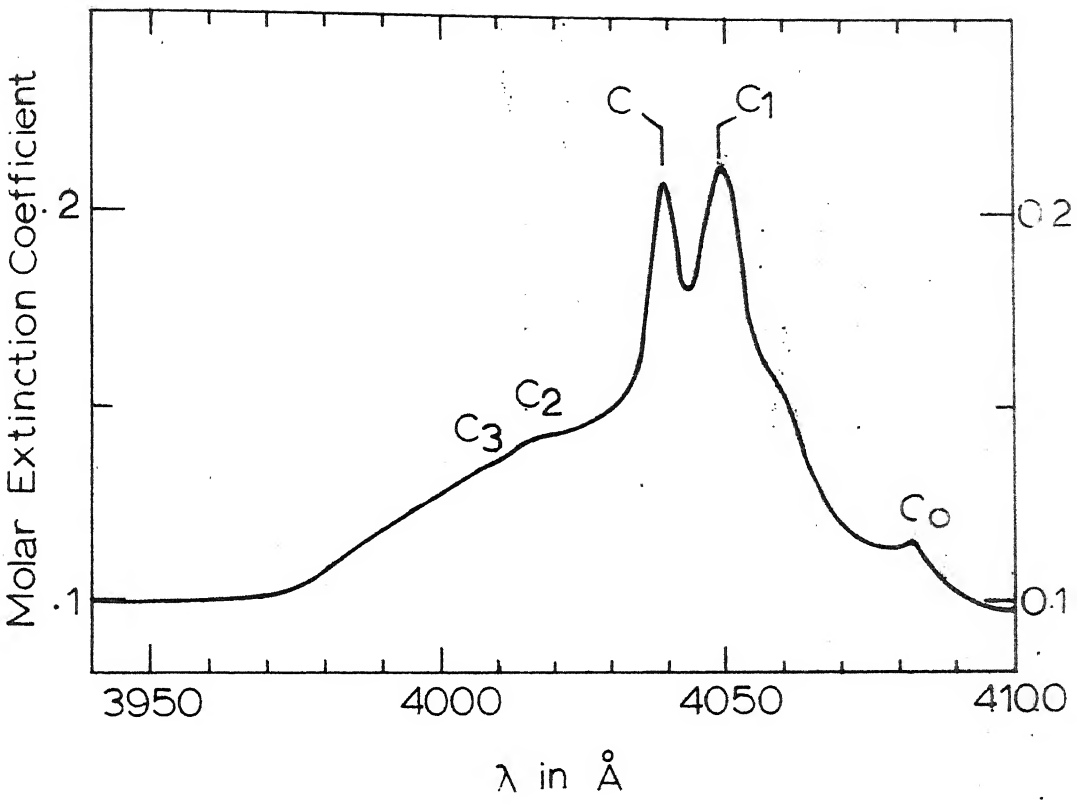

Fig. 4.3 $^6A_1(S) \rightarrow {}^4A_1(G)$, $^4E(G)$ band in $Mn(CH_3COO)_2 \cdot 4H_2O$ at liquid nitrogen temperature.

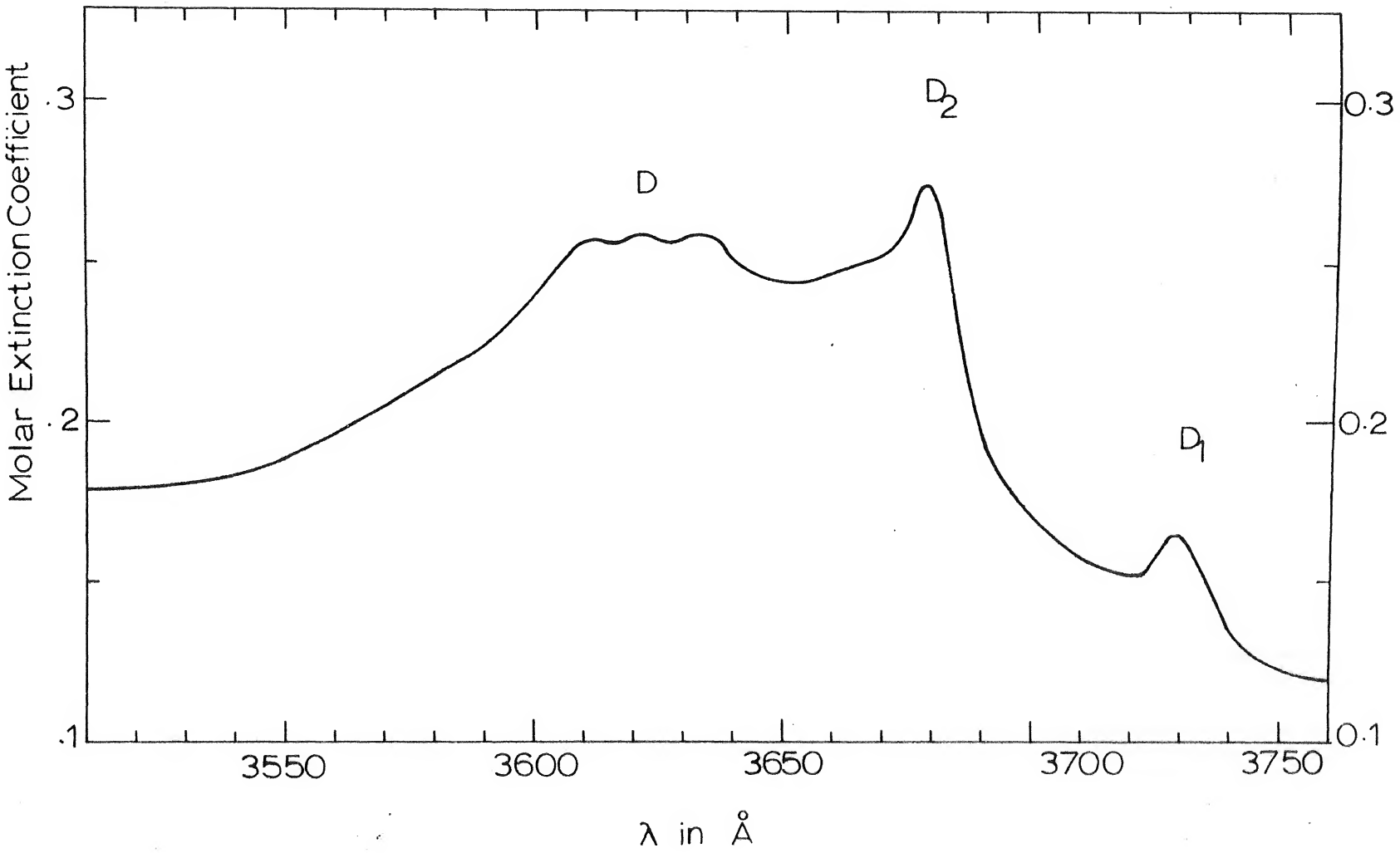

Fig. 4.4 $^6A_1(S) \rightarrow {}^4T_2(D)$ band in $Mn(CH_3COO)_2 \cdot 4H_2O$ at liquid nitrogen temperature.

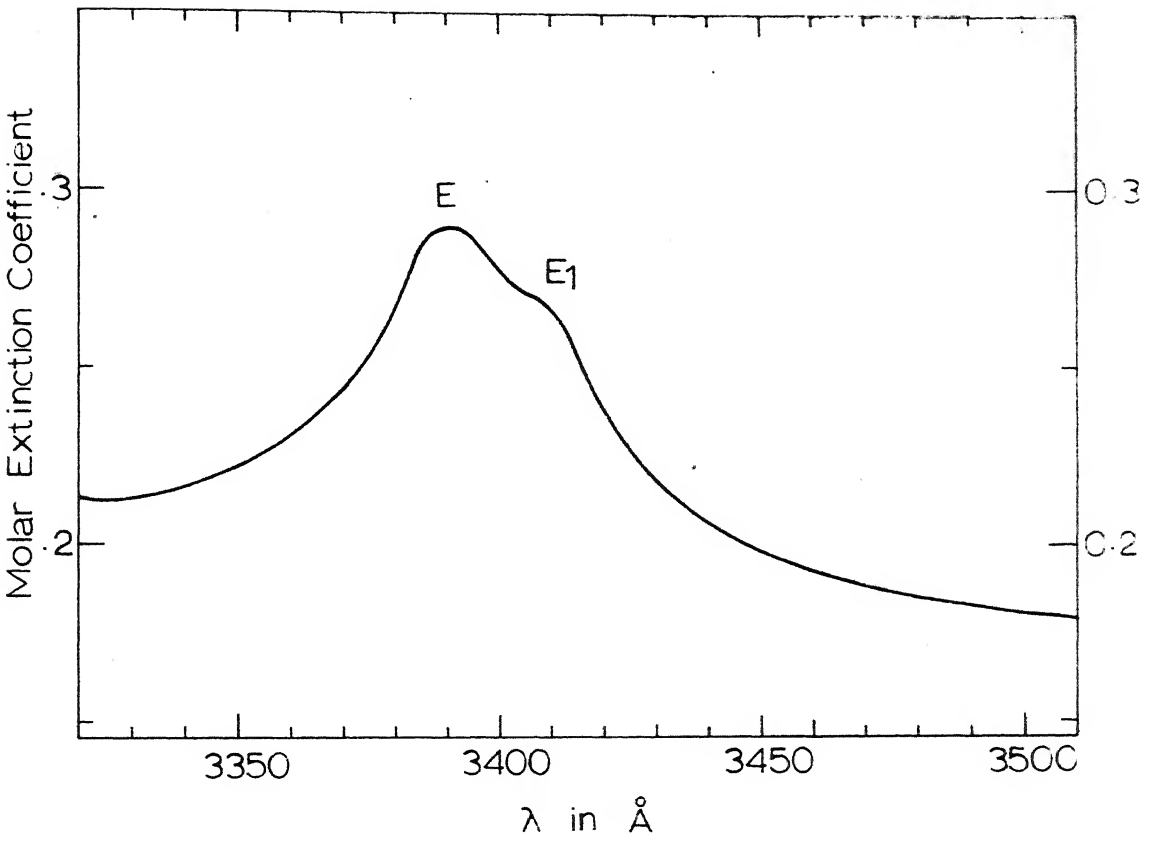

Fig. 4.5 $^6A_1(S) \rightarrow {}^4E(D)$ band in $Mn(CH_3COO)_2 \cdot 4H_2O$ at liquid nitrogen temperature.

Table 4.3

Fine structure of $^6A_1(S) \rightarrow (^4A_1(G), {}^4E(G))$ band in $Mn(CH_3COO)_2 \cdot 4H_2O$ at liquid nitrogen temperature. Tsujikawa's[55] notation and wavenumbers of lines at 4.2°K and E//a are given in the last column.

Absorption peaks	Wavelength A^o	Wavenumber cm^{-1}	Tsujikawa's wavenumber cm^{-1}
C_o	4079	24,515	S:24,496.1
	4058[a]	24,642	---
C_1	4049	24,697	Q_1:24,695.4 Q_2:24,708.5
C	4039	24,759	Q_3:24,756.9 Q_4:24,768.0
C_2	4016	24,901	---
C_3	4008	24,951	---

a. Observed as a weak shoulder.

considerable structure at liquid nitrogen temperature (Fig. 4.4 and Table 4.4). It shows two sharp lines D_1 and D_2 and a broad peak D which has three nearly equally spaced weak components.

The band E involving $^4E(D)$ level developes a weak shoulder E_1 on cooling (Fig. 4.5).

The true nature of the band F is masked by the heavy background absorption of the crystal (Fig. 4.2). It has probably $^4T_1(P)$ level for its upper state. An additional weak band marked X is seen around 3225A° in Fig. 4.2 but its upper state is not understood.

The crystal absorbs very heavily below 3000A° and therefore, no measurements could be performed in that region.

CUBIC FIELD CALCULATIONS

These calculations are discussed in detail in the previous chapters II and III. There are four parameters B, C, Dq and α. The parameter α is fixed at $76cm^{-1}$. Values of the adjustable parameters B, C and Dq for room temperature spectrum are found to be 820, 3000 and $760cm^{-1}$ respectively. The calculated energies are compared with the observed ones in Table 4.1. A schemetic transition diagram is drawn in Fig.4.6.

Parameters for liquid nitrogen temperature spectrum are B = 820, C = 3000, Dq = 795 and $-\alpha = 76cm^{-1}$. The shifts of bands C and E whose energies depend on the

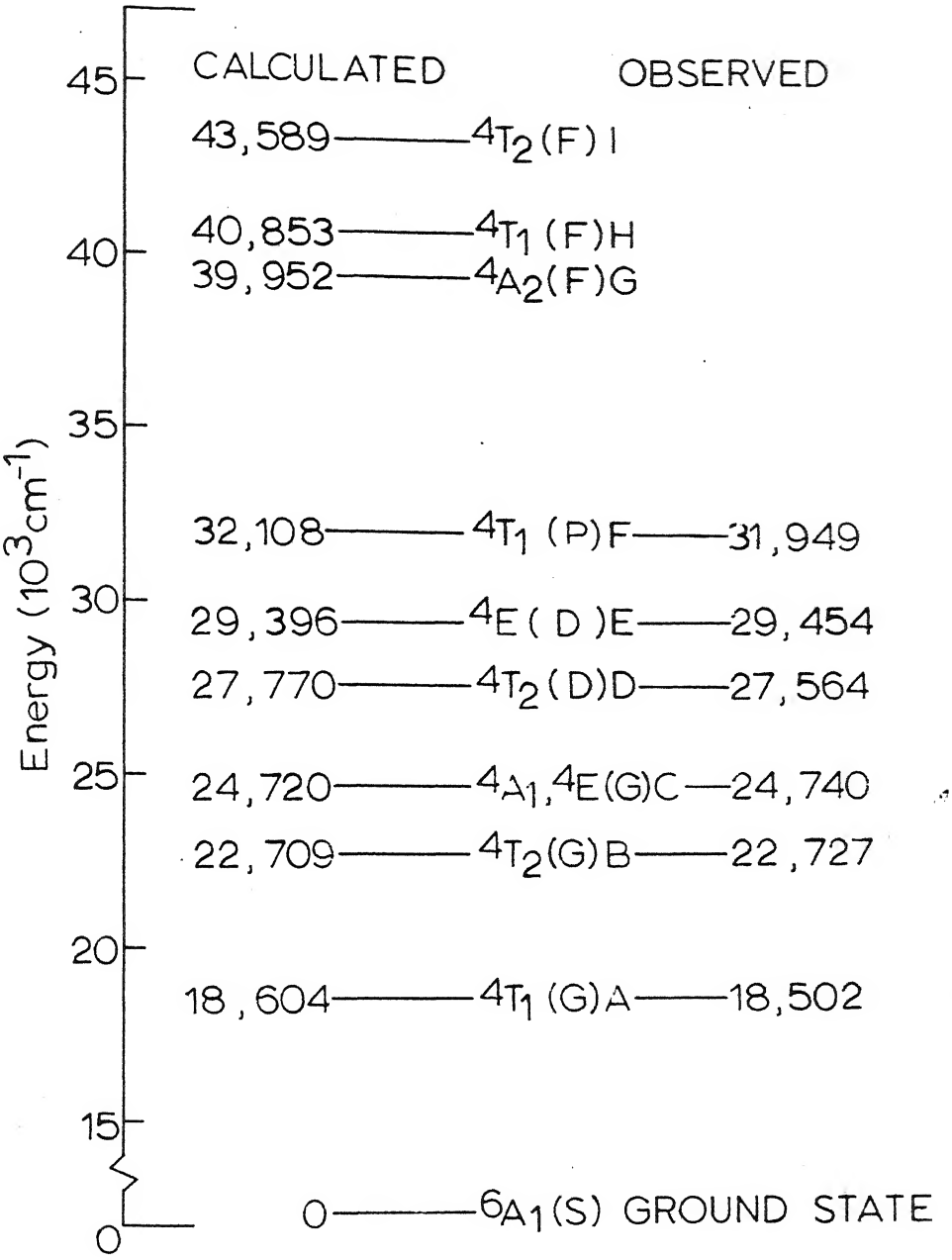

Fig. 4.6 Schemetic transition diagram for the absorption spectrum of $Mn(CH_3COO)_2 \cdot 4H_2O$ at room temperature. The calculated levels are for B= 820, C = 3000, Dq = 760 and α= 76 cm^{-1}.

parameters B and C only, are quite small on cooling the crystal and accordingly the parameters B and C have same values at both the temperatures. The slight increase in the Dq value over its room temperature value is responsible for the red shifts of A and B bands.

The agreement between the calculated and observed energies is satisfactory at both the temperatures. (Tables 4.1 and 4.2).

ANALYSIS OF THE FINE STRUCTURE: THEORETICAL FORMULATION

The interpretation of fine structure in the present case can be expected to be complicated and also difficult since the spin-orbit interaction, the vibrations and the lower symmetry field can all cause a splitting of the cubic field levels. We shall first find the possible splittings due to each of these and shall then try to analyse the observed structure taking all of these to be simultaneously present.

A. Spin Orbit Splitting

We have found in Chapter III that the spin orbit coupling parameter ξ in $RbMnF_3$ is $320cm^{-1}$. The ξ value in the present water coordinated case is expected to be only slightly smaller than this as F^- and H_2O lie quite close in the nephelauxetic series. This can be verified by considering the nephelauxetic decrease in the energy of the transition $^6A_1(S) \rightarrow (^4A_1(G)$,

$^4E(G)$) in going from $RbMnF_3$ to the present case. This decrease is negligible and less than 0.3 per cent. We shall therefore, assume the ξ value in the present case to be the same as in $RbMnF_3$. Because of this the magnitudes of spin orbit splittings here may be expected to be about the same as in $RbMnF_3$ (the spin orbit splittings for $RbMnF_3$ are given in Table 3.10).

B. Vibrational Modes of the Crystal

An exact analysis of the vibrational modes of the crystal is not possible, and for simplification we make an assumption of treating Mn^{2+} as surrounded by a regular octahedron of water molecules. The problem then reduces to finding the vibrational modes of an octahedron of water molecules which has been discussed in considerable detail by Koide and Pryce.[37] Possible modes found by them are A_{1g}, E_g, T_{2g}, T_{1u}, T_{1u} and T_{2u}. Out of these only last three have odd symmetry and their frequencies have been named as ν_3, ν_4 and ν_6 respectively. Koide and Pryce[37] theoretically find that $\nu_3 = 2\nu_6$ and $\nu_3 \sim 170cm^{-1}$, $\nu_4 \sim 320$ to $400cm^{-1}$ and $\nu_6 \sim 85cm^{-1}$. From the vibrational analysis of the optical spectrum of $MnSiF_6 \cdot 6H_2O$, Tsujikawa[44] finds the three vibrational frequencies as 80, 235, 350 cm^{-1}. These results are summarised in Table 4.5.

The observed separations in the expected vibrational structure can be equal to the vibrational frequencies as well as to the sum and differences of the individual

Table 4.5

Frequencies of odd symmetry vibrational modes of an octahedron of water molecules.

Symmetry	Name	Frequency	
		Theoretical Koide and Pryce's (cm^{-1})	Experimental Tsujikawa's (cm^{-1})
T_{1u}	ν_3	170	235
T_{1u}	ν_4	320 to 400	350
T_{2u}	ν_6	85	80

Table 4.6

Splitting of cubic field levels in tetragonal and rhombic symmetries.

O	D_4	C_2
A_1	A_1	A
A_2	B_1	B
E	$A_1 + B_1$	A + B
T_1	$A_2 + E$	A + 2B
T_2	$B_2 + E$	2A + B

vibrational frequencies.

C. Lower Symmetry Fields

The degenerate cubic field levels can split in lower symmetries. If the symmetry is as low as rhombic all the final levels will be orbital singlets. The expected splittings of the cubic field levels under tetragonal and rhombic perturbations are given in Table 4.6.

ANALYSIS OF THE FINE STRUCTURE: INTERPRETATION

While considering all ~~the~~ three, the spin orbit interaction, the vibrations and the lower symmetry fields, to be present, the main problem is the relative magnitudes of the three. We have estimated the order of magnitudes of spin orbit and vibrational parts but it is very hard to make any guess or find theoretically the order of splitting due to the lower symmetry fields. The theoretical order of splittings in a tetragonal field has been estimated by Goode[33] and we shall make use of that.

A. $^6A_1(S) \rightarrow {}^4E(D)$ Transition:

The band E assigned to this transition has a shoulder E_1 separated by nearly 145 ± 10 cm^{-1} from the peak E. It can not be spin orbit in origin since the spin orbit components of $^4E(D)$ level spread over less than $40cm^{-1}$. This can not be a part of simple vibrational

progression since the separation is not close to any one of the expected vibrational frequencies. However, the separation can be represented as the difference $\nu_4 - \nu_3$ as well as $\nu_3 - \nu_6$ if one uses the frequency values reported by Tsujikawa (Table 4.5). This indicates that different vibrational modes may be effective in inducing the transitions.

In lower symmetries this state splits into two orbital singlets. Goode[33] calculated a splitting of 53cm^{-1} for moderate tetragonal perturbations. A large perturbation due to lower symmetry combined with spin orbit splitting may account for the observed separation between E and E_1 but in our view the shoulder E_1 is more likely to be vibrational in origin.

B. $^6A_1(S) \rightarrow (^4A_1(G), {}^4E(G))$ Transition:

In the band C assigned to this transition, the lines C_0, C_1 and C are seen to be quite prominent and sharp. Tsujikawa[55] has found that at very low temperature C and C_1 separately get further resolved into two components; C_1 gets resolved into two peak Q_1 and Q_2 and C into Q_3 and Q_4. The separations Q_2-Q_3 are nearly same $\sim$ 12 cm^{-1}.

There are three cubic field levels, the ground state $^6A_1(S)$, and the two upper states $^4A_1(G)$ and $^4E(G)$, whose splitting under the combined action of spin orbit and lower symmetry one has to consider for explaining

the presence of above mentioned lines. The ground state $^6A_1(S)$ can split into three Kramers doublets, and ground state splitting is directly measurable in the paramagnetic resonance experiments. In most of the cases it is found to be less than 1 cm^{-1}. The splitting being so small, can be neglected in the present analysis and the ground state considered as essentially unsplit. $^4A_1(G)$ state can atmost split into two Kramers doublets but the state being an orbital singlet the total splitting is not expected to be more than $5cm^{-1}$. $^4E(G)$ state can split into four Kramers doublets. In lower symmetry an E state can split into two orbital singlets. Each of the orbital singlet can further split into two Kramers doublets under the spin orbit interaction because of the quartet spin multiplicity.

In our view the lines C and C_1 come from $^4E(G)$ state and the line C_o comes from $^4A_1(G)$ state. A probable analysis of the splitting of the $^4E(G)$ state for explaining the C and C_1 lines is as follows. Because of the lower symmetry the state first splits into two orbital singlets to which the lines C and C_1 may be assigned. Under the spin orbit interaction each of the orbital singlet further splits into two Kramers doublets. The lines Q_1 and Q_2 of Tsujikawa may be assigned to the two Kramers doublets arising from the orbital singlet corresponding to the line C_1 and likewise

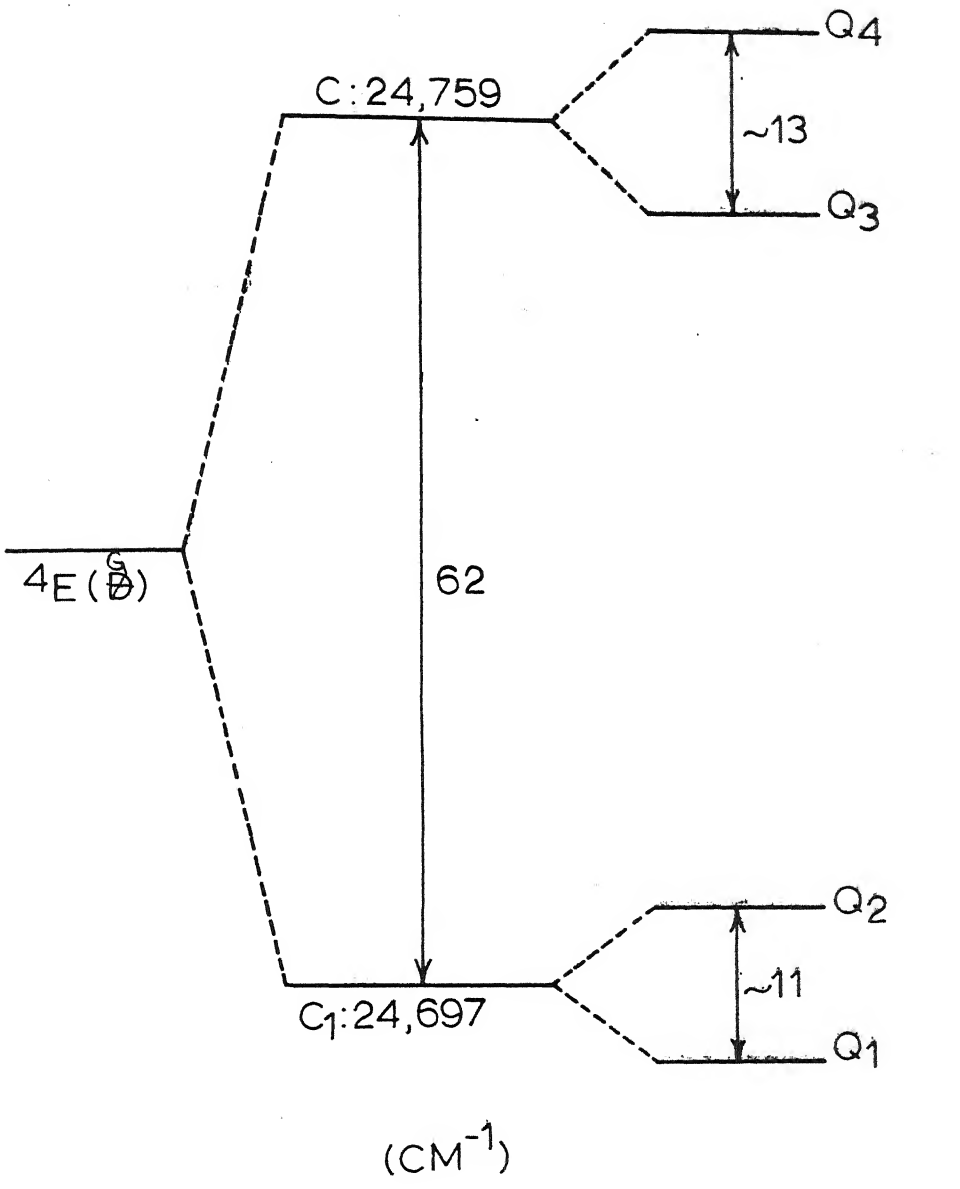

Fig. 4.7 Splitting of $^4E(G)$ level in $Mn(CH_3COO)_2 \cdot 4H_2O$.

the lines Q_3 and Q_4 may be the Kramers doublets arising from C. The separations Q_2-Q_1 and Q_4-Q_3 are of the expected order of spin orbit splitting. The comparatively larger separation of 62cm^{-1} between C and C_1 i.e. the orbital singlets suggest that the lower symmetry perturbation is larger than the spin orbit interaction. The qualitative splitting diagram is drawn in figure 4.7.

A lower symmetry perturbation does not directly split the $^4A_1(G)$ state. The state splits into two Kramers doublets only after the inclusion of spin orbit interaction but at a higher order perturbation. This splitting should therefore, be quite small, < 5 cm^{-1}, and hence not observed in the line B_0 corresponding to this state.

As indicated earlier, the broad shoulder around 4015A$^{\circ}$ gets resolved at low temperature into two components whose separation is nearly equal to the separation between C and C_1 lines. It is possible that these two resolved components may arise due to the coupling of same type of vibrational mode with the upper electronic levels of C and C_1.

C. $^6A_1(S) \rightarrow {}^4T_2(D)$ Transition:

Fine structure at low temperature of the band D assigned to this transition is given in Fig. 4.9. The components of this band are spread over more than 900cm^{-1}. This can not be solely due to the spin orbit

interaction since the spin orbit components are expected to spread over only 350cm^{-1}. In Chapter III we have found that the structure of $^4T_2(D)$ level is resolved in $RbMnF_3$ also. However, the components in $RbMnF_3$ are spread over only 400cm^{-1} while in the present case the total spread is more than 900cm^{-1}. This clearly shows that the lower symmetry perturbation which is absent in $RbMnF_3$, is quite prominent in the present case.

Under the tetragonal perturbation $^4T_2(D)$ state splits into an orbital singlet and a doublet. The orbital doublet can further split into two singlets if rhombic perturbation is also present. Each of the three orbital singlets can split into two Kramers doublets due to the spin orbit interaction. Fig. 4.4 shows that there are three intense lines D_1, D_2, and D. It is quite likely that these three lines may represent the three orbital singlets of rhombic field. In the peak D a further splitting into three equally spaced components with average separation around 80cm^{-1} is observed. This probably is the vibrational structure of the upper electronic state of the line D. It seems to be a simple vibrational progression whose average separation 80cm^{-1} is quite close to the ν_6 vibrational frequency. The other weak shoulders in this band could be spin orbit or vibrational in nature.

A further detailed study of this band under the polarized light is needed for any definite analysis. However, from the large extension of the fine structure we conclude that the perturbation due to the low symmetry field is quite large. Such a large low symmetry field will give rise to appreciable ground state splitting and paramagnetic resonance studies are desirable to confirm this.

CHAPTER V

ABSORPTION SPECTRUM OF Mn^{2+}-DOPED ALKALI HALIDES

CHAPTER V

ABSORPTION SPECTRUM OF Mn^{2+}-DOPED ALKALI HALIDES

INTRODUCTION

Very little work has been done on the absorption spectra of Mn^{2+}-doped alkali halides. This is perhaps because of the weak intensities of Mn^{2+} bands which makes their observation difficult for normal concentrations of the impurity ion. Recently, Kuwabara and Aoyagi[58] have observed a few bands in the ultraviolet region in Mn^{2+}:NaCl, but these are considered by them as charge transfer bands and not the usual crystal field bands of Mn^{2+}. In the present work the spectra of alkali halide crystals having high concentrations of Mn^{2+} have been studied and the bands characterstic of Mn^{2+} absorption in the visible region have been observed.

Paramagnetic resonance of Mn^{2+} in alkali halides has been studied extensively. Watkins[59] and more recently Shrivastava and Venkateswarlu[60] studied the electron spin resonance of Mn^{2+}:NaCl and Mn^{2+}:KCl. They have found in NaCl that depending upon concentration and heat treatment, the manganese could exist as a metallic precipitate, as substitutional Mn^{2+} near a first neighbor or second neighbor alkali vacancy, as Mn^{2+} near an impurity or as isolated Mn^{2+}. All these features except that of Mn^{2+} near an impurity were observed in Mn^{2+}:KCl.[59] In manganese-doped KCl Watkins[59]

observed an additional resonance in the cloudy areas of the crystal which contained a higher percentage of manganese and attributed it to K_4MnCl_6. However, the spin resonance studies are performed with smaller concentration of Mn^{2+} while the concentrations of Mn^{2+} used in the present optical studies are comparatively higher. At high concentrations, besides the entry of Mn^{2+} as substitutional impurity, the formation of some complexes of manganeus and alkali halides like K_4MnCl_6, $KMnCl_3$, and $NaMnCl_3$ is also possible. Because of the several possibilities for the symmetry around Mn^{2+} in the crystals we shall discuss the observed spectra and fine structure only qualitatively.

EXPERIMENTAL

The alkali halide crystals doped with various concentrations of Mn^{2+} were grown from melt by the Bridgeman method. The absorption spectra were recorded with a Cary-14 spectrophotometer at room temperature and also at liquid nitrogen temperature. The concentrations of manganese in the grown crystals could not be determined. The amount of dopant added varied from0.1 to 10 mole percent. Large single crystals could only be grown for smaller concentrations of the impurity. The high concentration crystals used in the measurements were of comparatively smaller dimensions because of the difficulty in growing large homogenous crystals and also because of the high background absorption which did not allow

the use of very thick samples particularly in the ultraviolet region.

RESULTS

The crystals grown with low impurity concentration (< 1 mole per cent) are quite clear and do not show any Mn^{2+} bands in the visible region. Such crystals of Mn^{2+}:KCl and Mn^{2+}:RbBr show a few bands in the ultraviolet region which are given in Figs. 5.1 and 5.2 at room temperature. These spectra are perhaps charge transfer spectra of the type reported by Kuwabara and Apyan[58] in Mn^{2+}:NaCl. We could not observe these bands in Mn^{2+}:NaCl or in any other alkali halide crystal with low impurity concentration.

The effect of increasing dopant concentration was studied only in NaCl and KCl. On increasing the dopant concentration (between 1 to 5 mole per cent) the grown crystals of both NaCl and KCl tend to become milky in appearance and some sort of white complex also seems to be formed. In KCl this is perhaps due to the formation of K_4MnCl_6 as proposed by Watkins.[59] These homogeneously milky crystals do not show any band in the visible region or in the ultraviolet region.

A further increase in the dopant concentration (> 5 mole per cent) causes a deterioration in the quality of grown crystal. The grown crystals are not completely homogenous and some sort of amorphous pink deposit on the top of grown bulk crystal which penetrates even

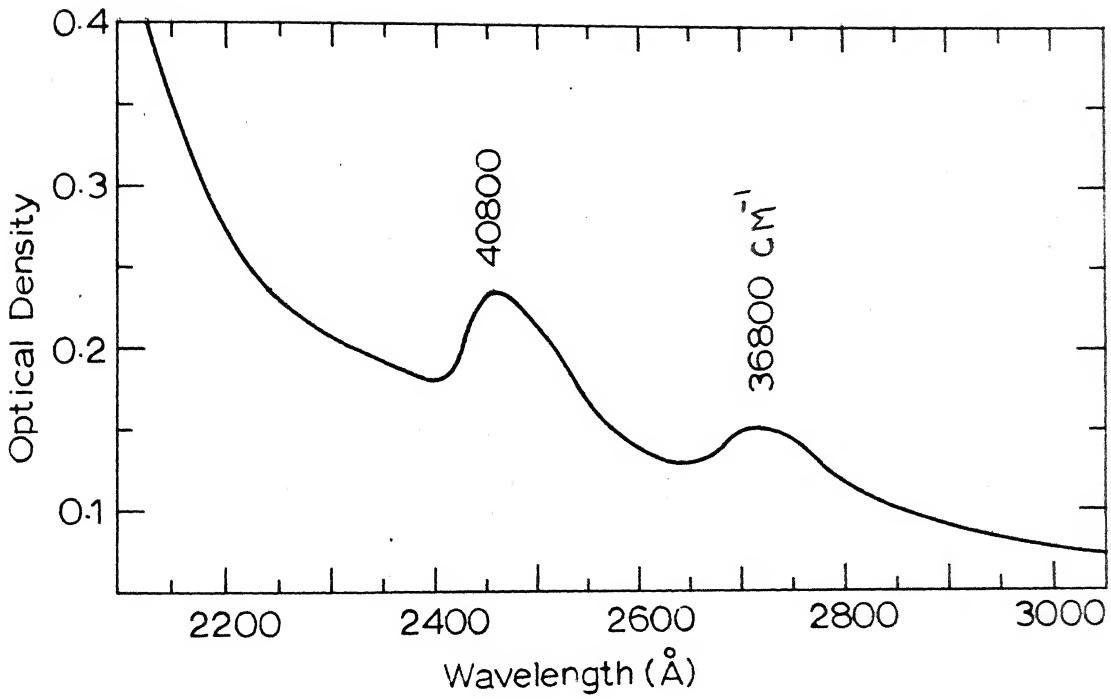

Fig. 5.1 Absorption spectrum in the ultraviolet region at room temperature of KCl crystal having low manganese concentration.

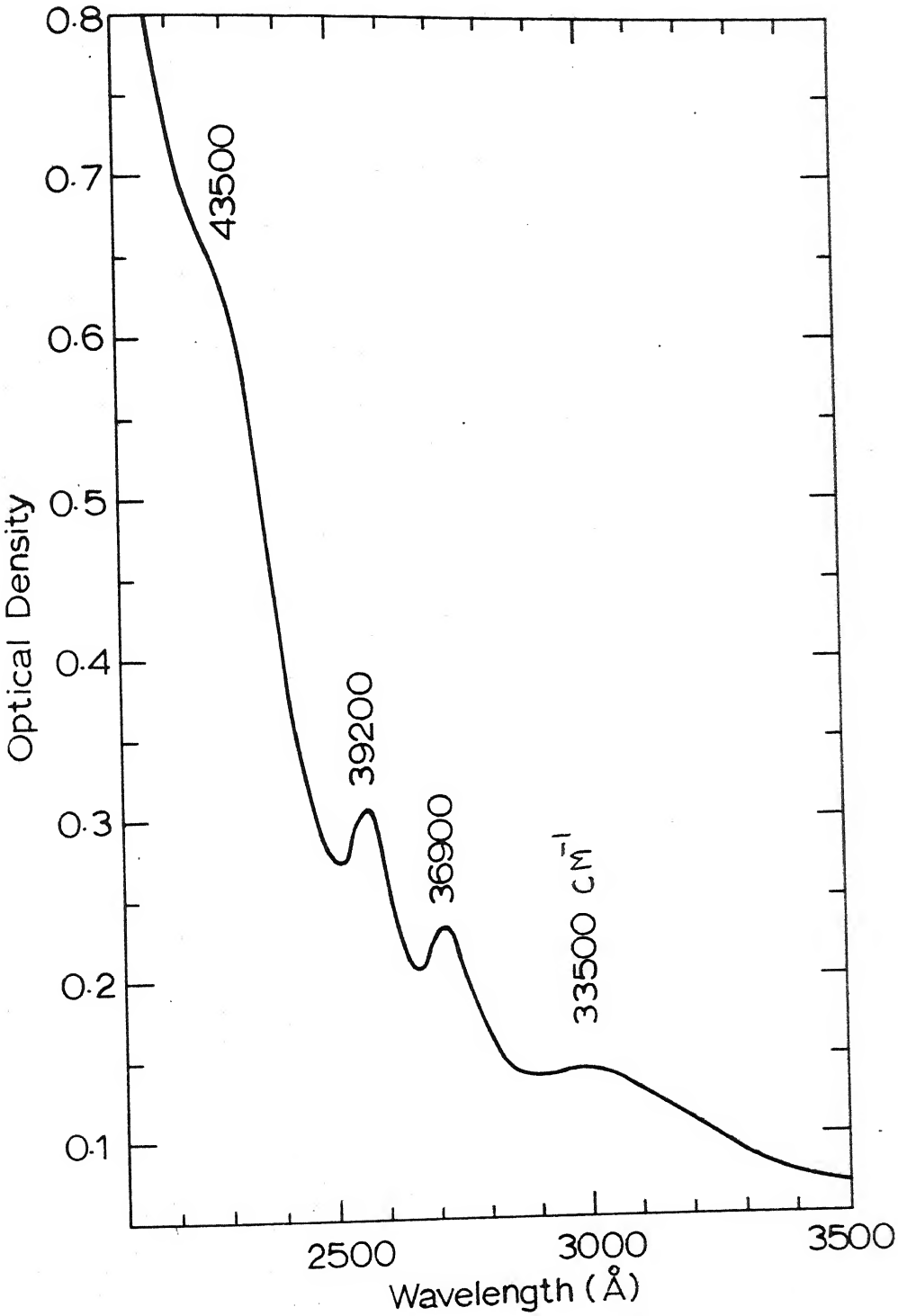

Fig. 5.2 Absorption spectrum in the ultraviolet region at room temperature of a RbBr crystal having low manganese concentration.

inside the lower crystalline portion is seen in both Mn^{2+}: NaCl and Mn^{2+}:KCl. The pink deposit could be some complex of the mixed halides. However, the bottom and central portions of the grown pieces were in the form of single crystals with a few small sized yellowish pink spots. The best crystals out of these were chosen for the optical absorption measurements which are described below.

The spectrum of one such crystal of Mn^{2+}:KCl at room temperature has been reported recently[61], and a copy of that article is given as Appendix IV in this thesis. The results on another crystal having larger concentration of impurity centers are described here. Except for the higher intensities of the bands in the spectrum of the present sample, the spectrum reported here is same as the one reported earlier. Fig. 5.3 and 5.4 show the visible region spectrum of the present sample and Tables 5.1 and 5.2 give the results of measurements at room temperature and liquid nitrogen temperature respectively. Two bands are observed in the ultraviolet region which are shown in Fig. 5.5 at room temperature. The positions and nature of these bands are different from the ultraviolet region bands shown in Fig. 5.1 observed in KCl having low concentration of impurity. This makes one conclude that absorbing Mn^{2+} centers in the two cases have different nature.

No fine structure is observed in any of the bands

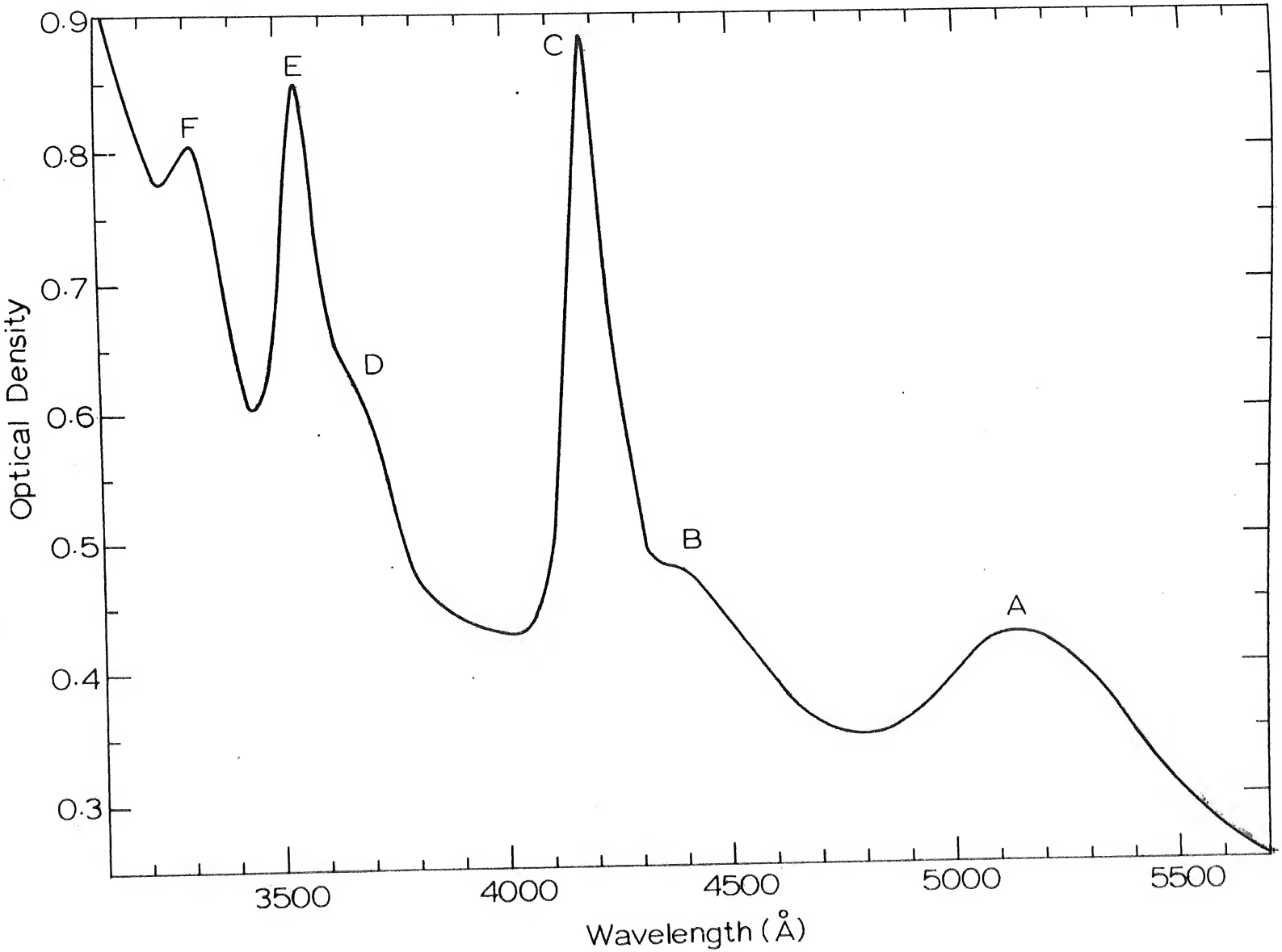

Fig. 5.3 Absorption spectrum of Mn^{2+}: KCl at room temperature.

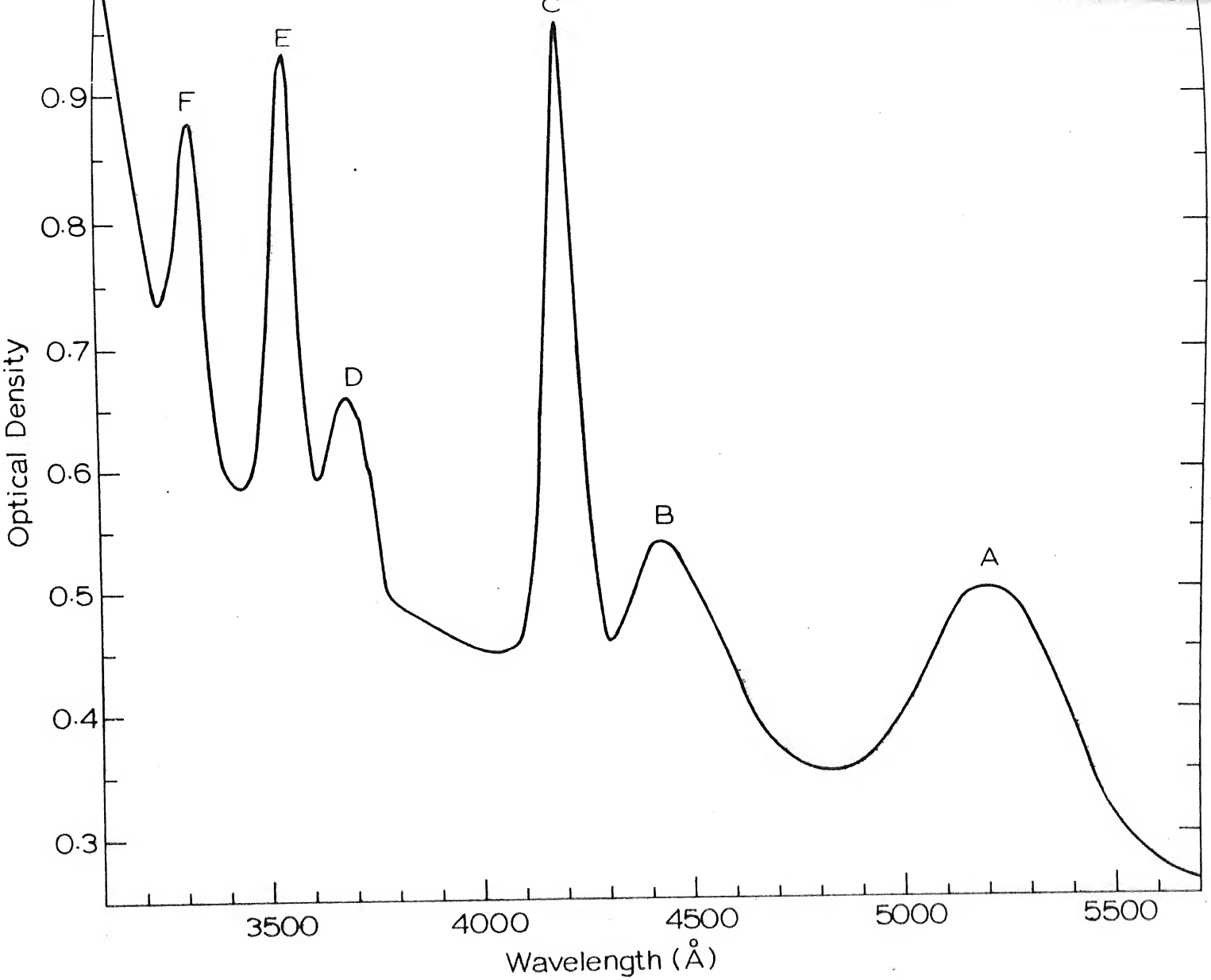

Fig. 5.4 Absorption spectrum of Mn^{2+}: KCl at liquid nitrogen temperature.

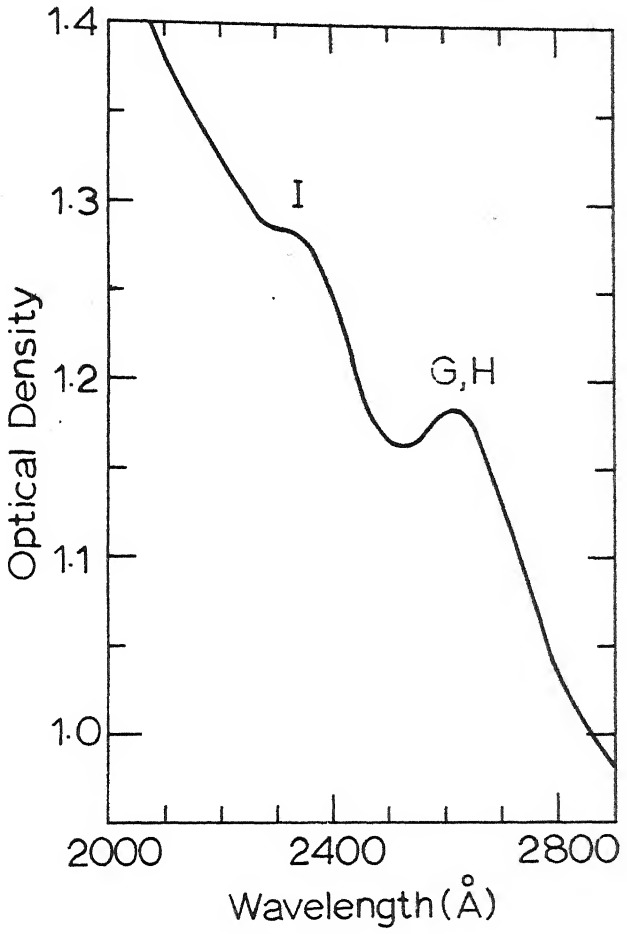

Fig. 5.5 Absorption spectrum of Mn^{2+}:KCl in the ultraviolet region at room temperature.

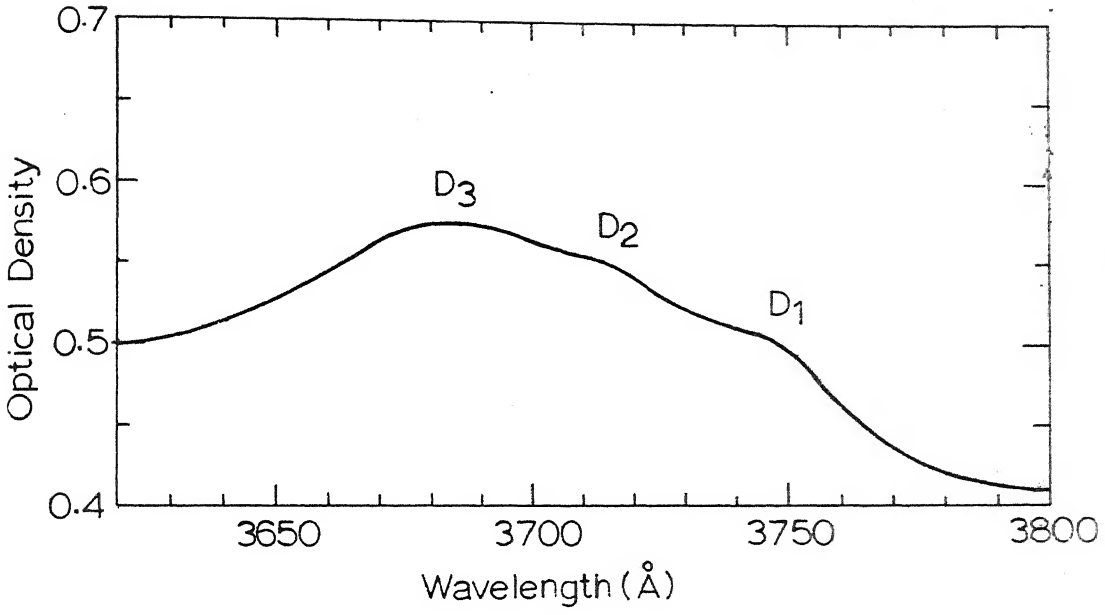

Fig. 5.6 $^6A_{1g}(S) \rightarrow {}^4T_{2g}(D)$ band in Mn^{2+}:KCl at liquid nitrogen temperature.

Table 5.1

Experimental data and analysis of the absorption spectrum of Mn^{2+}:KCl at room temperature.

Absorption peaks	Wave-length A^o	Wave-number cm^{-1}	Width cm^{-1}	Transition: $^6A_{1g}(S) \rightarrow$	Remark[a]	Calculated[b] energy cm^{-1}
A	5180	19,305	1900	$^4T_{1g}(G)$	b	19,403
B	4405	23,700		$^4T_{2g}(G)$	h	22,656
C	4187	23,882	660	$^4A_{1g}(G)$ $^4E_g(G)$	s	23,845
D	3675	27,210		$^4T_{2g}(D)$	h	26,931
E	3554	28,137	770	$^4E_g(D)$	s	28,151
F	3331	30,020		$^4T_{1g}(P)$		30,103
G	2600	38,500		$^4A_{2g}(F)$		38,317
H				$^4T_{1g}(F)$		38,862
I	2340	42,700		$^4T_{2g}(F)$	b	40,766

a. Abbreviations: s, sharp; h, hump; b, broad.

b. Calculated for B=760, C=2955, Dq=590 and α=76cm^{-1}.

Table 5.2

Experimental data and analysis of the absorption spectrum of Mn^{2+}:KCl at liquid nitrogen temperature.

Absorption peaks	Wave length A^{o}	Wave number cm^{-1}	Width cm^{-1}	Relative intensity	Transition $^6A_{1g}(S) \rightarrow$	Calculated energy[a] cm^{-1}
A	5210	19,194	1350	2.8	$^4T_{1g}(G)$	19,196
B	4435	22,547	1150	2.2	$^4T_{2g}(G)$	22,571
C	4182	23,911	450	2.9	$^4A_{1g}(G)$ $^4E_g(G)$	23,925
D_1	3740	26,738				
D_2	3708	26,970			$^4T_{2g}(D)$	26,921
D_3	3685	27,136				
E	3545	28,209	520	2.1	$^4E_g(D)$	28,202
F	3325	30,075	700	1.6	$^4T_{1g}(P)$	30,31[illegible]

a. Calculated for B=763, C=2955, Dq=615 and α=76cm^{-1}.

except in the case of the band D involving $^4T_{2g}(D)$ level. It appears that this band at liquid nitrogen temperature consists of three very weak components shown in Fig. 5.6. It may be noted that no structure is observed even in the two sharp bands C and E.

In contrast to Mn^{2+}:KCl, the spectrum of Mn^{2+}:NaCl is very rich in fine structure. The visible region spectra of Mn^{2+}:NaCl at room and liquid nitrogen temperatures are given in Figures 5.7 and 5.8 and the corresponding results of measurements are given in Tables 5.3 and 5.4. The positions of the two bands observed in the ultraviolet region are given in Table 5.3 at room temperature. This ultraviolet spectrum is different from the one reported by Kuwabara and Aoyagi[58] (see Table 5.3). Here again like Mn^{2+}:KCl one may conclude that the absorbing centers are of different type in the two cases.

The assignments of the bands to cubic field levels in both the cases, Mn^{2+}:KCl and Mn^{2+}:NaCl, are straightforward and are given in the tables along with the results of measurements. Fine structure of the bands will be discussed in the next section.

All the bands in Mn^{2+}:KCl and Mn^{2+}:NaCl show a decrease in width and intensity on cooling, indicating thereby that the transitions are vibrationally assisted ones.

Since the concentration of Mn^{2+} could not be

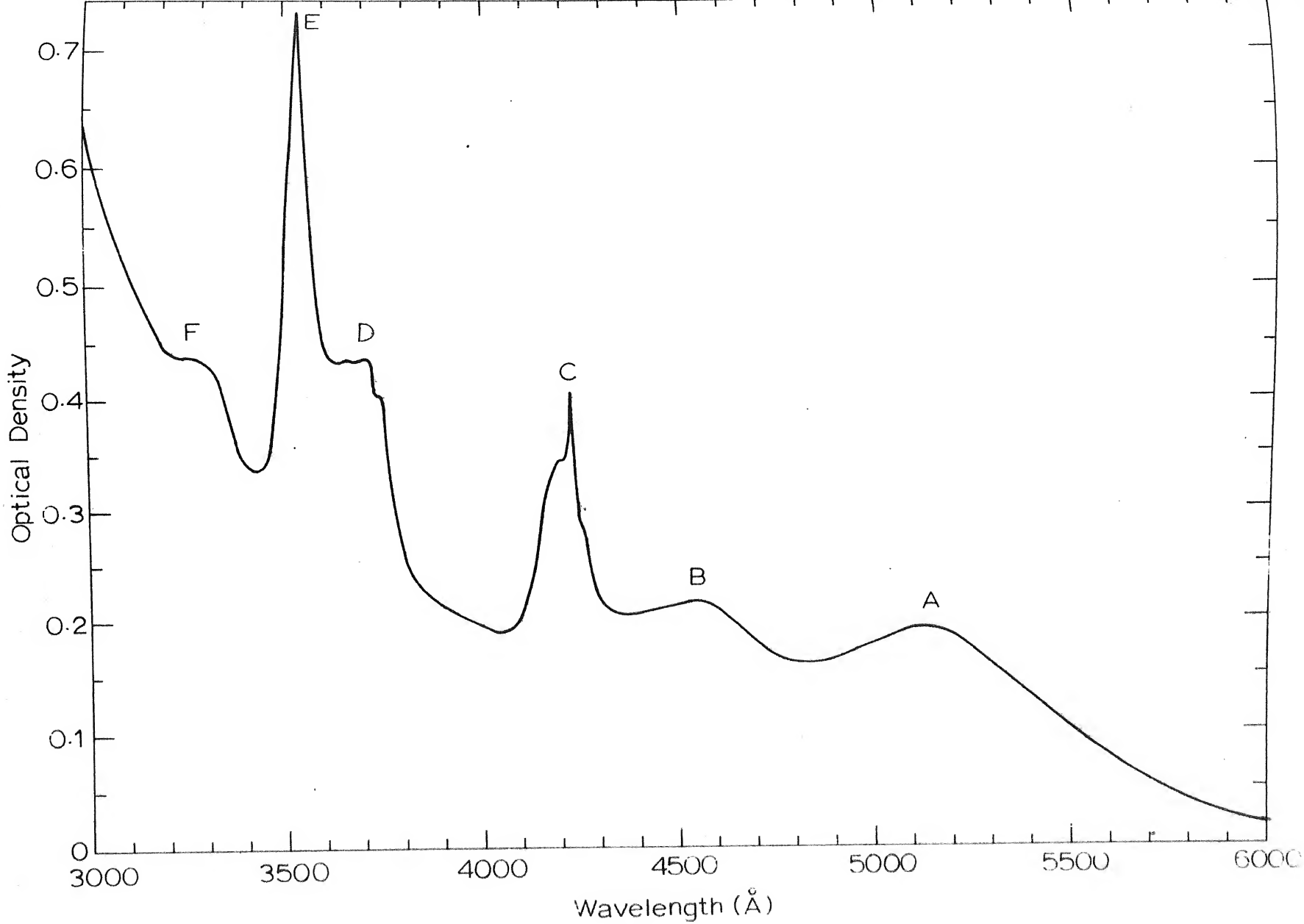

Fig 5.7 Absorption spectrum of Mn^{2+} NaCl at room temperature

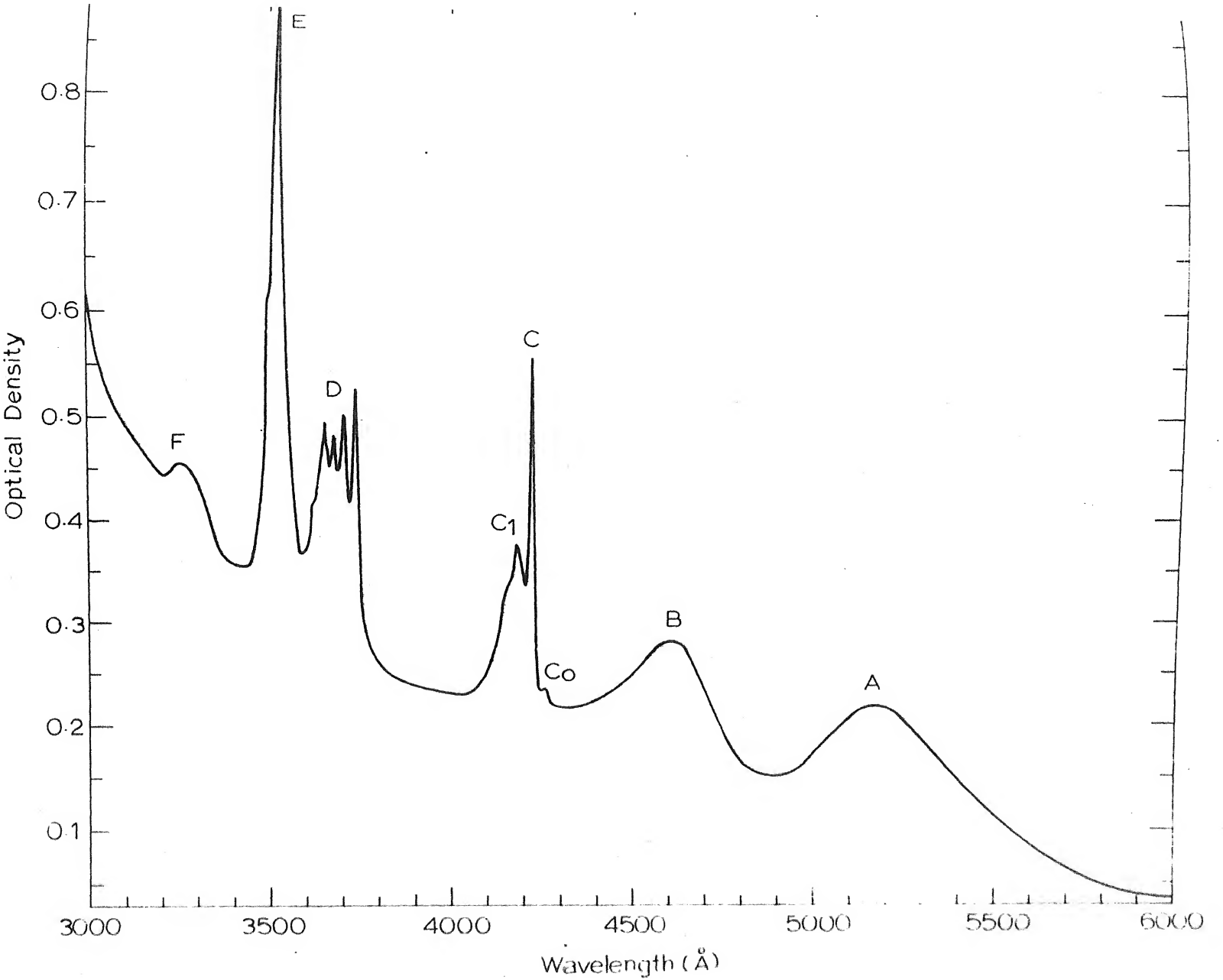

Fig. 5.8 Absorption spectrum of Mn^{2+} : NaCl at liquid nitrogen temperature

Table 5.3

Experimental data and analysis of the absorption spectrum of Mn^{2+}:NaCl at room temperature.

Absorption peaks	Wave length A^o	Wave number cm^{-1}	Transition. $^6A_{1g}(S) \rightarrow$	Calculated[a] energy cm^{-1}
A	5150	19,417	$^4T_{1g}(G)$	19,042
B	4550	21,978	$^4T_{2g}(G)$	22,510
C_o	4252	23,518	$^4A_{1g}(G)$	
C	4217	23,714	$^4E_g(G)$	23,870
C_1	4178	23,935		
D	3708	26,970	$^4T_{2g}(D)$	26,960
E	3530	28,329	$^4E_g(D)$	28,266
F	3270	30,581	$^4T_{1g}(P)$	30,216
G	2550	39,200[b]	$^4A_{2g}(F)$	38,442
H			$^4T_{1g}(F)$	39,042
I	2445	40,969[b]	$^4T_{2g}(F)$	41,108

a. Calculated for B=780, C=2910, Dq=620, and α=76cm^{-1}.

b. Wavenumbers of the four ultraviolet bands observed by Kuwabara and Aoyagi[58] at liquid nitrogen temperature are 51,500, 45,500, 38,200, and 36,500cm^{-1}.

Table 5.4

Experimental data and analysis of the absorption spectrum of Mn^{2+}:NaCl at liquid nitrogen temperature.

Absorption peaks	Wave length A^o	Wave number cm^{-1}	Relative intensity	Transition $^6A_{1g}(S) \rightarrow$	Calculated[a] energy cm^{-1}
A[b]	5180	19,305	2.6	$^4T_{1g}(G)$	18,901
B[b]	4605	21,716	2.5	$^4T_{2g}(G)$	22,436
C_o	4253	23,512			
C	4216	23,720	1.7	$^4A_{1g}(G)$	23,870
C_1	4175	23,882		$^4E_g(G)$	
D	3707	26,977	3.3	$^4T_{2g}(D)$	26,924
E	3530	28,329	4.4	$^4E_g(D)$	28,266
F	3260	30,675		$^4T_{1g}(P)$	30,318
G	2550	39,200		$^4A_{2g}(F)$	38,442
H				$^4T_{1g}(F)$	39,075
I	2455	40,732		$^4T_{2g}(F)$	41,217

a. Calculated for B=780, C=2910, Dq=635, and α=76cm^{-1}.

b. Half widths of A and B bands are 1250 and 1100 cm^{-1} respectively (widths at half intensity).

determined in Mn^{2+}:KCl or in Mn^{2+}:NaCl, only the relative intensities of the bands are given which have been obtained by comparing the area under the absorption curves.

ANALYSIS OF THE SPECTRUM OF Mn^{2+}:KCl

Parameters for room temperature spectrum are B = 760, C = 2955, Dq = 590 and $\alpha = 76cm^{-1}$ while those for the spectrum at liquid nitrogen temperature come out as B = 763, C = 2955, Dq = 615 and $\alpha = 76cm^{-1}$. The calculated energies given in Tables 5.1 and 5.2 are fairly close to the observed ones.

The structure observed in the band arising from $^4T_{2g}(D)$ level might be due to the combined effect of spin-orbit, lower symmetry and vibrational perturbations.

CUBIC FIELD CALCULATIONS FOR Mn^{2+}:NaCl

Parameters for room temperature spectrum are B = 780, C = 2910, Dq = 620 and $\alpha = 76cm^{-1}$ and those for liquid nitrogen temperature spectrum are B = 780, C = 2910, Dq = 635 and $\alpha = 76cm^{-1}$. The shifts of sharp bands C and E on cooling are negligibly small and consequently the parameters B and C are expected to have about the same values at both the temperatures. The Dq dependent bands A and B show red shift on cooling and accordingly the Dq value at liquid nitrogen temperature is slightly higher than the Dq value at room temperature.

FINE STRUCTURE OF THE BANDS IN Mn^{2+}:NaCl

$^4E_g(D)$

Fig. 5.9 gives the record and Table 5.5 gives the wave numbers of the observed lines in the band involving $^4E_g(D)$ level at liquid nitrogen temperature. The lines E, E_1 and E_2 seem to form a simple vibrational progression since the differences E_1-E and E_2-E_1 are quite close. The average difference is 211cm^{-1}.

$^4T_{2g}(D)$

The band D involving $^4T_{2g}(D)$ level is shown in Fig. 5.10 at liquid nitrogen temperature and the wavenumbers of the observed lines at the same temperature are listed in Table 5.6. At first sight the structure here appears similar to that of an analogous band in $RbMnF_3$. However, it does not here seem to be simple spin orbit in origin since the separations between the lines are largerthan those expected from a pure spin orbit interaction. It is therefore probable that the site symmetry of Mn^{2+} is lower than cubic. Probably, the observed structure will have to be understood by taking the combined action of spin orbit interaction, low symmetry and vibrational coupling into consideration.

$^4A_{1g}(G)$, $^4E_g(G)$

Results at liquid nitrogen temperature for the band C

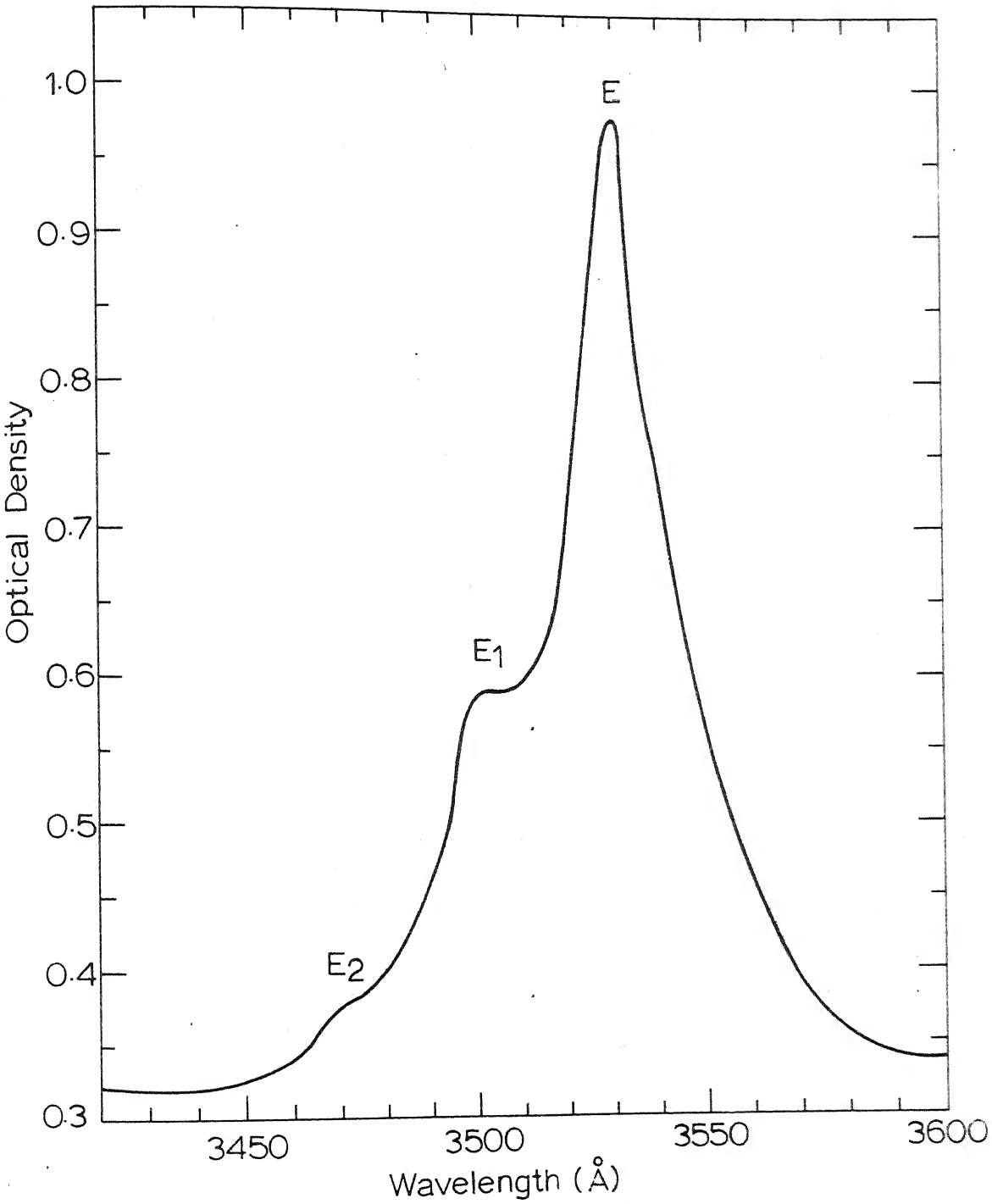

Fig. 5.9 $^6A_{1g}(S) \rightarrow {}^4E_g(D)$ band in Mn^{2+}: NaCl at liquid nitrogen temperature.

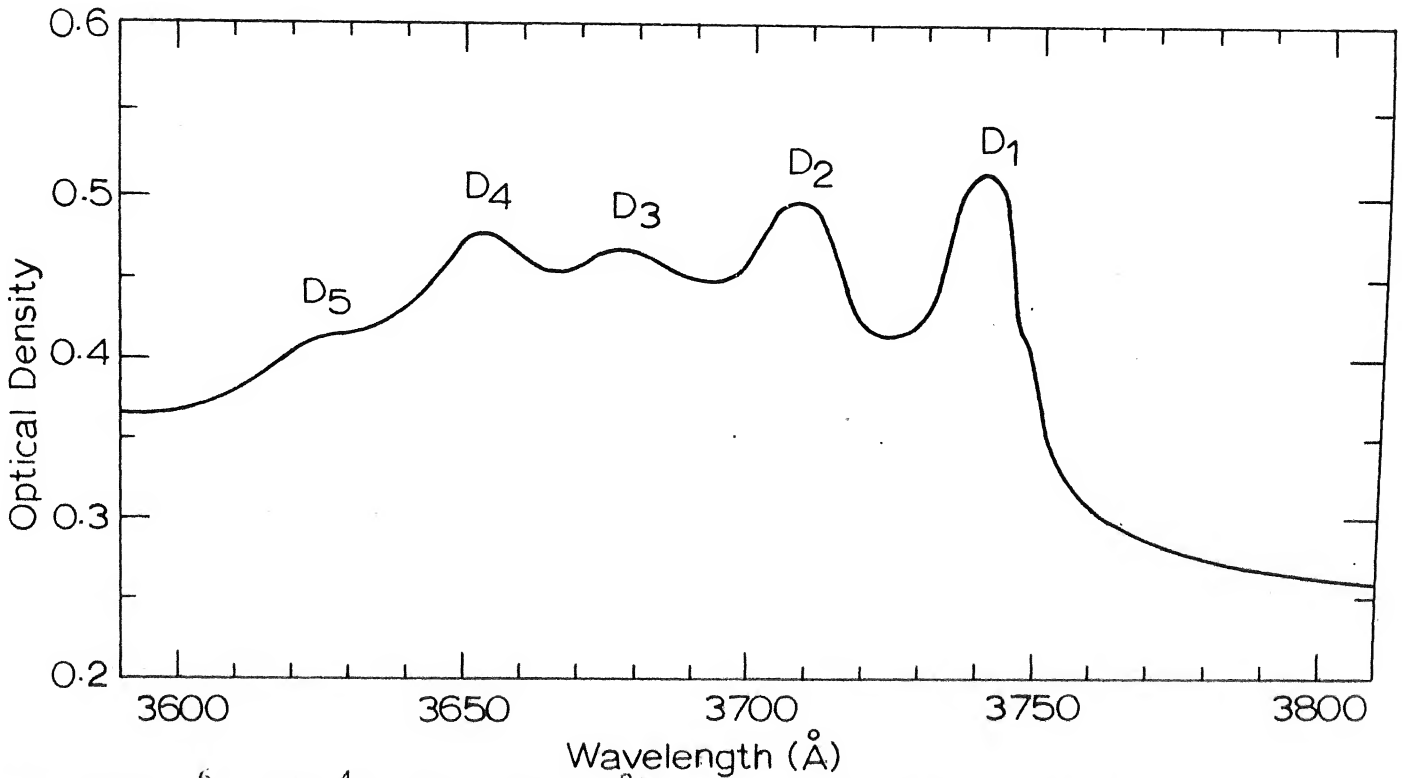

Fig. 5.10 $^6A_{1g}(S) \rightarrow {}^4T_{2g}(D)$ band in Mn^{2+} : NaCl at liquid nitrogen temperature.

Table 5.5

Fine structure of $^6A_{1g}(S) \rightarrow {}^4E_g(D)$ band in Mn^{2+}:NaCl at liquid nitrogen temperature.

Absorption peaks	Wavelength A^o	Wavenumber[c] cm^{-1}
	3536[a]	28,282
E[b]	3530	28,329
E_1	3503	28,547
E_2	3478	28,751

a. Observed as a weak shoulder.

b. Width of this line at half intensity is $210cm^{-1}$.

c. Differences in the observed wavenumbers of the lines are, in cm^{-1}, $E_1-E = 218$, $E_2-E_1 = 204$ and mean difference = 211.

Table 5.6

Fine structure of $^6A_{1g}(S) - {}^4T_{2g}(D)$ band in Mn^{2+}:NaCl at liquid nitrogen temperature.

Absorption peaks	Wavelength A^o	Wavenumber cm^{-1}
	3748[a]	26,681
D_1[b]	3740	26,738
D_2	3707	26,977
D_3	3677	27,195
D_4	3653	27,374
D_5	3626	27,579

a. Observed as a weak shoulder.

b. Width of this line at half intensity is $114cm^{-1}$.

involving these levels are given in Fig. 5.11 and Table 5.7. The prominence of C and C_1 lines suggests that probably these two lines represent the two closely spaced cubic field levels. The line C_o has a higher intensity at room temperature (Fig. 5.12) and its intensity decreases on cooling so that at liquid nitrogen temperature its intensity is very low. This suggests that the lower state of this line should be an excited vibrational level of thegroundstate. The closeness of the difference $C-C_o$ ($= 208cm^{-1}$) with the previously determined vibrational separation of $211cm^{-1}$ in the $^4E_g(D)$ band makes possible the construction of a simple transition diagram shown in Fig. 5.13.

Other lines in this band may be associated with the vibrational levels of the two electronic states.

It is worth mentioning that the appearance of this band is very similar to that of the corresponding band in $MnCl_2$ spectrum. The band C of $MnCl_2$ spectrum, i.e. the one involving $^4A_{1g}(G)$ and $^4E_g(G)$ levels, is shown in Fig. 5.14 which has been recorded with the Cary-14 spectrophotometer at room temperature.

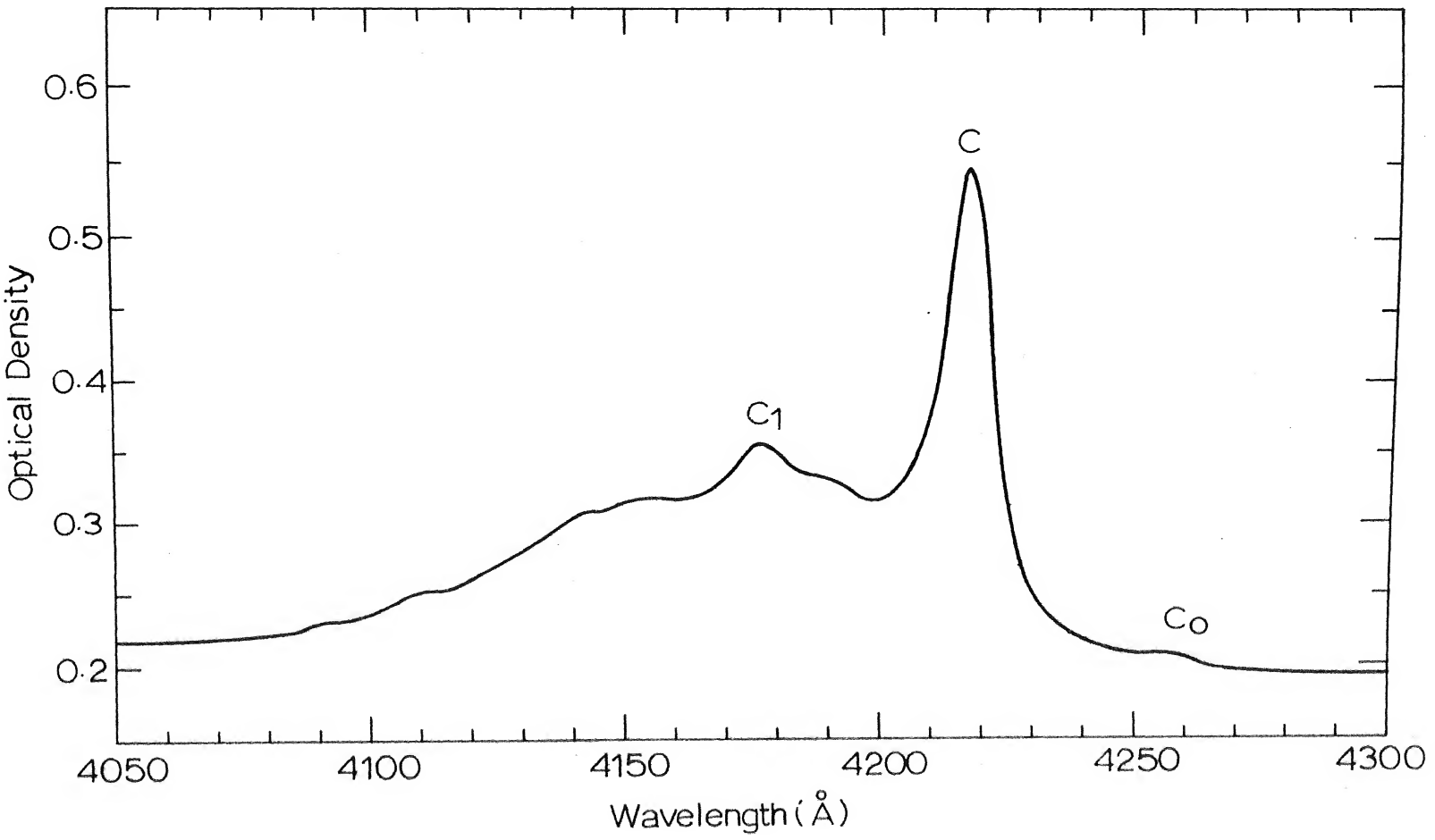

Fig. 5.11 $^6A_{1g}(S) \rightarrow {}^4A_{1g}(G)$, $^4E_g(G)$ band in Mn^{2+}: NaCl at liquid nitrogen temperature.

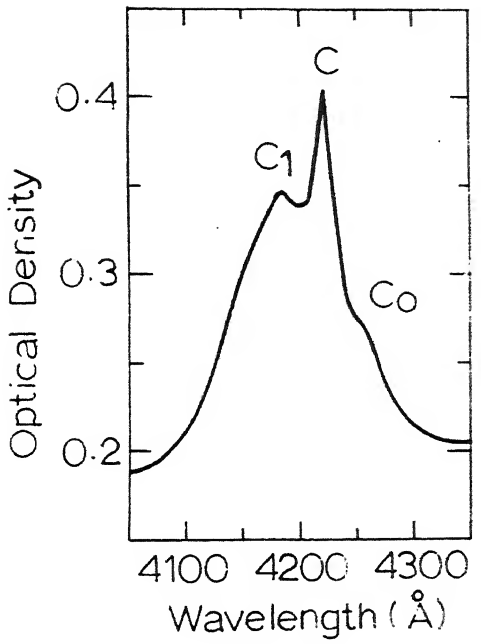

Fig. 5.12 $^6A_{1g}(S) \rightarrow {}^4A_{1g}(G)$, $^4E_g(G)$ band in Mn^{2+} : NaCl at room temperature.

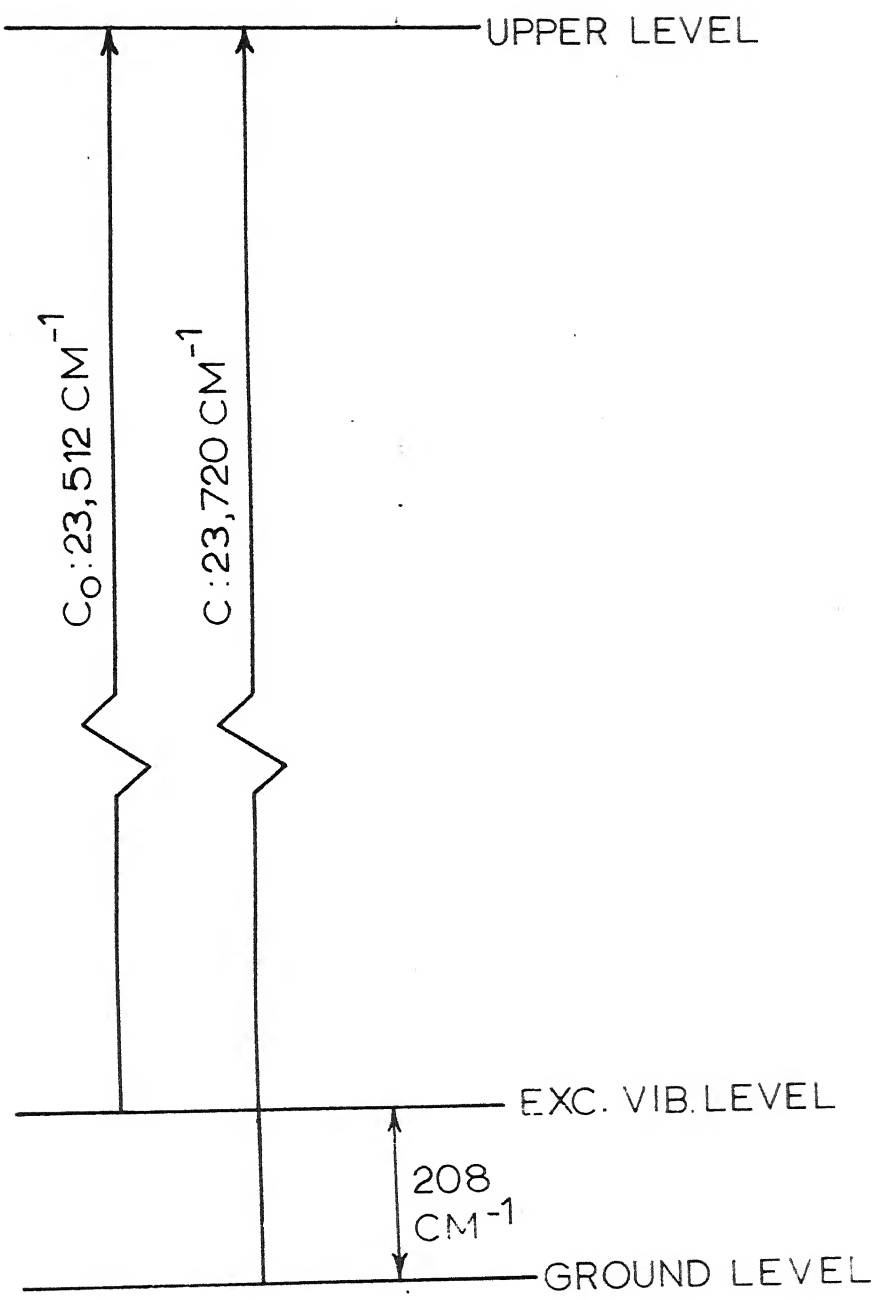

Fig. 5.13 Transition diagram for C and C_o lines in Mn^{2+} : NaCl.

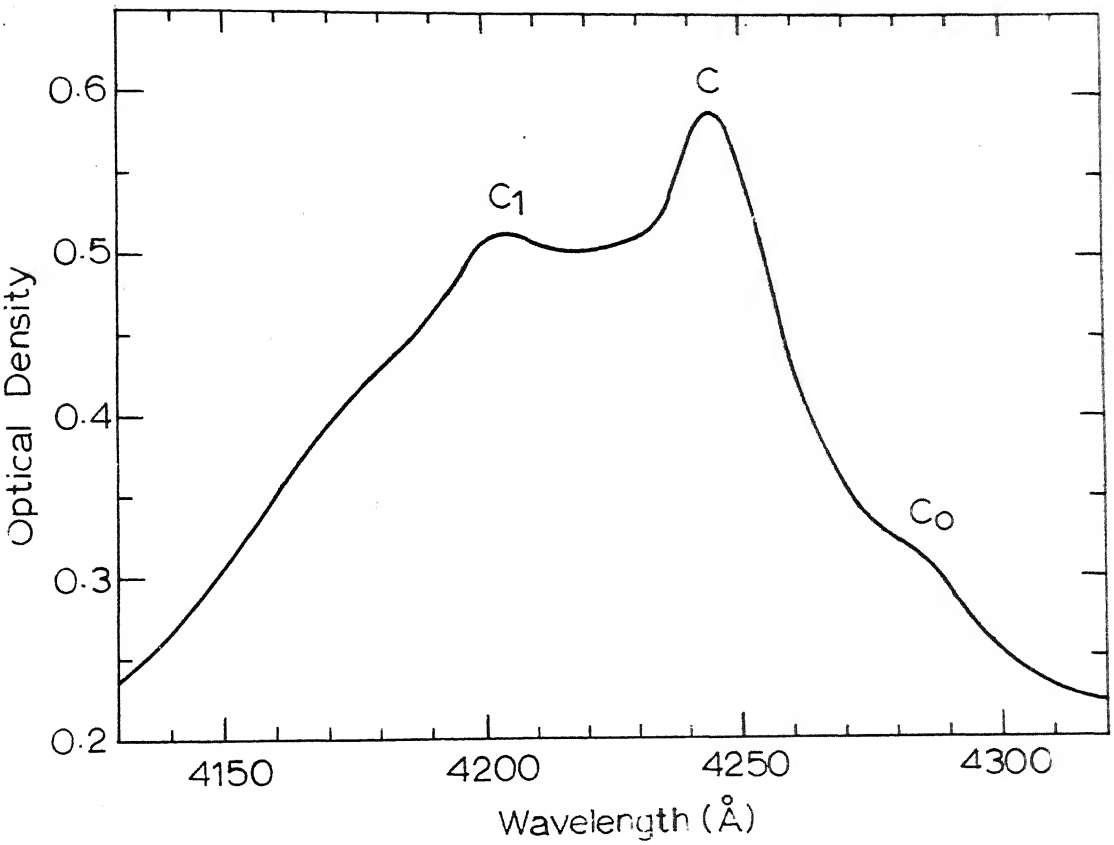

Fig. 5.14 $^6A_{1g}(S) \rightarrow {}^4A_{1g}(G)$, $^4E_g(G)$ band in $MnCl_2$ at room temperature.

Table 5.7

Fine structure of $^6A_{1g}(S)$- $^4A_{1g}(G)$, $^4E_g(G)$ band in Mn^{2+}:NaCl at liquid nitrogen temperature.

Absorption peaks	Wavelength A^o	Wavenumber cm^{-1}
C_o	4253	23,512
C^a	4216	23,720
	4187	23,882
C_1	4175	23,952
	4156	24,061
	4144	24,132
	4111	24,325

a. Width of this line at half intensity is $60cm^{-1}$.

CHAPTER VI

A COMPARATIVE STUDY OF Mn^{2+} SPECTRA

CHAPTER VI

A COMPARATIVE STUDY OF Mn^{2+} SPECTRA

A comparative study of Mn^{2+} spectra in various ligand coordinations is presented in this chapter. In Table 6.1 we have summarized the results on Mn^{2+} spectra in several coordinations. The values of the parameters B, C, and Dq given in this table for $RbMnF_3$, $Mn(CH_3COO)_2 \cdot 4H_2O$ Mn^{2+}:NaCl and Mn^{2+}:KCl are those obtained in the present work and discussed earlier. The values for other crystals MnF_2, $MnCl_2$, $MnBr_2$, MnO and $MnCl_2 \cdot 4H_2O$ and for manganese in perchloric acid ($Mn(ClO_4)_2 \cdot Aq$) have been calculated in the present work from the data of earlier workers for the sake of comparison.

Heidt, Koster and Johnson[13] have fitted the band energies in $Mn(ClO_4)_2 \cdot Aq$ by freely varying three parameters B, C, and Dq. The best values of parameters obtained by them are B = 670, C = 3710 and Dq = 848 cm^{-1}. Their observed and calculated band energies are given in Table 6.2. The calculated band energies in our formulation are also given in this table and the fit obtained by us is seen to be more satisfactory. For instance, the position of $^4T_1(P)$ level in the calculation of Heidt, Koster and Johnson is deviated by more than 2000cm^{-1} while in our calculation this deviation is less than 250cm^{-1}.

Table 6.1

Crystal field parameters and positions of ($^4A_1(G)$, $^4E(G)$) and $^4E(D)$ levels of Mn^{2+} in various coordinations. Values given in this table are from room temperature spectrum. Paranthesized values are from low temperature spectra.[a]

Systems	B	C	Dq	$^4A_1(G)$, $^4E(G)$ level C band	$^4E(D)$ level E band	Reference
Free ion	915	3235	---	26,850	32,340	ref.19
$RbMnF_3$	835	3080	760	25,278	30,067	this work
MnF_2	840	3095	750	25,270	30,230	ref.14
Mn^{2+}:NaF	835	3070	745	25,230	30,060	b
$Mn(ClO_4)_2 \cdot Aq$	820	3080	780	24,960	29,750	ref.13
$Mn(CH_3COO)_2 \cdot 4H_2O$	820	3000	760	24,740	29,454	this work
$MnCl_2 \cdot 4H_2O$	810	2980	710	24,590	29,100	ref.54
$MnCl_2$	770	2900	650	23,560	28,065	ref.15
Mn^{2+}:NaCl	780	2910	620	23,714	28,329	this work
Mn^{2+}:KCl	760	2955	590	23,882	28,137	this work
$MnBr_2$	(750)	(2860)	(630)	(23,084)	(27,505)	ref.15
MnO	(780)	(2900)	(895)	(23,810)	---	ref.62

a. All the values are given in cm^{-1}.

b. Unpublished work of the author.

Table 6.2

Calculated and observed band energies for the absorption spectrum of $Mn(ClO_4)_2 \cdot Aq$ at room temperature. The values are in cm^{-1}.

Transitions $^6A_1(S)$-	Observed[a] energy	Calculated[b] energy (I)	Calculated[c] energy (II)
$^4T_1(G)$	18,870	19,400	18,880
$^4T_2(G)$	23,120	22,800	23,013
$^4A_1(G)$	24,960	25,200	25,120
$^4E(G)$	25,275		
$^4T_2(D)$	27,980	28,200	28,141
$^4E(D)$	29,750	29,900	29,796
$^4T_1(P)$	32,960	35,000	32,747
$^4A_2(F)$	40,810	40,700	40,512

a. ref. 13.

b. Calculated energies of Heidt, Koster and Johnson (ref.13) for B = 670, C = 3710 and Dq = 848 cm^{-1}.

c. Calculated energies in the present case for B=820, C=3080, Dq=780 and α=76 cm^{-1}.

It is found for all the Mn^{2+} spectra that the deviations between calculated and experimental energies are larger for the higher energy bands. The theory used in the present work neglects the interactions with higher configurations and since the higher lying energy states are closer to excited configurations, the departures from the theory are more pronounced for the bands involving these states. A least squares fitting is not tried in the present work since, in view of the theory being less accurate at higher energies, such a fitting makes the set of parameters equally bad for all the levels and is not very useful for interpretation. In our fitting which gives preference to the lower levels, the errors from configurational mixing are minimized and the parameters may be evaluated for physical meaning in terms of the environment of the ion.

A comparison of the energies of C and E bands in different systems shows that the nephelauxetic series is obeyed. The order of ligands in the increasing power of decreasing the term separations or in other words in decreasing energies of C and E bands is:

$$F^-,\ H_2O,\ Cl^-,\ Br^-$$

On comparing the Dq values in different systems one gets the following spectrochemical series of ligands in the increasing order of Dq value:

$$Br^-,\ Cl^-,\ F^-,\ H_2O$$

A comparison of the hydrated systems manganese in perchloric acid, manganese acetate tetrahydrate and manganese chloride tetrahydrate shows that while nephelauxetically manganese acetate tetrahydrate is in between the other two, spectrochemically it is nearer to manganese in perchloric acid. In perchloric acid, all the six vertices of octahedron of ligands around Mn^{2+} are occupied by the water molecules while in $MnCl_2 \cdot 4H_2O$, water molecules at the two opposite vertices are replaced by Cl^-. The decrease in the parameters B and C, and Dq in going from $Mn(ClO_4)_2 \cdot Aq$ to $MnCl_2 \cdot 4H_2O$ are in agreement with this replacement. If all the six vertices of octahedron of ligands around Mn^{2+} in $Mn(CH_3COO)_2 \cdot 4H_2O$ were occupied by the water molecules, its parameters B and C should have been much nearer to those of $Mn(ClO_4)_2 \cdot Aq$. Similarity in the chemical formulae of $Mn(CH_3COO)_2 \cdot 4H_2O$ and $MnCl_2 \cdot 4H_2O$ suggests that probably the role played by Cl^- in the later crystal is played by $(CH_3COO)^-$ in the former. The requirements on the parameters B, C, and Dq of $Mn(CH_3COO)_2 \cdot 4H_2O$ will be fulfilled if oxygen of the acetic groups occupies the two opposite vertices of octahedron since oxygen is nephelauxetically nearer to Cl^- and spectrochemically nearer to H_2O (see the data on MnO spectrum).

The Dq value in $RbMnF_3$ is slightly larger than that in MnF_2. Mn-F distances in $RbMnF_3$ (~ 2.12 A^o) and MnF_2 (~ 2.10 and 2.13 A^o) are nearly same. It is possible

that this increase in Dq is due to the presence of Rb^{+} at the corners of the cube around Mn^{2+} in $RbMnF_3$ since the positive ions situated at the corners of a cube can cause a positive contribution to Dq.

APPENDICES

APPENDIX I

Table A-1

Character table for point group O_h and reduction of the fifteen dimensional mechanical representation T_M of the unit cell of $RbMnF_3$.

O_h	E	$8C_3$	$3C_2$	$6C_4$	$6C_2$	$\bar{1}$	$i8C_3$	$i3C_2$	$i6C_4$	$i6C_2$	Reduced representation
A_{1g}	1	1	1	1	1	1	1	1	1	1	...
A_{2g}	1	1	1	-1	-1	1	1	1	-1	-1	...
E_g	2	-1	2	0	0	2	-1	2	0	0	...
T_{1g}	3	0	-1	1	-1	3	0	-1	1	-1	...
T_{2g}	3	0	-1	-1	1	3	0	-1	-1	1	...
A_{1u}	1	1	1	1	1	-1	-1	-1	-1	-1	...
A_{2u}	1	1	1	-1	-1	-1	-1	-1	1	1	...
E_u	2	-1	2	0	0	-2	1	-2	0	0	...
T_{1u}	3	0	-1	1	-1	-3	0	1	-1	1	...
T_{2u}	3	0	-1	-1	1	-3	0	1	1	-1	...
T_M	15	0	-5	3	-3	-15	0	5	-3	3	$4T_{1u}+T_{2u}$

Table A-2

Splitting of the even parity atomic states in O_h symmetry.

Atomic state	Crystal field terms
S	A_{1g}
P	T_{1g}
D	E_g+T_{2g}
F	$A_{2g}+T_{1g}+T_{2g}$
G	$A_{1g}+E_g+T_{1g}+T_{2g}$
H	$E_g+2T_{1g}+T_{2g}$
I	$A_{1g}+A_{2g}+E_g+T_{1g}+2T_{2g}$

Table A-3

Character table for the double group O!

O	E	R	$8C_3$	$8RC_3$	$6C_4$	$6RC_4$	$3C_2 + 3RC_2$	$6C_2 + 6RC_2$
Γ_6	2	-2	1	-1	$\sqrt{2}$	$-\sqrt{2}$	0	0
Γ_7	2	-2	1	-1	$-\sqrt{2}$	$\sqrt{2}$	0	0
Γ_8	4	-4	-1	1	0	0	0	0

Table A-4

Reduction of the direct product of spin and orbital parts of the quartet terms of Mn^{2+} into the irreducible representations of the double group O´

Term	Product representation	Reduced representation
$^6A_1$	$(\Gamma_7+\Gamma_8)\times A_1$	$\Gamma_7+\Gamma_8$
$^4A_1$	$\Gamma_8 \times A_1$	Γ_8
$^4A_2$	$\Gamma_8 \times A_2$	Γ_8
^4E	$\Gamma_8 \times E$	$\Gamma_6+\Gamma_7+\Gamma_8$
$^4T_1$	$\Gamma_8 \times T_1$	$\Gamma_6+\Gamma_7+2\Gamma_8$
$^4T_2$	$\Gamma_8 \times T_2$	$\Gamma_6+\Gamma_7+2\Gamma_8$

Correlation between Bethe's and Mulliken's notation

Bethe's: Γ_1 Γ_2 Γ_3 Γ_4 Γ_5 Γ_6 Γ_7 Γ_8

Mulliken's: A_1 A_2 E T_1 T_2 $E_{\frac{1}{2}}$ $E_{\frac{5}{2}}$ G

APPENDIX II

ENERGY MATRICES FOR QUARTET LEVELS IN CUBIC FIELD

Table A-5

Energy matrices used in the present work for the quartet levels of d^5 configuration in cubic field. The matrices are in the strong field scheme. These are obtained by adding the strong field matrices of α term to the matrices of Tanabe and Sugano.[30] The ground state $^6A_1(S)$ is taken as zero of the energy scale. The matrices are symmetric.

. . . .

$^4A_1(G) : t^3e^2 : 10B + 5C + 20\alpha$

$^4A_2(F) : t^3e^2 : 22B + 7C + 12\alpha$

$^4E(D,G)$:

$t^3(^4A_2)e^2(^1E)$	$t^3(^2E)e^2(^3A_2)$
$14B + 5C + 12\alpha$	$-2\sqrt{3}B + 4\sqrt{3}\alpha$
	$13B + 5C + 14\alpha$

Table A-5 (Contd.)

$^4T_1(P,F,G)$:

t^4e	t^3e^2	t^2e^3
$10B+5C+12\alpha-10Dq$	$-3\sqrt{2}B-2\sqrt{2}\alpha$	$C-8\alpha$
	$19B+7C+10\alpha$	$-3\sqrt{2}B-2\sqrt{2}\alpha$
		$10B+5C+12\alpha+10Dq$

$^4T_2(D,F,G)$:

t^4e	t^3e^2	t^2e^3
$18B+5C+12\alpha-10Dq$	$\sqrt{6}B-2\sqrt{6}\alpha$	$4B+C$
	$13B+5C+14\alpha$	$-\sqrt{6}B+2\sqrt{6}\alpha$
		$18B+5C+12\alpha-10Dq$

APPENDIX III

The matrices of Trees correction term (α term) in the strong field scheme and the procedure adopted for finding them are given in this Appendix.

The procedure adopted here uses the unitary transformation matrices connecting strong and weak field schemes. If U is the matrix which transforms the weak field (w.f.) basis functions to the strong field (s.f.) ones, then it can be shown that any operator T is related in the two schemes by means of the following similarity transformations:[31]

$$T_{s.f.} = U\, T_{w.f.}\, U^{\dagger}$$

and $$T\, T_{w.f.} = U^{\dagger} T_{s.f.}\, U$$

where $U^{\dagger}$ is the Hermitian conjugate of U. Hence, if the matrix representation of any operator is known in one scheme, its matrix representation in other scheme can be determined with the help of above equations, provided U is known. Alternatively, if the matrix representations of any operator are known in both the schemes, the transformation matrix U may also be determined by means of above equations. Since the matrix representation of α term is known in the weak field scheme, the problem is to determine the suitable transformation matrices U. The determination of U's by finding the basis functions in the two schemes is not very practical and hence U's are found with the help of operators whose matrix representations are known in both the schemes. The electrostatic interaction is quite convenient for this purpose as the electrostatic matrices in the analytic form are known in both the schemes.[1,21,30] These

are diagonal in the weak field scheme[1,21] and non-diagonal in strong field scheme.[30] The diagonal elements in the weak field matrices are, obviously, the eigenvalues of strong field matrices. This makes the evaluation of U's particularly simple as these can be easily formed out of the eigenvectors of the strong field matrices. In other words, U's in this case are the matrices which diagonalise the strong field electrostatic matrices.

After finding the U, the task is simply to make a similarity transformation $U\alpha U^{\dagger}$ of the weak field α matrices which are diagonal, the diagonal elements being L(L+1). Since α term has got only diagonal elements in the weak field case, the arbitrariness in the sign of eigenvectors forming U causes no trouble in the present case as a change in sign of any of the column of U is accompanied by the change in sign of the corresponding row of its transpose $\tilde{U}$ (U being real, $U^{\dagger} = \tilde{U}$). This can be demonstrated in the following way:

$$\alpha_{s.f.} = U\, \alpha_{w.f.}\, \tilde{U}$$

On expanding the matrix product,

$$(\alpha_{s.f.})_{ij} = \sum_{kl} U_{ik}\, (\alpha_{w.f.})_{kl}\, \tilde{U}_{lj}$$

$$\text{but } \tilde{U}_{lj} = U_{jl}$$

$$\text{and hence } (\alpha_{s.f.})_{ij} = \sum_{kl} U_{ik}\, (\alpha_{w.f.})_{kl}\, U_{jl} \ .$$

Moreover, since $(\alpha_{w.f.})$ has only diagonal elements, the summation over l can be contracted and the double summation reduces to single summation so that,

$$(\alpha_{s.f.})_{ij} = \sum_{k} U_{ik}\, U_{jk}\, (\alpha_{w.f.})_{kk}$$

Thus the elements of any column of U always occur in pairs.

A change in sign of the column results in the change of sign of both the elements in the pair appearing as product (U_{ik} and U_{jk}) and therefore, does not cause any change in any of the terms appearing in the summation. Hence, the total sum that is the transformed matrix element is independent of the sign of the columns of U.

In this way the strong field matrices of α term have been found for all the doublet and quartet levels of d^5 configuration. The matrices for doublet levels of d^5 configuration are given in Table A-6 while the matrices for the quartet levels are included in the complete energy matrices for the quartet levels given in Table A-5 (Appendix II). The unitary transformation matrices, U, have been omitted for the sake of brevity.

Table A-6

Strong field matrices of the α term for the doublet Γ levels of d^5 configuration. The matrix elements are in unit of the parameter α. The matrices are symmetric.

$^2A_2(_3F,\ _5F,\ _5I)$:

t^4e	t^3e^2	t^2e^3
24	$-6\sqrt{2}$	-12
	18	$6\sqrt{2}$
		24

Table A-6 (Contd.)

$^2A_1(^5S, {}^3G, {}^5G, {}^5I)$:

t^4e	$t^3(^2E)e^2$	$t^3(^4A_2)e^2$	$t^2(^1E)e^3$
16	$6\sqrt{2}$	0	4
	18	$8\sqrt{3}$	$-6\sqrt{2}$
		32	0
			16

$^2E(^1D, {}^3D, {}^5D, {}^3G, {}^5G, {}^3H, {}^5I)$:

$t^4(^1A_1)e$	14	-4	0	0	0	-4	-8
$t^4(^1E)e$		20	6	$-6\sqrt{3}$	0	-4	4
$t^3(^2E)e^2(^1A_1)$			18	0	0	6	0
$t^3(^2E)e^2(^3A_2)$				26	$-4\sqrt{6}$	$6\sqrt{3}$	0
$t^3(^2E)e^2(^1E)$					18	0	0
$t^2(^1E)e^3$						20	4
$t^2(^1A_1)e^3$							14

Table A-6 (Contd.)

$^2T_1(^3P, {}^3F, {}^5F, {}^3G, {}^5G, {}^3H, {}^3H, {}^5I)$:

$t^4(^3T_1)e$	30	6	$3\sqrt{2}$	$-3\sqrt{2}$	$-\sqrt{2}$	$-\sqrt{6}$	0	-8
$t^4(^1T_2)e$		18	$-3\sqrt{2}$	$-3\sqrt{2}$	$-\sqrt{2}$	$-\sqrt{6}$	0	0
$t^3(^2T_1)e^2(^1A_1)$			18	0	0	$-4\sqrt{3}$	$-3\sqrt{2}$	$3\sqrt{2}$
$t^3(^2T_1)e^2(^1E)$				18	0	0	$3\sqrt{2}$	$3\sqrt{2}$
$t^3(^2T_2)e^2(^3A_2)$					22	$-4\sqrt{3}$	$-3\sqrt{2}$	$-\sqrt{2}$
$t^3(^2T_2)e^2(^1E)$						14	$-\sqrt{6}$	$-\sqrt{6}$
$t^2(^1T_2)e^3$							18	6
$t^2(^3T_1)e^3$								30

Table A-6 (Contd.)

$^2T_2(^1D,\ ^3D,\ ^5D,\ ^3F,\ ^5F,\ ^3G,\ ^5G,\ ^3H,\ ^5I,\ ^5I)$:

t^5	22	$-2\sqrt{6}$	$2\sqrt{6}$	0	$-4\sqrt{3}$	-8	4	0	0	0
$t^4(^3T_1)e$	18	-6	$-\sqrt{6}$	$3\sqrt{2}$	$\sqrt{6}$	$\sqrt{6}$	0	0	0
$t^4(^1T_2)e$		22	$-3\sqrt{6}$	$3\sqrt{2}$	$-\sqrt{6}$	$\sqrt{6}$	-8	0	0
$t^3(^2T_1)e^2(^3A_2)$			26	$-4\sqrt{3}$	0	0	$3\sqrt{6}$	$\sqrt{6}$	0
$t^3(^2T_1)e^2(^1E)$				18	$4\sqrt{3}$	0	$-3\sqrt{2}$	$-3\sqrt{2}$	$-4\sqrt{3}$
$t^3(^2T_2)e^2(^1A_1)$					14	0	$\sqrt{6}$	$-\sqrt{6}$	-8
$t^3(^2T_2)e^2(^1E)$						14	$\sqrt{6}$	$\sqrt{6}$	-4
$t^2(^1T_2)e^3$							22	-6	$-2\sqrt{6}$
$t^2(^3T_1)e^3$								18	$2\sqrt{6}$
te^4									22

APPENDIX IV†

ABSORPTION SPECTRUM OF Mn^{2+} IN KCl

ABSTRACT

The absorption spectrum of an Mn^{2+}-doped KCl crystal has been measured at room temperature. The observed bands are assigned as transitions from the $^6A_1(S)$ ground state to various excited quartet levels of a Mn^{2+} ion in a cubic crystalline field. The observed band energies are fitted with four parameters B,C,Dq, and α and the values obtained for the parameters in cm^{-1} are B = 760, C = 2955, Dq = 590, and α = 76.

---

† This appendix is a repreduction of paper entitled :Absorption Spectrum of Mn^{2+} in KCl: published by Author and Venkateswarlu in the Journal of Chemical Physics 45, 3381 (1966) and supplements the study of Mn^{2+}-doped alkali halides given in Chapter V. This appendix has separate numbering for its references which are given as footnotes.

INTRODUCTION

The absorption spectra of several manganous salts in the form of single crystals have been reported by earlier workers.[1,2] However, there have been only a few investigations on the electronic absorption spectra of Mn^{2+}-doped crystals and particularly on the Mn^{2+}-doped alkali halides.[3] Watkins[4] and more recently Shrivastava and Venkateswarlu[5] have made extensive electron spin resonance studies on Mn^{2+}:NaCl and Mn^{2+}:KCl. They have found in NaCl that depending upon concentration and heat treatment, the manganese could exist as a matallic precipitate, substitutional Mn^{2+} near a first-neighbor or a second-neighbor alkali vacancy, Mn^{2+} near an impurity or isolated Mn^{2+}. All these features except that of Mn^{2+} near an impurity were observed in Mn^{2+}:KCl.[4] In manganese-doped KCl Watkins[4] observed an additional resonance in the cloudy areas of the crystal which contained a higher percentage of manganese and attributed it to K_4MnCl_6. In order to obtain a measure of crystalline-field strength in these alkali halide crystals which have predominently ionic character, a study of Mn^{2+}-doped KCl and NaCl was

---

1. R. Pappalardo, J. Chem. Phys. 31, 1050 (1959)
2. J.W. Stout, J. Chem. Phys. 31, 709 (1959).
3. G. Kuwabara and K. Aoyagi, Japan J. Appl. Phys. 4, 627 (1965).
4. G.D. Watkins, Phys. Rev. 113, 79 (1959).
5. K.N. Shrivastava and P. Venkateswarlu, Proc. Indian Acad. Sci. A63, 284, 311 (1966)

undertaken and the results obtained in KCl are reported here.

EXPERIMENTAL

The crystals were grown from melt by the Bridgeman method and the optical absorption was measured with a Cary-14 spectrophotometer at room temperature. The amount of $MnCl_2$ added to the KCl flux was around 5 mole per cent, but the absolute concentration of Mn^{2+} in the grown crystal was not determined. The crystal used had a thickness of about 2 cm. It is possible that Mn^{2+} might have gone in the crystal partly in the substitutional positions and partly in the ways indicated by Watkins.[4]

RESULTS AND ANALYSIS

The spectrum obtained in the visible region is shown in Fig. 1. It has features characteristic of Mn^{2+} absorption and except for smaller separations between the bands it is very similar to the spectra of Mn^{2+} in pure crystals such as MnF_2.[2] The wavelengths and the wavenumbers of the bands are given in Table I along with the assignments which to a large extent are based upon the analysis of Mn^{2+} spectra by earlier workers, assuming the symmetry to be octahedral. The uncertainty in the observed wavelengths for the sharp bands is around ± 3 A^{o} and that for the broad bands is

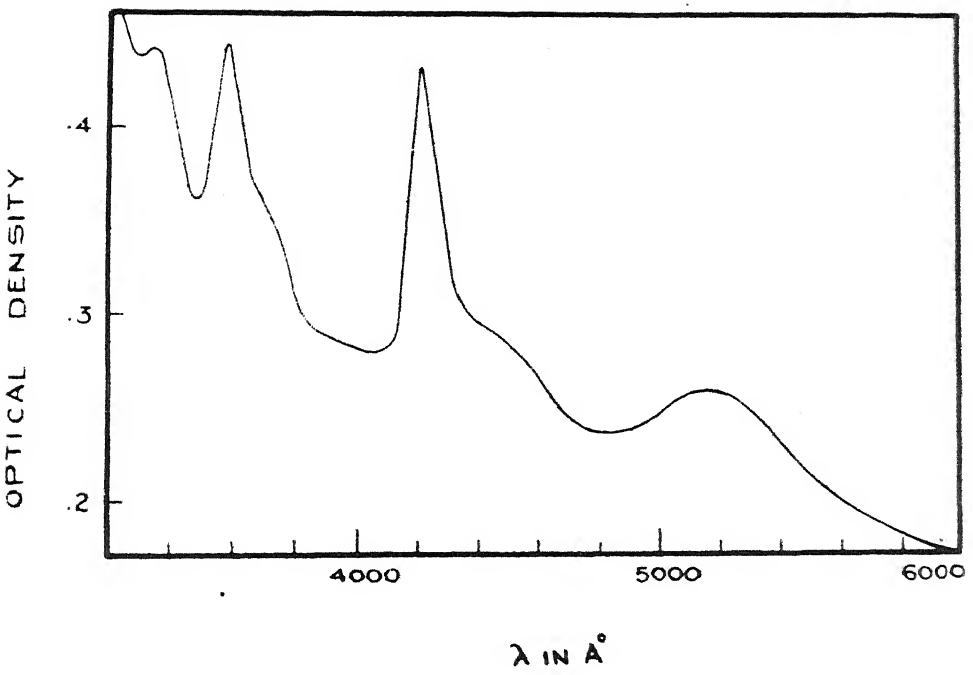

Fig. 1 The absorption spectrum of Mn^{2+} — doped KCl in the visible region at room temperature.

Table I

The experimental data at room temperature and the analysis of the absorption spectrum of Mn^{2+} in KCl.

Transition[a,b] $^6A_1(S) \rightarrow$	Observed $\lambda(A^o)$	Observed ν (cm^{-1})	Calculated[c] ν (cm^{-1})	Remark[d]
$^4T_1(G)$	5180	19 300	19 403	b
$^4T_2(G)$	4405	22 700	22 656	h
$^4A_1(G)$ $^4E(G)$	4187	23 880	23 895	s
$^4T_2(D)$	3675	27 200	26 931	h
$^4E(D)$	3554	28 135	28 151	s
$^4T_1(P)$	3331	30 020	30 103	b
$^4A_2(F)$ $^4T_1(F)$	2600	38 500	38 317 38 862	b
$^4T_2(F)$	2340	42 700	40 766	b

a. The nomenclature of the states is based on the one adopted by Stout (Ref. 2). The parent free-ion orbital states are given in the parentheses.

b. All the states are gerade states.

c. Calculated with B = 760, C = 2955, Dq = 590 and α = 76cm^{-1}.

d. Abbreviations: s, sharp; h, hump; b, broad.

around ± 10A°. The sharp band at 4200 A° and the next two bands on its higher-wavelength side arise due to the transitions from the ground state to the states ($^4A_1$, ^4E), $^4T_2$ and $^4T_1$, respectively, all of which arise from the ^4G level of the free ion (Fig. 2). The next sharp band around 3600 A° and its longer-wavelength side shoulder have ^4E and $^4T_2$, respectively, for their upper states both of which arise from the ^4D state of the free ion. The last band around 3300 A° is because of a transition to $^4T_1$ state which arises from the ^4P state of the free ion. The overlapping of the bands assigned to the $^4T_2(G)$ and $^4T_2(D)$ levels with their respective neighboring sharp bands indicates a low value for the cubic crystalline-field parameter Dq. The energy-level calculations discussed later show that this is indeed true.

In the ultraviolet region two broad bands superposed over a strong background absorption were observed and the approximate positions of these two-band maxima are also included in Table I. The assignments of these two bands are not as clear as those of the visible region bands and are discussed in the next section.

DISCUSSION

The calculation of energy levels was performed using four parameters B, C, Dq, and α in the weak-field scheme. The parameters B and C are the electrostatic parameters called Racah coefficients and are the linear

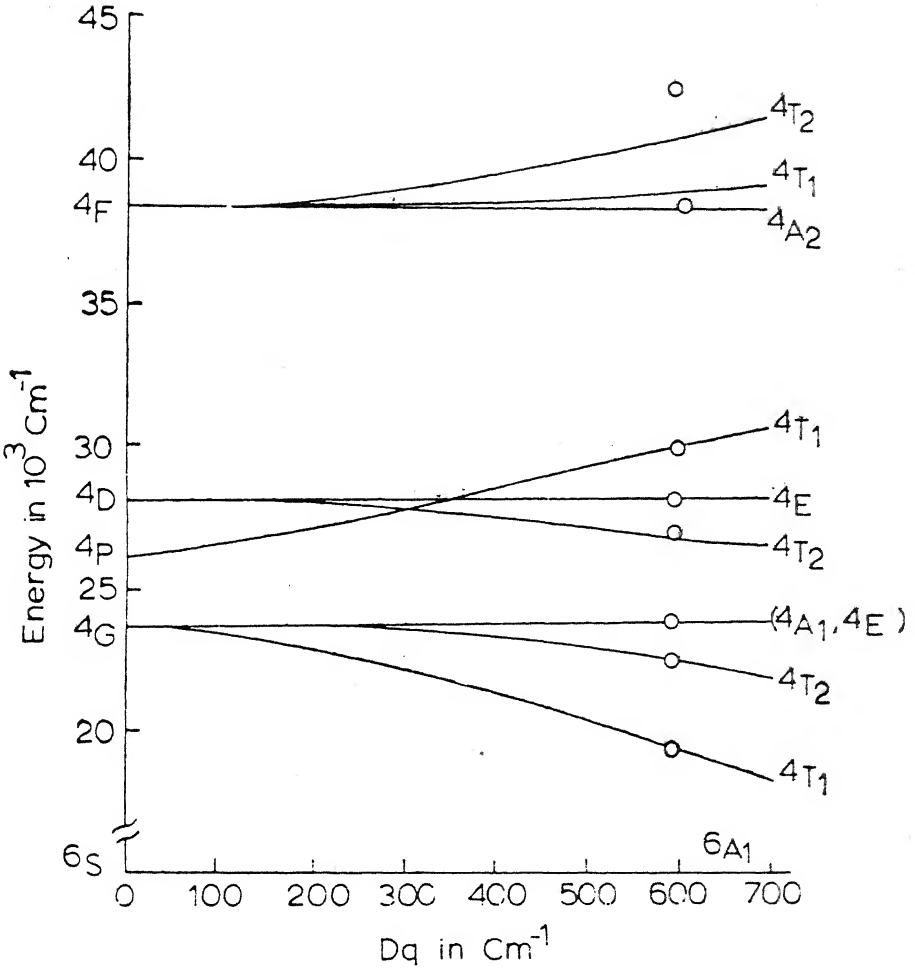

Fig. 2 The energy level diagram of Mn^{2+} in a cubic field showing the variation of the levels with Dq for a case with B = 760, C = 2955, and α = 76 cm^{-1}. The observed energies are marked o around the Dq value of 590 cm^{-1}.

combinations of the Slater-Condon parameters for the radial integrals. Because of the deformation of the free-ion orbitals in the crystal, the free-ion values of B and C cannot be carried over to the crystals. These are treated as adjustable parameters in the calculation. The parameter Dq describes the splitting due to the cubic crystalline field and this too is treated as an adjustable parameter. The parameter α is the one introduced by Trees[6] and later attributed by Racah[7] to the polarization effects. The correction term introduced by it is relatively small and therefore, it was arbitrarily fixed at the free-ion value of 76cm^{-1}. Its inclusion was found necessary for a good agreement between the observed and calculated values. The set of parameters used by us is similar to the one used by Low and Rosengarten[8] in their extensive calculations on Mn^{2+}. However, the spin-orbit coupling parameter ξ used by them is not introduced in the present calculations as its effects which show up as fine structures are not observed. Thus only three parameters B, C, and Dq were varied so as to give a best over-all fit with the observed energies and the agreement obtained is satisfactory. The values of parameters found in cm^{-1} are B = 760, C = 2955, and Dq = 590. The calculated energies

---

6. R.E. Trees, Phys. Rev. 83, 756 (1951).
7. G. Racah, Phys. Rev. 85, 381 (1952).
8. W. Low and G. Rosengarten, J. Mol. Spectry. 12, 319 (1964).

are included in Table I. The energy levels plotted against Dq for B = 760, C = 2955 and α = 76cm^{-1} are shown in Fig. 2 and the observed energies are also marked in it for comparison.

Calculations show that the transitions from the ground state to the levels arising from the ^4F state of the free ion lie in the ultraviolet region. The calculated energies of the two lower levels $^4A_2(F)$ and $^4T_1(F)$ are respectively, at 38, 317 and 38,867 cm^{-1}. It seems that the observed single broad band with its maximum at 38 500cm^{-1} is perhaps due to an overlapping of the transitions to these two levels. The 42 700cm^{-1} band might be thought of as having $^4T_2(F)$ for its upper state but the agreement between the observed and the calculated values for this transition is not good.

It may be mentioned here that Goode[9] has recently obtained the spectrum of Mn^{2+} in solid solutions of $KCl \cdot MnCl_2 \cdot 2H_2O$ and found that its nature is similar to what he obtained in $MnCl_2 \cdot 2H_2O$. Both these spectra are different from what is reported in the present paper.

---

9. D.H. Goode, J. Chem. Phys. 43, 2830 (1965).

APPENDIX V

EXPERIMENTAL DETAILS

Crystal Growing:

The alkali halide crystals were grown from melt and for this purpose a vertical cylindrical muffle furnace was constructed. The crystals were grown by Bridgeman method in evacuated quartz crucibles.[63] The method was found to be very successful for growing large single crystals. Pure crystals and also the crystals with small impurity concentrations could be grown upto 5 cm. in length. Increase in the impurity concentration causes a deterioration in the quality of the grown crystal.

The crystals of manganese acetate tetrahydrate were grown from saturated water solution at room temperature. $Mn(CH_3COO)_2 \cdot 4H_2O$ used in growing the crystals was of high purity grade. The crystals of $Mn(CH_3COO)_2 \cdot 4H_2O$ grow in the form of six sided plates. Single crystals upto the size of 1 x 1 x 0.5 cm. were successfully grown. The crystal gets spoiled by a long exposure to atmosphere and care has to be taken for preserving the crystal.

Spectral Measurements:

All the spectra were recorded on a Cary-14 spectrophotometer. This is a double beam spectrophotometer which operates in the 26000 to 2000A^{o} range. Separate detectors and sources are provided for the infrared, visible and ultraviolet regions. None of the Mn^{2+} bands are found in the infrared

region and so the measurements were needed only in the visible and ultraviolet regions. It has been found that the instrument works very well in the visible region where the main Mn^{2+} spectrum lies. An accurate wavelength calibration is needed in the region of sharp bands C and E since the uncertainty in the peak position of the broad band itself is of the order of $10A^{o}$. A standard mercury arc lamp was used for this purpose and in the region of sharp bands the calibration was found to be true within $2A^{o}$.

Uncertainty in the wavelength measurement varies from line to line and depends on the sharpness of the line. Uncertainty for the lines in the sharp bands lies between 1 to $3A^{o}$ and that in the region of broad bands lies between 5 to $10A^{o}$. It may be mentioned that the separations between the fine structure components of a band are more accurately found than the absolute positions of the fine structure components.

The instrument directly records the optical density. It has two recording scales one for optical densities between 0 to 1 and another for optical densities between 1 and 2. Optical densities higher than 2 may be measured by inserting a suitable density screen in the reference beam, but this reduces the sensitivity and accuracy of the instrument.

Molar extinction coefficient ε(litre cm^{-1} $mole^{-1}$) is defined as (M/1000 Dt) x optical density, where M is the molecular weight, D is the density, and t is the thickness

of the specimen used. The oscillator strength of a band is given by:

$$f = 2.303 \times 10^{3} \, (mc/N \pi e^{2}) \int_{c} \varepsilon(\nu) \, d\nu$$

$$= 0.43 \times 10^{-8} \int_{c} \varepsilon \, d\nu$$

The integral in all the cases was evaluated by measuring the area under the absorption curve. The individual f-values of the fine structure components of the bands were not measured and only the total oscillator strengths of the bands are reported. It is estimated that the errors in the oscillator strength may be at great as 25%.

The band widths reported in this work are always the widths at half of the maximum absorption.

The spectra were measured at room temperature as well as at liquid nitrogen temperature. A brass disc with a circular aperture was used as a crystal holder at room temperature. For low temperature measurements a dewar of the type shown in Fig. A-1 was constructed. In this dewar the crystal is pasted on a copper plate with a circular hole attached to copper disc which is in direct contact with the coolant, liquid nitrogen in the present case. The chamber around the crystal is kept evacuated while taking the spectra.

Computations:

Some of the calculations were performed on IBM 7044 and IBM 1620 computers. Eigenvalues of the energy matrices were found by an iterative procedure.

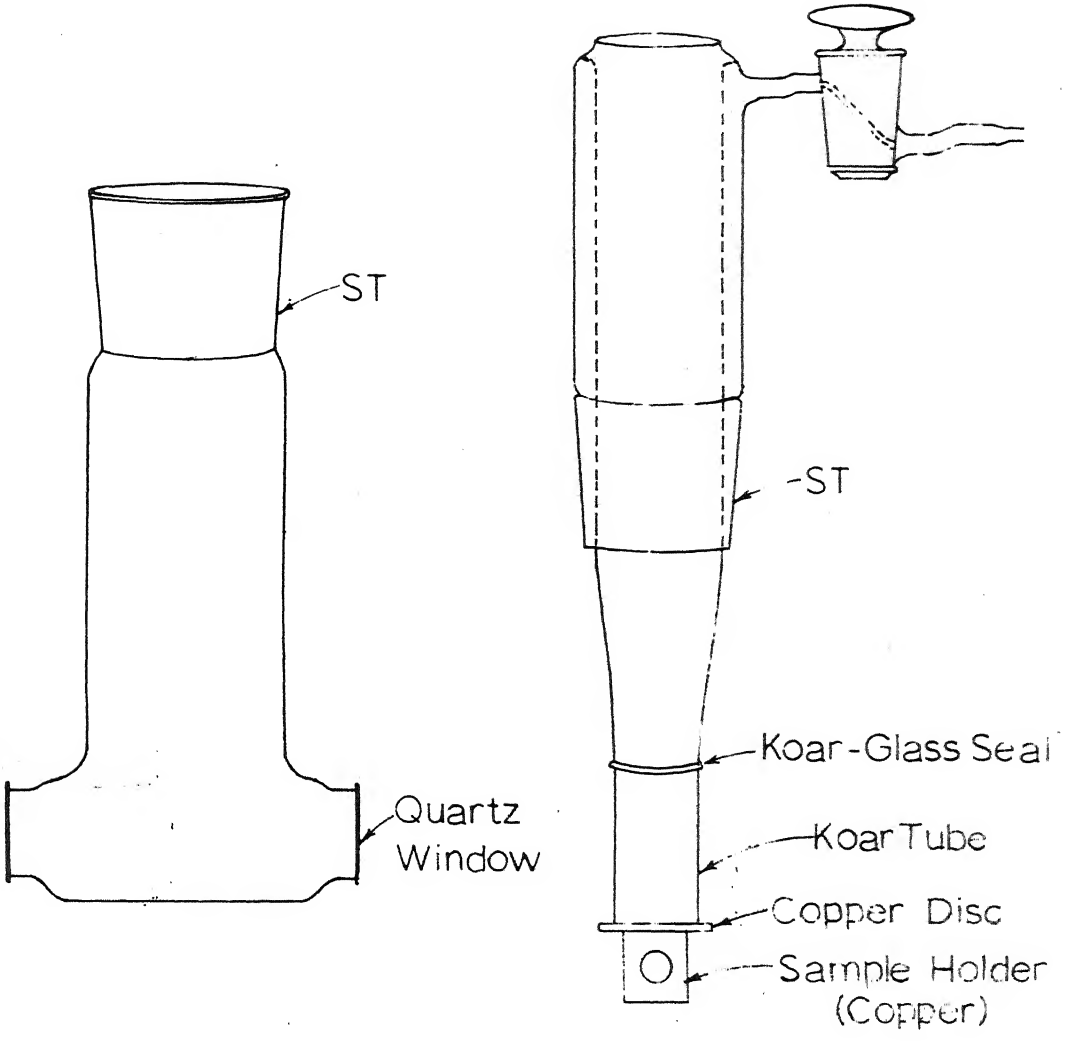

LOW TEMPERATURE DEWAR

Fig. A-1 Dewar used for taking the spectra at low temperatures.

REFERENCES

1 C.J. Ballhausen: "Introduction to Ligand Field Theory", McGraw-Hill Book Company, Inc., New York, 1962.

2 H. Bethe: Ann. Physik [5], 3, 133 (1929).

3 J. Owen: Discussion Faraday Soc., 19, 127 (1955).

4 C.J. Ballhausen and A.D. Liehr: J. Mol. Spectry 2, 342 (1958); 4, 190 (1960).

5 M. Tinkham: Proc. Roy. Soc. (London) A236, 535 (1956).

6 M.D. Sastri: (unpublished work).

7 J.H. VanVleck: J. Chem. Phys. 3, 803, 807 (1935).

8 J.H. Van Vleck and A. Sherman: Revs. Modern. Phys. 7, 167 (1935).

9 D.S. McClure: Solid State Physics , Vol. 9, Academic Press, Inc., New York,(1959.

10 Proceedings of the Symposium on Optical Masers, New York, 1963, John. Wiley and Sons, Inc., New York, 1963.

11 C.K. Jorgensen: Acta Chem. Scand. 8, 1502 (1954); 11, 53 (1957).

12 O.G. Holmes and D.S. McClure: J. Chem. Phys. 26, 1686 (1957).

13 L.J. Heidt, G.F. Koster, and A.M. Johnson: J. Am. Chem. Soc. 80, 6471 (1958).

14 J.W. Stout: J. Chem. Phys. 31, 709 (1959).

15 R. Pappalardo: J. Chem. Phys. 31, 1050 (1959).

16 D.M. Finlayson, I.S. Robertson, T. Smith and R.W.H. Stevenson: Proc. Phys. Soc. 76, 355 (1960).

17 R.J. Ginther: J. Electrochemical Soc. 98, 74 (1951).

18 R.B. Flippen and S.A. Friedberg: Phys. Rev. 121, 1591 (1961).

19 C. Moore: Atomic Energy Levels, N.B.S. Circ. 467, Vol. II, 1952.

20 J.C. Slater: "Quantum Theory of Atomic Structure", McGraw-Hill Book Company, Inc., New York, 1960.

21 G. Racah: Phys. Rev. 62, 438 (1942); 63, 367 (1943).

22 R.E. Watson: Phys. Rev. 118, 1036 (1960).

23 R.E. Trees: Phys. Rev. 83, 756 (1951); 84, 1089 (1951); 85, 382 (1952).

24 G. Racah: Phys. Rev. 85, 381 (1952).

25 J.S. Griffith: "The Theory of Transition Metal Atoms", Cambridge University Press, 1960.

26 J. Ferguson: Rev. Pure and Appl. Chem. 14, 1 (1964).

27 Y. Shadmi: Thesis, Jerusalem (1961).

28 J.R. Gabriel, D.F. Johnston and M.J.D. Powell: Proc. Roy. Soc. A264, 503 (1961).

29 L.E. Orgel: J. Chem. Phys. 23, 1004 (1955).

30 Y. Tanabe and S. Sugano: J. Phys. Soc. Japan: 9, 753, 766 (1954).

31 A.D. Liehr and C.J. Ballhausen: Ann. Phys. (N.Y.) 6, 134 (1959).

32 K.A. Shroeder: J. Chem. Phys. 37, 1587 (1962).

33 D.H. Goode: J. Chem. Phys. 43, 2830 (1965).

34 W. Low and G. Rosengarten: J. Mol. Spectry 12, 319 (1964).

35 L.E. Orgel: J. Chem. Phys. 23, 1824 (1955).

36 J.H. Van Vleck: J. Phys. Chem. 41, 67 (1937).

37 S. Koide and M.H.L. Pryce: Phil. Mag. 3, 607 (1958).

38 R. Englman: Mol. Phys. 4, 183 (1961).

39 J. Ferguson, H.J. Guggenheim, L.F. Johnson and H. Kamimura: J. Chem. Phys. 38, 2579 (1963).

40 C.C. Klick and J.H. Shulman: J. Opt. Soc. Am. 42, 910 (1952).

41 R. Tsuchida: Bull. Chem. Soc. Japan 13, 388, 436 (1938).

42 C.E. Shaffer and C.K. Jorgensen: J. Inorg. and Nuc. Chem. 8, 143 (1958).

43 I. Tsujikawa and E. Kanda: J. Phys. Soc. Japan 18, 1382 (1963).

44 I. Tsujikawa: J. Phys. Soc. Japan 18, 1391 (1963).

45 J. Ferguson and H.J. Guggenheim: J. Chem. Phys, 44, 1095 (1966).

46 S. Sugano and R.G. Shulman: Phys. Rev. 130, 517 (1963).

47 D.T. Teaney, M.J. Freesen and R.W.H. Stevenson: Phys. Rev. Letters 9, 212 (1962).

48 J. Ferguson, H.J. Guggenheim and Y. Tanabe: a) J. Phys. Soc. Japan 21, 692 (1966); b) J. Appl. Phys. 36, 1046 (1965).

49 R. Stevenson: Canadian J. Phys. 43, 1732 (1965).

50 V.L. Moruzzi and D.T. Teaney: Bull. Am. Phys.Soc. 8, 382 (1965).

51 Measurements of Windsor and Wilson quoted by M.B. Walker and R.W.H. Stevenson: Proc. Phys. Soc. 87, 35 (1966).

52 M. Balkanski, P. Mock and M.K. Teng: (private communication).

53 G.R. Hunt, C.H. Perry, and J. Ferguson: Phys. Rev. 134, A688 (1964).

54 R. Pappalardo: Phil. Mag. 2, 1397 (1957).

55 I. Tsujikawa: J. Phys. Soc. Japan 18, 1407 (1963).

56 P. Groth: Chemische Kristallographie, Leipzig, Vol. 3, p. 69, 1910.

57 J. Gielessen: Ann. Phys. 22, 537 (1935).

58 G. Kuwabara and K. Aoyagi: Japan J. Appl. Phys. 4, 627 (1965).

59 G.D. Watkins: Phys. Rev. 113, 79 (1959).

60 a) K.N. Shrivastava and P. Venkateswarlu: Proc. Indian Acad. Sci. A63, 284, 311 (1966).

b) K.N. Shrivastava: Ph.D. Thesis, Indian Institute of Technology, Kanpur, India, 1966.

61 A. Mehra and P. Venkateswarlu: J. Chem. Phys. 45, 3381 (1966).

62 G.W. Pratt and R. Coelho: Phys. Rev. 116, 281 (1959).

63 K. Lark -Horovitz and V. Johnson (Editors): Methods of Experimental Physics, Vol. VI, Academic Press, New York, 1959. Chapter 11.7 by J.H. Shulman and H.W. Etzel (This reference gives the details for growing crystals from melt).

-o-O-o-

VITAE

Born on July 24, 1945 in Bareilly of Uttar Pradesh, Anjani Mehra passed the High School examination in 1958 from Government High School, Bareilly. He pursued his later studies at Allahabad in Government Inter College from where he passed the Intermediate examination in 1960, and afterwards in Allahabad University from where he obtained the degrees of Bachelor of Science and Master of Science (Physics) in 1962 and 1964, respectively. He then joined the Department of Physics, Indian Institute of Technology Kanpur, in August 1964, and was awarded a Junior Research Fellowship of the Council of Scientific and Industrial Research, India. At present he holds a Senior Research Fellowship of the National Bureau of Standards, U.S.A.